Analytical and Numerical Investigation of Long-term Behavior of Microbial Flocculation Equations

by

Inom Mirzaev

B.S., Middle East Technical University, Turkey, 2012

A thesis submitted to the

Faculty of the Graduate School of the

University of Colorado in partial fulfillment

of the requirement for the degree of Doctor of Philosophy

Department of Applied Mathematics

2017

This thesis entitled:
Analytical and Numerical Investigation of Long-term Behavior of Microbial Flocculation Equations
written by Inom Mirzaev
has been approved for the Department of Applied Mathematics

Prof. David M. Bortz

Prof. Keith Julien

Prof. Jeffrey Cameron

Prof. Zachary Kilpatrick

Prof. Vanja Dukic

Date

The final copy of this thesis has been examined by the signatories, and we find that both the content and the form meet acceptable presentation standards of scholarly work in the above mentioned discipline.

Mirzaev, Inom (Ph.D., Applied Mathematics)

Analytical and Numerical Investigation of Long-term Behavior of Microbial Flocculation Equations

Thesis directed by Prof. David M. Bortz

Flocculation is the reversible combination and separation of suspended particles in a fluid. It is a phenomenon ubiquitous in a wide variety of fields such as meteorology, marine science, astronomy, polymer science, and biotechnology. Flocculation is an efficient liquid-solid separation technique and has a broad range of industrial applications including fermentation, biofuel production, mineral processing, and wastewater treatment. A common mathematical model for the microbial flocculation is a 1D nonlinear partial integro-differential equation, which has been used successfully in matching many flocculation experiments.

In this dissertation, we rigorously investigate the long-term behavior of the microbial flocculation equations. When the long-term behavior of biological populations is considered, many populations converge to a stable time-independent state. Towards this end, using results from fixed point theory, we first derive conditions for the existence of continuous, non-trivial stationary solutions. We further apply the principle of linearized stability and semigroup compactness arguments to provide sufficient conditions for local stability of stationary solutions as well as sufficient conditions for instability. Consequently, we develop a numerical framework for computing approximations to stationary solutions of the microbial flocculation equations, which can also be used to produce approximate existence and stability regions for steady states. Furthermore, this numerical framework can be used to numerically investigate stationary solutions of general evolution equations. We develop several efficient and high-precision numerical schemes based on Finite Difference and Spectral Collocation methods to approximate stationary solutions of the microbial flocculation equations. We exploit spectral accuracy of the Spectral Collocation method for the numerical spectral analysis, which in turn allows us to heuristically deduce local stability of numerically computed steady states. We explore the stationary solutions of the model for various biologically relevant parameters and give valuable insights for the efficient removal of suspended particles. Lastly, we investigate the inverse

problem of identifying a conditional probability measure in measure-dependent evolution equations arising in size-structured population modeling. We illustrate that a particular form of the microbial flocculation equations is one realization of a system satisfying the hypotheses in our framework.

Dedication

To my parents, Ilhom Mirzaev and Davronoy Mirzaeva.

Acknowledgments

First of all, I would like to express my sincere gratitude to my advisor Prof. David M. Bortz for his cooperation and for all of the support I was given throughout my Ph.D. life at the University of Colorado Boulder. His valuable guidance and supervision helped me to choose the right direction and successfully complete my dissertation.

A very special gratitude goes out to all my fellow graduate students and friends at the University of Colorado Boulder for all the fun we have had in the last five years. With a special mention to John Nardini, Taisa Kushner, Jacqueline Wentz, Eric Kightley, Anna Broido, Edward Yasutake, Jay Stotsky, and Sama Shrestha.

I owe special thanks to my best roommate/friend Sina Erturk and his wife Hulya Erturk for keeping things lively and for the enlightening discussions.

Finally, I would like to thank my parents for their wise counsel, enduring support and encouragement throughout writing this thesis and my life in general.

Contents

List of Figures

Chapter 1

Introduction

Flocculation is the process whereby particles (i.e., flocs) in suspension reversibly combine and separate. The process is crucial for mineral processing, biochemical polymerization, sewage treatment, and for many other industrial processes. Flocculation is one of the most significant solid-liquid separation techniques used in mineral industry (Laskowski & Ralston, 2015). The technique aims at recovering valuable minerals from liquid ore slurries and attained by addition of charged polymers (i.e., flocculants) to improve separation, settling and filtration rates. Flocculation is also essential in downstream processing, i.e., recovery and purification, of biosynthetic products from natural sources in the manufacturing of the pharmaceuticals (Ladisch, 2001). The first step in downstream processing is the removal of insoluble materials from fermentation broth containing pharmaceuticals. Consequently, the feed streams containing large amounts of dispersed particles are clarified by flocculation process (Buyel & Fischer, 2014).

Adhesion properties of microorganisms have also been a focus of extensive biological research (Enmon et al., 2002; Aceto et al., 2014; Haaber et al., 2012). It has been shown that adhesive features of cells are crucial for many biological processes such as biofilm formation (Bottero et al., 2013), tissue invasion during cancer metastasis (Aceto et al., 2014), sexual reproduction (Chen & Thorner, 2007) and others. For instance, microbial flocculation is a detrimental condition in bloodstream infections. Aggregates in the bloodstream provide bacteria with antibiotic resistance making them difficult to eradicate (Haaber et al., 2012). Moreover, recent studies demonstrate that bacterial floc formation initiates blood coagulation, which in turn causes life-threatening septic shocks (Borenstein, 2008).

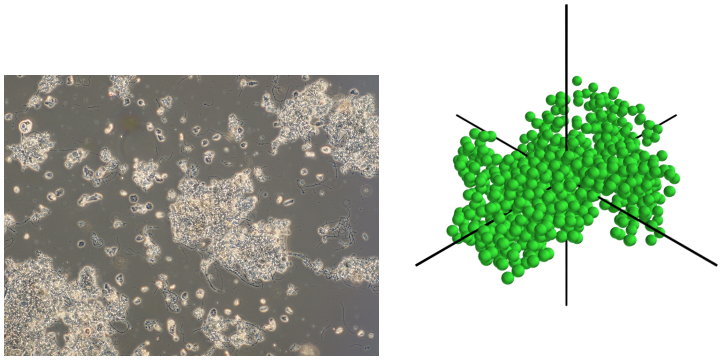

(a) (b)

Figure 1.1: Flocs, compactly aggregated cell communities in suspension a) Microscopy image of microbial floc in activated sludge formed from filamentous bacteria[1]. b) Computer rendering of *Klebsiella pneumoniae* floc imaged in the Younger and Solomon labs (Bortz et al., 2008).

Many microscopic lifeforms in suspension form highly compact cell communities to promote survival and proliferation. Figure 1.1 illustrates a microscopy image of microbial floc formed from filamentous bacteria and a computer rendering of *Klebsiella pneumoniae* floc imaged in the Younger and Solomon labs (Bortz et al., 2008). Flocculation of microorganisms has been exploited to improve various processes in microalgal biofuel production (Salim et al., 2011), brewing (Bauer et al., 2010), winemaking (Caridi, 2006) and wastewater treatment (Bache & Gregory, 2007). Due to its low energy consumption and relative simplicity compared to centrifugation and filtration, flocculation processes are often used to enhance suspended solids removal in fields such as water treatment and industrial fermentation.

Activated sludge flocculation process is a widely used inorganic and organic material removal method in wastewater treatment. Activated sludge process includes two main items: aeration tank and settling tank (usually referred to as "secondary clarifier"). In an aeration tank, the sewage water is injected with oxygen to promote bacterial growth and floc formation (a typical aeration tank is depicted Figure 1.2a). Consequently, the sewage water is treated in a secondary clarifier (see Figure 1.2b for illustration of a typical secondary clarifier) to allow suspended biological flocs to settle out of the final effluent. Thorough control of floc formation is crucial for proper operation of bioreactors and thus for efficient removal of suspended particles. It is usually desirable to have larger and denser flocs that settle faster under gravitational forces. Therefore, one of the most

[1] Activated sludge floc formed from filamentous bacteria. *UNBC Blogs site*, 4 April 2014, Retrieved from `http://blogs.unbc.ca`

(a) (b)

Figure 1.2: a) Aeration tank in a wastewater treatment plant[2] b) Secondary clarifiers in a wastewater treatment plant[3]

important designs and control parameters in the flocculation process is the size distribution of the flocs in a bioreactor. A popular mathematical model describing the time-evolution of the particle size distribution in a stirring tank is a 1D nonlinear partial integro-differential equation based on the population-balance equations proposed by van Smoluchowski (1917). The model (also known as *population balance equations* in the engineering literature) has been successful in matching many flocculation experiments (Li et al., 2004; Ducoste, 2002; Spicer & Pratsinis, 1996; Nopens et al., 2005).

In this dissertation, we rigorously investigate the long-term behavior of the microbial flocculation equations. When the long-term behavior of biological populations is considered, many populations converge to a stable time-independent state. Towards this end, using results from fixed point theory, we first derive conditions for the existence of continuous, non-trivial stationary solutions. We further apply the principle of linearized stability and semigroup compactness arguments to provide sufficient conditions for local stability of stationary solutions as well as sufficient conditions for instability. Consequently, we develop a numerical framework for computing approximations to stationary solutions of the microbial flocculation equations, which can also be used to produce approximate existence and stability regions for steady states. Furthermore, this numerical framework can be used to numerically investigate stationary solutions of general evolution equations. We develop several

[2]Aeration tank. *Downers Grove Sanitary District*, 10 May 2015, Retrieved from `https://www.dgsd.org/`

[3]Secondary clarifier in a wastewater treatment plant. *IndiaMart*, 17 March 2017, Retrieved from `https://www.indiamart.com/global-enviro-care/`

efficient and high-precision numerical schemes based on Finite Difference and Spectral Collocation methods to approximate stationary solutions of the microbial flocculation equations. We exploit spectral accuracy of the Spectral Collocation method for the numerical spectral analysis, which in turn allows us to heuristically deduce local stability of numerically computed steady states. We explore the stationary solutions of the model for various biologically relevant parameters and give valuable insights for the efficient removal of suspended particles. Lastly, we investigate the inverse problem of identifying a conditional probability measure in measure-dependent evolution equations arising in size-structured population modeling. We illustrate that a particular form of the microbial flocculation equations is one realization of a system satisfying the hypotheses in our framework.

The rest of this chapter is organized as follows. In Section 1.1, we present the microbial flocculation equations that will be investigated numerically and analytically in this dissertation report. Consequently, in Section 1.2, we briefly overview the results of each chapter.

1.1 Mathematical Preliminaries

The model accounts for four important phenomena that arise in a wide range of applications: fragmentation, proliferation, aggregation, and sedimentation. The equations for the microbial flocculation model track the time-evolution of the particle size number density $u(t,\, x)$ and can be written as

$$u_t \;=\; \mathcal{F}(u) \tag{1.1}$$

where

$$\mathcal{F}(u) := \mathcal{G}(u) + \mathcal{A}(u) + \mathcal{B}(u),$$

$\mathcal{G}$ denotes growth

$$\mathcal{G}(u) := -\partial_x(gu) - \mu(x)u(t,\, x)\,, \tag{1.2}$$

$\mathcal{A}$ denotes aggregation

$$\mathcal{A}(u) := \frac{1}{2}\int_0^x k_a(x-y,\, y)u(t,\, x-y)u(t,\, y)\, dy \\ - u(t,\, x)\int_0^{\overline{x}-x} k_a(x,\, y)u(t,\, y)\, dy\,, \tag{1.3}$$

and $\mathcal{B}$ denotes breakage

$$\mathcal{B}(u) := \int_x^{\overline{x}} \Gamma(x;\, y)k_f(y)u(t,\, y)\, dy - \frac{1}{2}k_f(x)u(t,\, x)\,. \tag{1.4}$$

The boundary condition is traditionally defined at the smallest size 0 and the initial condition is defined at $t = 0$

$$g(0)u(t,\, 0) = \int_0^{\overline{x}} q(x)u(t,\, x)dx, \quad u(0,\, x) = u_0(x)\,,$$

where the renewal rate $q(x)$ represents the number of new flocs entering the population. A floc size is usually expressed as volume. Moreover,since the equations model flocculation of particles in a confined space, the flocs are assumed to have a maximum size $\overline{x} < \infty$. The function $g(x)$ represents the average growth rate of the flocs of size x due to proliferation, and the coefficient $\mu(x)$ represents a size-dependent removal rate due to gravitational sedimentation and death.

The function $k_a(x,\, y)$ is the aggregation kernel, which describes the rate with which the flocs of size x and y agglomerate to form a floc of size $x + y$. Since the flocs $\{x - y,\, y\}$ and $\{y,\, x - y\}$ can aggregate and construct the floc of x, the factor of $1/2$ is included to avoid double-counting. When $\overline{x} = \infty$, for the aggregation kernels satisfying the inequality $k_a(x,\, y) \leq 1 + x + y$, existence of mass conserving global in time solutions were proven (Dubovskii & Stewart, 1996; Fournier & Laurençot, 2005; Menon & Pego, 2005) (for some suitable initial coditions). Conversely, for aggregation kernels satisfying $(xy)^{\gamma/2} \leq k_a(x,\, y)$ with $1 < \gamma \leq 2$, it has been shown that the total mass of the system blows up in a finite time (referred as a *gelation time*) (Escobedo et al., 2002). For a review of further mathematical results, we refer readers to review articles by Aldous (1999), Menon & Pego (2006), and Wattis (2006) and the book by Dubovskii (1994).

The breakage of flocs due to fragmentation is modeled by the terms in (1.4), where the frag-

mentation kernel $k_f(x)$ calculates the rate with which a floc of size x fragments. The breakage process assumes the fragmentation of a floc of size x into sizes $\{x-y,\, y\}$ and $\{y,\, x-y\}$ as two separate events. Therefore, the factor of $1/2$ is included in the second sum to avoid double-counting. The integrable function $\Gamma(x;y)$ represents the post-fragmentation probability density of daughter flocs for the fragmentation of the parent flocs of size y. The post-fragmentation probability density function Γ is one of the least understood terms in the flocculation model. Many different forms are used in the literature, among which normal and log-normal densities are the most common (Spicer et al., 1996). Recent modeling and computational work suggests that normal and log-normal forms for Γ are not correct and that a form closer to an $\arcsin(x;y)$ density would be more accurate (Mirzaev et al., 2016; Byrne et al., 2011). However, in this work we do not restrict ourselves to any particular form of Γ, and instead simply assume that the function Γ satisfies the mass conservation requirement. In other words, all the fractions of daughter flocs formed upon the fragmentation of a parent floc sum to unity,

$$\int_0^y \Gamma(x;\, y)\, dx = 1 \text{ for all } y \in (0,\, \overline{x}]. \tag{1.5}$$

The microbial flocculation equation, presented in (1.1), is a generalization of many mathematical models appearing in the size-structured population modeling literature and has been widely used, e.g., to model the formation of clouds and smog in meteorology (Pruppacher & Klett, 2012), the kinetics of polymerization in biochemistry (Ziff & Stell, 1980), the clustering of planets, stars and galaxies in astrophysics (Makino et al., 1998), and even schooling of fish in marine sciences (Niwa, 1998). For example, when the fragmentation kernel is omitted, $k_f \equiv 0$, the flocculation model reduces to algal aggregation model used to describe the evolution of a phytoplankton community (Ackleh & Fitzpatrick, 1997). When the removal and renewal rates are set to zero, the flocculation model simplifies to a model used to describe the proliferation of *Klebsiella pneumonia* in a bloodstream (Bortz et al., 2008). Furthermore, the flocculation model, with only growth and fragmentation terms, was used to investigate the elongation of prion polymers in infected cells (Calvez et al., 2012; Doumic-Jauffret & Gabriel, 2009; Calvez et al., 2010).

The equation (1.1) has also been the focus of considerable mathematical analysis. Well-posedness of the general flocculation model was first established by Ackleh and Fitzpatrick (Ackleh & Fitzpatrick, 1997; Ackleh, 1997) in an L^2-space setting and later by Banasiak & Lamb (2009) in an

L^1-space setting. Although the population balance equation has received substantial theoretical work, the derivation of analytical solutions for many realistic aggregation kernels has proven elusive. Towards this end, many discretization schemes for numerical simulations of the PBEs have been proposed. For instance, to approximate steady state solutions of PBEs, numerical schemes based on the least squares spectral method (Dorao & Jakobsen, 2006a,b, 2007) and the finite element method (Nicmanis & Hounslow, 1998, 2002; Hounslow, 1990) have been developed. For the further review of approximation methods, we refer interested readers to the review by Bortz (2015).

Investigating asymptotic behavior of the equation (1.1) has been a challenging task because of the nonlinearity introduced by the aggregation terms. Nevertheless, under suitable conditions on the kernels, the existence of a positive steady state has been established for the pure aggregation and fragmentation case (Laurencot & Walker, 2005). For the case $\overline{x} = \infty$, Banasiak (2011) establishes that for certain range of parameters, the solutions of the flocculation model do blow up in finite time. To the best of our knowledge, for the case $\overline{x} < \infty$ the long-term behavior of this model has not been considered. Hence, our main goal in this dissertation is to rigorously investigate the long-term behavior of the broad class of flocculation models described in (1.1). Consequently, in the subsequent section, we outline the work presented in this dissertation.

1.2 Outline

When the long-term behavior of biological populations is considered, many populations converge to a stable time-independent state. It is trivially true that a zero stationary solution of the microbial flocculation model exists and Figure 1.3a depicts that for sufficiently large removal rates the solutions of the microbial flocculation equation converge to this trivial zero stationary solution. Conversely, as illustrated in Figure 1.3b, for sufficiently large renewal rates the solutions diverge. Furthermore, under some restrictions on the model rates, which balance removal, growth, fragmentation and renewal rate, one might expect that the solutions of the microbial flocculation equations converge to a positive stationary size-distribution. In fact, as illustrated in Figure 1.3c, the solutions of the microbial flocculation equation converge to a nontrivial stationary size-distribution. To this end, our central objective in Chapter 2 is to prove the existence of positive steady states of this generalized flocculation model. Using results from fixed point theory we derive conditions for the

existence of continuous, non-trivial stationary solutions. We further apply the principle of linearized stability and semigroup compactness arguments to provide sufficient conditions for local stability of stationary solutions as well as sufficient conditions for instability. The end results of this analytical development are relatively simple inequality-criteria which thus allows for the rapid evaluation of the existence and stability of a non-trivial stationary solution. To our knowledge, this work is the first to derive precise stability criteria for such a generalized model.

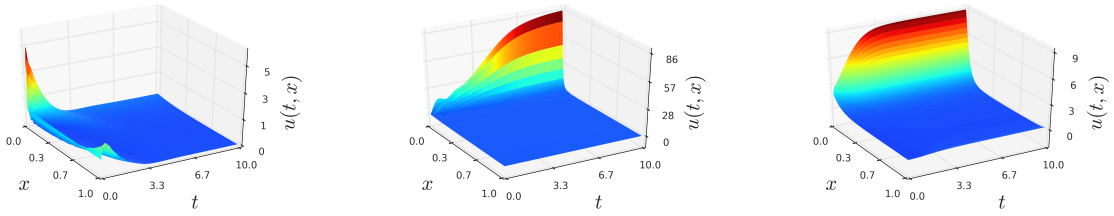

(a) (b) (c)

Figure 1.3: Transient behavior of solutions of the microbial flocculation equation. a) Convergence to trivial zero stationary solution. b) Divergence of the solutions c) Convergence to a nontrivial size-distribution

The flocculation equation (1.1) and all its extensions in the literature can be classified as so-called *evolution equations*. Evolution equations are differential laws that model time evolution of physical systems. They are a popular framework for studying the dynamics of biological populations. Many theoretical methods are available for establishing existence and stability of steady states of general evolution equations. However, except for very special cases, finding an analytical form of stationary solutions for evolution equations is a challenging task. Therefore, the content presented in Chapter 3 consist of our results in (Mirzaev & Bortz, 2017), where we develop a numerical framework for computing approximations to stationary solutions of general evolution equations, which can *also* be used to produce approximate existence and stability regions for steady states. In particular, we use the Trotter-Kato Theorem to approximate the infinitesimal generator of an evolution equation on a finite dimensional space, which in turn reduces the evolution equation into a system of ordinary differential equations. Consequently, we approximate and study the asymptotic behavior of stationary solutions. We illustrate the convergence of our numerical framework by applying it to a linear Sinko-Streifer structured population model for which the exact form of the steady state is known. To further illustrate the utility of our approach, we apply our framework

to nonlinear flocculation equation (1.1). We also demonstrate that our numerical framework can be used to gain insight into the theoretical stability of the stationary solutions of the evolution equations. Furthermore, the open source Python program that we have developed for our numerical simulations is freely available from our GitHub repository *(github.com/MathBioCU)*.

In a exploratory study presented in Chapter 4, we develop several efficient and high-precision numerical schemes based on Finite Difference and Spectral Collocation methods to approximate stationary solutions of the microbial flocculation equations. We exploit spectral accuracy of the Spectral Collocation method for the numerical spectral analysis. Particularly, we illustrate that the eigenvalues of the Fréchet derivative of the operator $\mathcal{F}$, defined in (1.1), evaluated at the stationary solutions can be approximated using spectral collocation method. This in turn allows to heuristically deduce local stability of numerically computed steady states. Furthermore, we explore the stationary solutions of the model for various biologically relevant parameters and give valuable insights for the efficient removal of suspended particles.

In Chapter 5, we investigate the inverse problem of identifying a conditional probability measure in measure-dependent evolution equations arising in size-structured population modeling. We formulate the inverse problem as a least squares problem for the probability measure estimation. Using the Prohorov metric framework, we prove existence and consistency of the least squares estimates and outline a discretization scheme for approximating a conditional probability measure. For this scheme, we prove general method stability. The work is motivated by Partial Differential Equation (PDE) models of flocculation for which the shape of the post-fragmentation conditional probability measure greatly impacts the solution dynamics. To illustrate our methodology, we apply the theory to a particular PDE model that arises in the study of population dynamics for flocculating bacterial aggregates in suspension, and provide numerical evidence for the utility of the approach. Lastly, in Chapter 6, we finish with our conclusions and remarks.

Chapter 2

On the existence and stability of steady-state size-distributions of the microbial flocculation equations[1]

When the long-term behavior of biological populations is considered, many populations converge to a stable time-independent state. Thus, identifying conditions under which a population converges to a stationary state is one of the most important applications of mathematical population modeling. Hence, our main goal in this chapter is to prove the existence of positive steady states of the microbial flocculation model (1.1). It is trivially true that a zero stationary solution of the microbial flocculation model exists, but we are also interested in non-trivial stationary solutions of the microbial flocculation model. Consequently, in Section 2.1 we first show that under some suitable conditions on the model parameters the equation (1.1) has a unique non-trivial (non-zero and non-negative) stationary solution.

Once a stationary solution to a model is shown to exist, the next natural question is whether it is stable or unstable. When the associated evolution equation of a population model is linear, many of stability properties can be deduced from the spectral properties of this linear operator (Diekmann et al., 1984; Greiner & Nagel, 1988). However, almost no information about the operator can be deduced from the spectrum of a nonlinear operator (Appell et al., 2004). Moreover, there is no

[1] This chapter is being prepared for a publication.

general consensus among mathematicians on how to define spectrum of a nonlinear operator. Thus, our stability analysis in this work is based on the *principle of linearized stability* for nonlinear evolution equations (Webb, 1985; Kato, 1995). Hence, in Section 2.2 we summarize the principle of linearized stability and linearize the flocculation model around its stationary solutions. In Section 2.2 we also derive conditions for the regularity of the linearized flocculation model. Next, in Sections 2.3 and 2.4 we derive sufficiency conditions for the linearized stability and instability of zero and non-zero stationary solutions, respectively. Finally, in Section 4.5, we summarize and discuss the conclusions of this chapter.

2.1 Existence of a positive stationary solution

The flocculation model under our consideration (1.1), accounts for physical mechanisms such as growth, removal, fragmentation, aggregation and renewal of microbial flocs. Thus, under some conditions, which balance these mechanisms, one could reasonably expect that the model possesses a non-trivial stationary solution. Hence, our main goal in this section is to derive sufficient conditions for the model terms such that the equation (1.1) engenders a positive stationary solution.

The flocculation model in this form (1.1) was first considered by Banasiak and Lamb in (Banasiak & Lamb, 2009), where they employed the flocculation model to describe the dynamical behavior of phytoplankton cells. The authors showed that under some conditions the flocculation model is well-posed, i.e., there exist a unique, global in time, positive solution for every absolutely integrable initial distribution. For the remainder of this work, we make the following assumptions on the model rates for which well-posedness of the solutions of the microbial flocculation equations has

been established by Banasiak & Lamb (2009):

$$
\begin{aligned}
&(\mathbf{A}1) \qquad g \in C^1(I) \qquad g(x) > 0 \ \text{ for } x \in I = [0,\, \overline{x}] \\
&(\mathbf{A}2) \qquad k_a \in L^\infty(I \times I), \quad k_a(x,\, y) = k_a(y,\, x) \\
&\qquad\qquad \text{and } k_a(x,\, y) = 0 \quad \text{if } x + y \geq \overline{x}\,, \\
&(\mathbf{A}3) \qquad \mu \in C(I) \qquad \text{and } \mu \geq 0 \text{ a.e. on } I\,, \\
&(\mathbf{A}4) \qquad q \in L^\infty(I) \qquad \text{and } q \geq 0 \text{ a.e. on } I\,, \\
&(\mathbf{A}5) \qquad k_f \in C(I) \qquad k_f(0) = 0 \text{ and } k_f \geq 0 \text{ a.e. on } I\,, \\
&(\mathbf{A}6) \qquad \Gamma(\cdot,\, y) \in L^\infty(I), \quad \Gamma(x;\, y) \geq 0 \text{ for } x \in (0,\, y]; \\
&\qquad\qquad \text{and } \Gamma(x;\, y) = 0 \text{ for } x \in (y,\, \overline{x})\,.
\end{aligned}
$$

Assumption (**A**1) states that the floc of any size has strictly positive growth rate. This in turn implies that flocs can grow beyond the maximal size $\overline{x}$, i.e., the model ignores what happens beyond the maximal size $\overline{x}$ (as many authors in the literature have done (Ackleh, 1997; Farkas & Hagen, 2007; Ackleh & Fitzpatrick, 1997)). We also note that although the Assumption (**A**1) is widely used in the literature it does generate biologically unrealistic condition $g(0) > 0$, i.e., the flocs of size zero also have positive growth rate. However, this assumption is crucial for our work, and thus we postpone the analysis of the case $g(0) = 0$ for our future research. Assumption (**A**2) states that for the aggregates of size x and y the aggregation rate is zero if the combined size of the aggregates is larger than the maximal size. Lastly, Assumption (**A**3) on $\mu(x)$ enforces continuous dependence of the removal on the size of a floc and ensures that every floc is removed with a non-negative rate.

Recall that at a steady state we should have

$$u_t = 0 = \mathcal{F}[u]\,. \tag{2.1}$$

By Assumption (**A**1), we know that $1/g \in C(I)$ and thus we can define $u = f/g$ for some $f \in C(I)$. The substitution of this f into (2.1), integration between 0 and an arbitrary x, and rearrangment

of the terms yields

$$f(x) = f(0) - \int_0^x \frac{k_f(y)/2 + \mu(y)}{g(y)} f(y)\,dy + \int_0^x \int_z^{\overline{x}} \frac{\Gamma(z;\,y) k_f(y)}{g(y)} f(y)\,dy\,dz$$
$$+ \frac{1}{2}\int_0^x \int_0^z \frac{k_a(z-y,\,y)}{g(z-y)g(y)} f(z-y)f(y)\,dy\,dz - \int_0^x \frac{f(z)}{g(z)} \int_0^{\overline{x}} \frac{k_a(z,\,y)}{g(y)} f(y)\,dy\,dz\,. \tag{2.2}$$

At this point we set

$$f(0) = 1 = g(0)p(0) = \int_0^{\overline{x}} q(y)u(y)\,dy\,. \tag{2.3}$$

Note that if there is a function f satisfying the equations (2.2) and (2.3), then u_* is a steady state for the modified choice of $q(x)$

$$q(x) := \frac{q(x)}{\int_0^{\overline{x}} \frac{q(y)f(y)}{g(y)}\,dy}\,. \tag{2.4}$$

We now define the operator Φ as

$$\Phi[f](x) := 1 - \int_0^x \frac{k_f(y)/2 + \mu(y)}{g(y)} f(y)\,dy + \int_0^x \int_z^{\overline{x}} \frac{\Gamma(z;\,y) k_f(y)}{g(y)} f(y)\,dy\,dz$$
$$+ \frac{1}{2}\int_0^x \int_0^z \frac{k_a(z-y,\,y)}{g(z-y)g(y)} f(z-y)f(y)\,dy\,dz - \int_0^x \frac{f(z)}{g(z)} \int_0^{\overline{x}} \frac{k_a(z,\,y)}{g(y)} f(y)\,dy\,dz\,. \tag{2.5}$$

and will use a fixed point theorem to prove the existence of a fixed point f of Φ . This in turn will allow us to claim that equation (2.1) has at least one non-trivial positive solution.

The use of fixed point theorems for showing existence of non-trivial stationary solutions is not new in size-structured population modeling. For example, fixed point theorems, based on Leray-Schauder degree theory, have been used to find stationary solutions of linear Sinko-Streifer type equations (Prüss, 1983a; Farkas & Hinow, 2012). Moreover, the Schauder fixed point theorem has been used to establish the existence of steady state solutions of nonlinear coagulation-fragmentation equations (Laurençot & Walker, 2005). For our purposes we will use the Contraction Mapping Theorem.

We carry out the analysis of this work on the space of continuous functions $\mathcal{X} = C(I)$ with usual uniform (supremum) norm $\|\cdot\|_u$. We also denote the usual essential supremum of a function by $\|\cdot\|_\infty$. Since the positive cone in $C(I)$, denoted by $(C(I))_+$, is closed and convex, we choose K to be $(C(I))_+$. Then $K_r = \overline{K \cap B_r(0)}$, where $B_r(0) \subset \mathcal{X}$ is an open ball of radius r and centered

at zero, and r has yet to be chosen. Note that since K_r is also Banach space since it is closed subspace of $\mathcal{X}$. Next, we show that one can choose model rates such that the operator Φ defined in (2.5) maps K_r to K_r and is also contraction. This in turn implies existence of a positive stationary solution of the operator $\mathcal{F}$. We are now in a position to state the main result of this section in the following theorem.

Theorem 2.1. *Assume that the condition*

$$0 \leq \frac{1}{2}k_f(x) - \mu(x), \tag{C1}$$

holds true for all $x \in I$. For sufficiently small choice of $\left\|\frac{1}{g}\right\|_1$ the operator Φ defined in (2.5) has a unique non-zero fixed point, $f_* \in K$ satisfying

$$1 \leq \|f_*\|_u \leq r \tag{2.6}$$

for some $r \geq 1$. Moreover, for the modified choice of the renewal rate in (2.4), the non-zero and non-negative function

$$u_* = \frac{f_*}{g} \in C(I) \tag{2.7}$$

is a unique stationary solution of the flocculation model defined in (1.1) on K.

Proof. For $f \in K_r$ we have

$$\begin{aligned}
\Phi[f] &\geq 1 - \int_0^x \frac{k_f(y)/2 + \mu(y)}{g(y)} f(y)\,dy \\
&\quad + \int_0^x \int_z^x \frac{\Gamma(z;\,y) k_f(y)}{g(y)} f(y)\,dy\,dz - \int_0^x \frac{f(z)}{g(z)} \int_0^{\overline{x}} \frac{k_a(z,\,y)}{g(y)} f(y)\,dy\,dz \\
&\geq 1 - \int_0^x \frac{f(z)}{g(z)} (k_f(z)/2 + \mu(z))\,dz + \int_0^x \frac{k_f(y) f(y)}{g(y)} \underbrace{\int_0^y \Gamma(z;\,y)\,dz}_{=1}\,dy - \|f\|_u^2 \|k_a\|_\infty \left\|\frac{1}{g}\right\|_1^2 \\
&\geq \int_0^x \frac{f(z)}{g(z)} \left(\frac{1}{2}k_f(z) - \mu(z)\right) dz + 1 - r^2 \cdot \|k_a\|_\infty \left\|\frac{1}{g}\right\|_1^2,
\end{aligned}$$

where $\|\cdot\|_1$ represents the usual L^1 norm on I. The first condition of the theorem (**C**1) guarantees that

$$\frac{1}{2}k_f(z) - \mu(z) > 0 \text{ for all } z \in I\,,$$

so we can choose

$$r = \left\| \frac{1}{g} \right\|_1^{-1} \|k_a\|_\infty^{-1/2} \tag{2.8}$$

in K_r such that $\Phi[f] \geq 0$, i.e., $\Phi : K_r \to K$. On the other hand, using the assumptions (**A**1)-(**A**6), it is straightforward to show that $\Phi(K_r) \subset C(I)$.

Next we prove that the operator Φ maps K_r to K_r. Consequently, for $f \in K_r$ it follows that

$$\begin{aligned}
0 \leq \Phi[f](x) &\leq 1 - \int_0^x \frac{k_f(y)/2 + \mu(y)}{g(y)} f(y)\, dy + \int_0^{\overline{x}} \int_z^{\overline{x}} \frac{\Gamma(z;\, y) k_f(y)}{g(y)} f(y)\, dy\, dz \\
&\quad - \int_x^{\overline{x}} \int_z^{\overline{x}} \frac{\Gamma(z;\, y) k_f(y)}{g(y)} f(y)\, dy\, dz + \frac{1}{2} \int_0^x \int_0^z \frac{k_a(z-y,\, y)}{g(z-y) g(y)} f(z-y) f(y)\, dy\, dz \\
&\leq 1 + \int_x^{\overline{x}} \frac{1}{g(y)} k_f(y) f(y)\, dy + \int_0^x \frac{1}{g(y)} \left(\frac{1}{2} k_f(y) - \mu(y) \right) f(y)\, dy \\
&\quad + \frac{1}{2} \|f\|_u^2 \cdot \|k_a\|_\infty \cdot \left\| \frac{1}{g} \right\|_1^2 \\
&\leq 1 + \|f\|_u \left\| \frac{1}{g} \right\|_1 \left[\|k_f\|_u + \left\| \frac{1}{2} k_f - \mu \right\|_u + r \|k_a\|_\infty \left\| \frac{1}{g} \right\|_1 \right] \\
&\leq 1 + r \left\| \frac{1}{g} \right\|_1 \left[\|k_f\|_u + \left\| \frac{1}{2} k_f - \mu \right\|_u + \|k_a\|_\infty^{1/2} \right] .
\end{aligned}$$

At this point choosing $\left\| \frac{1}{g} \right\|_1$ sufficiently small yields $r > 1$ in (2.8), and thus we can guarantee that

$$\|\Phi[f]\| \leq r$$

for all $f \in K_r$. Hence the operator Φ maps K_r to K_r.

Next we will prove that the operator Φ is in fact a contraction mapping, i.e., for all f, $h \in K_r$

$$\|\Phi[f] - \Phi[h]\|_u \leq c \|f - h\|_u$$

for some $c \in [0,1)$.

$$\begin{aligned}
|\Phi[f](x) - \Phi[h](x)| \leq & \int_0^x \frac{k_f(y)/2 - \mu(y)}{g(y)} |f(y) - h(y)| \, dy + \int_x^{\overline{x}} \frac{k_f(y)}{g(y)} |f(y) - h(y)| \, dy \\
& + \frac{1}{2} \int_0^x \int_0^z \frac{k_a(z-y,\, y)}{g(z-y)g(y)} f(z-y) \, |f(y) - h(y)| \, dy \, dz \\
& + \frac{1}{2} \int_0^x \int_0^z \frac{k_a(z-y,\, y)}{g(z-y)g(y)} h(y) \, |f(z-y) - h(z-y)| \, dy \, dz \\
& + \int_0^x \frac{f(z)}{g(z)} \int_0^{\overline{x}} \frac{k_a(z,\, y)}{g(y)} |f(y) - h(y)| \, dy \, dz \\
& + \int_0^x \frac{|f(z) - h(z)|}{g(z)} \int_0^{\overline{x}} \frac{k_a(z,\, y)}{g(y)} h(y) \, dy \, dz \, .
\end{aligned}$$

Taking the supremum of both sides at this point yields

$$\|\Phi[f] - \Phi[h]\|_u \leq \|f - h\|_u \left\| \frac{1}{g} \right\|_1 \left[\|k_f\|_u + \left\| \frac{1}{2} k_f - \mu \right\|_u + \frac{3}{2} \|k_a\|_\infty^{1/2} \right] .$$

Once again by choosing $\left\| \frac{1}{g} \right\|_1$ sufficiently small, we can guarantee that the constant

$$c = \left\| \frac{1}{g} \right\|_1 \left[\|k_f\|_u + \left\| \frac{1}{2} k_f - \mu \right\|_u + \frac{3}{2} \|k_a\|_\infty^{1/2} \right]$$

is less than 1. This in turn implies that the operator Φ defined in (2.5) is also a contraction mapping. Hence, the Contraction Mapping Theorem guarantees the existence of a unique positive fixed point of Φ satisfying the bounds (2.6). Therefore, the function $u_* = f_*/g$ is a stationary solution of the flocculation equations (1.1). Moreover, from the assumption (**A**1) and the continuity of the fixed point f_* it follows that u_* is non-zero, non-negative and continuous on I. □

2.2 Principle of linearized stability and regularity properties of the linearized semigroup

In this section we summarize the principle of linearized stability as it applies to semigroups in general and our flocculation equation in particular.

For a given autonomous ordinary differential equation,

$$\dot{u} = f(u)\,,$$

the method for determining the local asymptotic behavior of a stationary solution u_*, $f(u_*) = 0$, by the eigenvalues of the Jacobian $\mathbf{J}_f(u_*)$ is quite well-known. In semigroup theory the analogous method is known as the *principle of linearized stability* and was developed in the context of semilinear partial differential equations in (Henry, 1981; Smoller, 1983; Webb, 1985). Later, Kato (1995) extended this principle to a broader range of nonlinear evolution equations. Before presenting the principle of linearized stability we introduce some terminology, which can be found in many functional analysis books (see (Belleni-Morante & McBride, 1998) for instance).

The *growth bound* $\omega_0(\mathbf{A})$ of a strongly continuous semigroup $(S(t))_{t\geq 0}$ with an infinitesimal generator $\mathbf{A}$ is defined as

$$\omega_0(\mathbf{A}) := \inf \left\{ \omega \in \mathbb{R} \,:\, \begin{array}{c} \exists M_\omega \geq 1 \text{ such that} \\ \|S(t)\| \leq M_\omega e^{\omega t} \text{ for all } t \geq 0 \end{array} \right\}.$$

The operator $D\mathbf{A}(f)$ denotes the Fréchet derivative of an operator $\mathbf{A}$ evaluated at f, which is defined as

$$D\mathbf{A}(u)h = \mathbf{A}[u+h] - \mathbf{A}[u] + o(h), \qquad \forall u,\, h \in \mathcal{D}(\mathbf{A})\,,$$

where o is little-o operator satisfying $\|o(h)\| \leq b(r)\,\|h\|$ with increasing continuous function $b : [0,\,\infty) \to [0,\,\infty)$, $b(0) = 0$.

The *discrete spectrum* $\sigma_D(\mathbf{A})$ of an arbitrary operator $\mathbf{A}$ on a Banach space X, is the subset of the point spectrum of $\mathbf{A}$,

$$\sigma_p(\mathbf{A}) = \{\lambda \in \mathbb{C}\,|\,\exists \phi \neq 0 \in X \text{ s.t. } \mathbf{A}\phi = \lambda\phi\}\,,$$

such that $\lambda \in \sigma_D(\mathbf{A})$ is an isolated eigenvalue of finite multiplicity, i.e., the dimension of the set

$$\{\psi \in X \,:\, \mathbf{A}\psi = \lambda\psi\}$$

is finite and nonzero. Let $(T(t))_{t\geq 0}$ be a C_0 semigroup on the Banach space X with its infintesimal generator $\mathbf{A}$. Then the limit $\omega_1(\mathbf{A}) = \lim_{t\to\infty} t^{-1}\log(\alpha[T(t)])$ is well-defined and called the α-*growth bound* of $(T(t))_{t\geq 0}$. The function $\alpha[T(t)]$ is a measure of non-compactness of the semigroup $T(t)$ as defined as in (Kuratowski, 1966). This measure associates non-negative numbers to operators (or sets), which tells how close an operator (or a set) is to a compact operator (or set). For example, for a bounded set M in a Banach space, $\alpha[M] = 0$ implies that $\overline{M}$ (closure of M) is a compact set. Analogously, for a semigroup $(T(t))_{t\geq 0}$, $\alpha[T(t)] = 0$ indicates that the semigroup is eventually compact.

With the above definitions, we are now ready to present the principle of linearized stability in the form of the following proposition (see (Webb, 1985) for the complete discussion of the proof of the following proposition).

Proposition 2.2. *Define the nonlinear operator $\mathcal{N} : \mathcal{D}(\mathcal{F}) \subset L^1(I) \to L^1(I)$ and let $f_* \in \mathcal{D}(\mathcal{N})$ be a stationary solution of (1.1), i.e., $\mathcal{N}[f_*] = 0$. If $\mathcal{N}$ is continuously Fréchet differentiable on $L^1(I)$ and the linearized operator $\mathcal{L} = D\mathcal{N}(f_*)$ is the infinitesimal generator of a C_0-semigroup $T(t)$, then the following statements hold:*

1. *If $\omega_0(\mathcal{L}) < 0$, then f_* is locally asymptotically stable in the following sense: There exists η, $C \geq 1$, and $\alpha > 0$ such that if $\|f - f_*\| < \eta$, then a unique mild solution $T(t)f$, satisfies $\|T(t)f - f_*\| \leq Ce^{-\alpha t}\|f - f_*\|$ for all $t \geq 0$.*

2. *If there exists $\lambda_0 \in \sigma(\mathcal{L})$ such that $Re\,\lambda > 0$ and*

$$\max\left\{\omega_1(\mathcal{L}), \sup_{\lambda\in\sigma_D(\mathcal{L})\setminus\{\lambda_0\}} Re\,\lambda\right\} < Re\,\lambda_0\,, \tag{2.9}$$

then f_* is an unstable equilibrium in the sense that there exists $\varepsilon > 0$ and sequence $\{f_n\}$ in X such that $f_n \to f_*$ and $\|T(n)f_n - f_*\| \geq \varepsilon$ for $n = 1, 2, \ldots$.

Having the explicit statement of the principle of linearized stability in hand, we now show that the nonlinear operator $\mathcal{F}$ defined in (1.4) satisfies all the conditions of Proposition 2.2. Towards this end, we first establish the elementary assumption of Proposition 2.2 in the following lemma.

Lemma 2.3. *The nonlinear operator $\mathcal{F}$ defined in (1.4) is continuously Fréchet differentiable on $L^1(I)$.*

Proof. The Fréchet derivative of the nonlinear operator $\mathcal{F}$ is given explicitly as

$$\begin{aligned} D\mathcal{F}(\phi)[h(x)] = -\partial_x[gh](x) - \left(\mu(x) + \frac{1}{2}k_f(x)\right)h(x) + \int_x^{\overline{x}} \Gamma(x;\, y)k_f(y)h(y)\, dy \\ + \frac{1}{2}\int_0^x k_a(x-y,\, y)\left[\phi(y)h(x-y) + h(y)\phi(x-y)\right] dy \\ - h(x)\int_0^{\overline{x}-x} k_a(x,\, y)\phi(y)dy - \phi(x)\int_0^{\overline{x}-x} k_a(x,\, y)h(y)dy\,. \end{aligned} \tag{2.10}$$

For the arbitrary functions $u_1,\, u_2 \in L^1(I)$ we have

$$\begin{aligned} |D\mathcal{F}(u_1)h(x) - D\mathcal{F}(u_2)h(x)| \leq \frac{1}{2}\left\|k_a\right\|_\infty \int_0^x |u_1(y) - u_2(y)||h(x-y)|\, dy \\ + \frac{1}{2}\left\|k_a\right\|_\infty \int_0^x |h(y)||u_1(x-y) - u_2(x-y)|\, dy \\ + |h(x)|\left\|k_a\right\|_\infty \int_0^{\overline{x}} |u_1(y) - u_2(y)|dy \\ + |u_1(x) - u_2(x)|\left\|k_a\right\|_\infty \int_0^{\overline{x}} |h(y)|dy \end{aligned}$$

Consequently, taking the integral of both sides with respect to x and an application of Young's inequality for convolutions (see (Adams & Fournier, 2003, Theorem 2.24)) to the first two integrals yields

$$\left\|D\mathcal{F}(u_1)h(x) - D\mathcal{F}(u_2)h(x)\right\|_1 \leq \left\|k_a\right\|_\infty \left\|u_1 - u_2\right\|_1 \left\|h\right\|_1 + \left\|k_a\right\|_\infty \left\|u_1 - u_2\right\|_1 \left\|h\right\|_1 + \left\|u_1 - u_2\right\|_1 \left\|k_a\right\|_\infty \left\|h\right\|_1$$

for all $h \in L^1(I)$. Then it follows that

$$\left\|D\mathcal{F}(u_1) - D\mathcal{F}(u_2)\right\|_1 \leq 3\left\|k_a\right\|_\infty \left\|u_1 - u_2\right\|_1\,,$$

which in turn implies that the nonlinear operator $\mathcal{F}$ is continuously Fréchet differentiable on $L^1(I)$.

□

In the previous section we have shown that the nonlinear operator $\mathcal{F}$ (1.4) has at least one non-trivial stationary solution, u_* (in addition to trivial zero stationary solution). To derive stability results for this stationary solutions we first linearize the equation (1.1) around u_*. A simple

calculation yields that the Fréchet derivative of the nonlinear operator $\mathcal{F}$ evaluated at a stationary solution u_* (see Theorem 2.1) is given explicitly by

$$\mathcal{L}[h](x) = D\mathcal{F}(u_*)[h](x) = -\partial_x(g(x)h(x)) - A(x)h(x) + \int_x^{\overline{x}} \Gamma(x;\, y)k_f(y)h(y)\, dy \\ - \int_0^{\overline{x}-x} E(x,\, y)h(y)\, dy + \int_0^x E(x-y,\, y)h(y)\, dy\,, \tag{2.11}$$

where

$$E(x,\, y) = k_a(x,\, y)u_*(x)$$

and

$$A(x) = \frac{1}{2}k_f(x) + \mu(x) + \int_0^{\overline{x}-x} E(y,\, x)\, dy\,.$$

We first prove that the linear operator $\mathcal{L}$ is an infinitesimal generator of a strongly continuous semigroup $\mathscr{T} = (T(t))_{t\geq 0}$. Consequently, we will prove two regularity results for the semigroup $\mathscr{T}$, which will prove useful in the spectral analysis of the operator $\mathcal{L}$. Particularly, we will show that under some conditions on the model ingredients the semigroup $\mathscr{T}$ is positive and eventually compact. The main implication of eventual compactness is that the Spectral Mapping Theorem holds (see (Engel & Nagel, 2000)) for the semigroup $\mathscr{T}$,

$$\sigma\left(T(t)\right)\setminus\{0\} = \exp\left(t\sigma(\mathcal{L})\right), \quad t \geq 0\,.$$

Consequently, we will use the positivity of the semigroup $\mathscr{T}$ in Section 2.4.2, where we employ the positive perturbation method introduced in (Farkas & Hinow, 2012).

Lemma 2.4. *If we define the domain of the linearized operator $\mathcal{L}$ as*

$$\mathcal{D}(\mathcal{L}) = \left\{\phi \in L^1(I)\,|\,(g\phi)' \in L^1(I),\, (g\phi)(0) = \int_0^{\overline{x}} q(x)u(t,\, x)dx\right\}, \tag{2.12}$$

then the operator $\mathcal{L}$ generates a C_0 semigroup on $\mathcal{D}(\mathcal{L})$.

Proof. The linear operator $\mathcal{L}$ can be written as the sum of an unbounded operator

$$\mathcal{L}_1[h](x) = -\partial_x(g(x)h(x)) - A(x)h(x) \tag{2.13}$$

and bounded operators

$$\mathcal{L}_2[h](x) = \int_x^{\overline{x}} \Gamma(x;\, y)k_f(y)h(y)\,dy - \int_0^{\overline{x}-x} E(x,\, y)h(y)\,dy, \qquad \mathcal{L}_3[h](x) = \int_0^x E(x-y,\, y)h(y)\,dy\,. \tag{2.14}$$

From the fact that $g(x),\, A(x) \in C(I)$ and from the Lemma 2.4 of (Banasiak & Lamb, 2009) it follows that $\mathcal{L}_1$ generates a C_0 semigroup on $\mathcal{D}(\mathcal{L})$. Consequently, the bounded perturbation theorem of (Pazy, 1992, §3, Theorem 1.1) yields that the operator $\mathcal{L}$ is also an infinitesimal generator of a C_0 semigroup. □

Lemma 2.5. *For a given stationary solution $u_* \in C(I)$ the operators $\mathcal{L}_2 : \mathcal{D}(\mathcal{L}) \to L^1(I)$ and $\mathcal{L}_3 : \mathcal{D}(\mathcal{L}) \to L^1(I)$ defined in (2.14) are compact operators.*

Proof. We first prove that the operator $\mathcal{L}_2$ is compact. Then compactness of the operator $\mathcal{L}_3$ follows from analogous arguments. Let us denote a unit ball centered at zero in $L^1(I)$ by $B = \left\{\phi \in L^1(I) \mid \|\phi\|_1 \leq 1\right\}$. Recall that an operator is compact if it maps a unit ball into a relatively compact set. Consequently, observe that the assumptions (**A**2) and (**A**6) together imply that the operator

$$\begin{aligned}\partial_x\mathcal{L}_2[h](x) = k_a(x,\, \overline{x}-x)u_*(x)h(\overline{x}-x) - \int_0^{\overline{x}-x} \partial_x(k_a(x,\, y)u_*(x))h(y)\,dy \\ + \int_x^{\overline{x}} \partial_x\Gamma(x;\, y)k_f(y)h(y)\,dy - \Gamma(x;\, x)k_f(x)h(x)\end{aligned}$$

is also bounded. Hence $\mathcal{L}_2[B] \subset W^{1,1}(I)$ and from the Rellich-Kondrachov embedding theorem (see *Adams & Fournier (2003, Theorem 6.3)* for a statement of the theorem) it follows that the set $\mathcal{L}_2[B]$ is relatively compact. □

Lemma 2.6. *The operator $\mathcal{L}$ defined in (2.11) generates an eventually compact C_0 semigroup. And thus, the spectrum of the operator $\mathcal{L}$ consists of isolated eigenvalues of a finite multiplicity only, i.e., $\sigma(\mathcal{L}) = \sigma_D(\mathcal{L})$.*

Proof. The operator $\mathcal{L}_1$ defined in (2.13) is well-known operator in size-structured dynamics literature. If $g \in C^1(I)$ and $A \in C(I)$, then in Farkas & Hagen (2007, Theorem 3.1) it has been shown that the C_0 semigroup generated by the operator $\mathcal{L}_1$ is compact for $t > 2\int_0^{\overline{x}} \frac{1}{g(y)}\, dy$. The condition $g \in C^1(I)$ follows from our main assumption (**A**1), and continuity of the function

$$A(x) = \frac{1}{2}k_f(x) + \mu(x) + \int_0^{\overline{x}-x} k_a(x,\, y)u_*(y)\, dy$$

follows from the assumptions (**A**1)-(**A**6). Thus the semigroup generated by $\mathcal{L}_1$ is eventually compact. Conversely, in Lemma (2.5) we have shown that the operators $\mathcal{L}_2$ and $\mathcal{L}_3$ are compact. Hence, the C_0 semigroup generated by the operator $\mathcal{L} = \mathcal{L}_1 + \mathcal{L}_2 + \mathcal{L}_3$ is also compact for $t > 2\int_0^{\overline{x}} \frac{1}{g(y)}\, dy$.

Therefore, the eventual compactness of the semigroup $\mathscr{T}$ (generated by $\mathcal{L}$) combined with Theorem 3.3 of Pazy (1992, §2.3) and Corollary 1.19 of (Engel & Nagel, 2000, §4) together imply that the spectrum of $\mathcal{L}$ consists of isolated eigenvalues of finite multiplicity. □

Lemma 2.7. *For a steady state solution u_* assume that the model rates satisfy the following conditions*

$$\partial_x \left(k_a(x,\, y)u_*(x)\right) \leq 0 \text{ for all } x \in I \text{ and } y \in (0,\, x) \tag{2.15}$$

and

$$\Gamma(x;\, y)k_f(y) \geq k_a(x,\, y)u_*(x) \text{ for all } x \in I \text{ and } y \in [x,\, x_1) \tag{2.16}$$

Then the operator $\mathcal{L}$ generates a positive C_0 semigroup.

Proof. In Farkas & Hagen (2007, Theorem 3.3) it has been shown that the operator $\mathcal{L}_1 : \mathcal{D}(\mathcal{L}) \to L^1(I)$ generates a positive C_0 semigroup under the main assumptions (**A**1)-(**A**6). On the other hand, from the conditions (2.15) and (2.16) it follows that

$$\begin{aligned}
\mathcal{L}_2[h](x) + \mathcal{L}_3[h](x) &\geq \int_0^x k_a(x-y,\, y)u_*(x-y)h(y)\, dy + \int_x^{\overline{x}} \Gamma(x;\, y)k_f(y)h(y)\, dy \\
&\quad - \int_0^{\overline{x}} k_a(x,\, y)u_*(x)h(y)\, dy \\
&\geq \int_0^x \left[k_a(x-y,\, y)u_*(x-y) - k_a(x,\, y)u_*(x)\right] h(y)\, dy \\
&\quad + \int_x^{\overline{x}} \left[\Gamma(x;\, y)k_f(y) - k_a(x,\, y)u_*(x)\right] h(y)\, dy \geq 0\,,
\end{aligned}$$

which in turn ensures that the operator $\mathcal{L}_2 + \mathcal{L}_3$ is a positive operator. Since the positivity of a semigroup is invariant under a bounded and positive perturbation of its generator (see (Engel & Nagel, 2000, §6, Corollary 1.11)), the result follows immediately. □

Remark 2.8. Lemma 2.7 has very important consequence. Specifically, if the positivity conditions (2.15) and (2.16) hold and the spectral bound $s(\mathcal{L}) = \sup\{Re\,\lambda \,|\, \lambda \in \sigma(\mathcal{L})\}$ is not equal to $-\infty$, then $s(\mathcal{L})$ belongs to the spectrum $\sigma(\mathcal{L})$ (Engel & Nagel, 2000, §Theorem 1.10). Moreover, the positivity and eventual compactness of the semigroup $\mathscr{T}$ together imply that the spectral bound $s(\mathcal{L})$ is one of the eigenvalues of $\mathcal{L}$ with finite multiplicity.

2.3 Linearized stability and instability criteria for the zero stationary solution

In this section we will derive linearized stability results for the zero stationary solution of the flocculation equation. In contrast to non-trivial stationary solutions, zero stationary solution always exists (provided that the well-posedness assumptions (**A**1)-(**A**6) hold true). As we have discussed in Section 2.2 the stability of the steady states depends on the spectral properties of the linear operator $\mathcal{L}$ defined in (2.11). We define the operator $\mathcal{M}$ as the linear operator $\mathcal{L}$ evaluated at the trivial stationary solution, $u_* \equiv 0$

$$\mathcal{M}[h](x) = -\partial_x[gh](x) - \left(\mu(x) + \frac{1}{2}k_f(x)\right)h(x) + \int_x^{\overline{x}} \Gamma(x;\, y)k_f(y)h(y)\,dy\,. \tag{2.17}$$

The assumptions (**A**1)-(**A**6) also ensure that the regularity conditions of Section 2.2 are all satisfied. Hence, the operator $\mathcal{M}$ generates a positive, eventually compact and strongly continuous semigroup. By Remark 2.8 we know that the spectral bound $s(\mathcal{M})$ of the operator $\mathcal{M}$ is a dominant eigenvalue of $\mathcal{M}$ with finite multiplicity. Then, by the principle of linearized stability (Proposition 2.2), the stability of the zero stationary solution depends on the sign of this dominant eigenvalue. Thus, in the subsequent two subsections we derive conditions which guarantee positivity and negativity of the spectral bound $s(\mathcal{M})$, respectively. For a more thorough discussion of the stability of the zero stationary solution we refer readers to (Mirzaev & Bortz, 2015a).

2.3.1 Instability of the trivial stationary solution

The operator $\mathcal{M}$ can be written as the sum of an unbounded operator

$$\mathcal{M}_1[h](x) = -\partial_x[gh](x) - \left(\mu(x) + \frac{1}{2}k_f(x)\right) h(x)$$

and a bounded operator

$$\mathcal{M}_2[h](x) = \int_x^{\overline{x}} \Gamma(x;\, y) k_f(y) h(y)\, dy\,.$$

In (Farkas, 2005), the authors have shown that the operator $\mathcal{M}_1$ generates a positive, eventually compact semigroup. Moreover, they have shown that the spectral bound of $\mathcal{M}_1$ is positive if

$$\int_0^{\overline{x}} \frac{q(x)}{g(x)} \exp\left(-\int_0^x \frac{\mu(s) + \frac{1}{2}k_f(s)}{g(s)}\, ds\right) dx > 1\,. \tag{2.18}$$

On the other hand, we note that $\mathcal{M}_2$ is a positive operator. Then, Corollary 1.11 of (Engel & Nagel, 2000, §6) yields that the operator $\mathcal{M} = \mathcal{M}_1 + \mathcal{M}_2$ also generates a positive, eventually compact semigroup. Furthermore, the following inequality holds for spectral bound of $\mathcal{M}_1$ and $\mathcal{M}$,

$$s(\mathcal{M}_1) \leq s(\mathcal{M}_1 + \mathcal{M}_2) = s(\mathcal{M})\,. \tag{2.19}$$

Consequently, this implies that the operator $\mathcal{M}$ also has a positive spectral bound provided that the condition (2.18) is satisfied. At this point, in Proposition 2.2, choosing λ_0 equal to the eigenvalue of $\mathcal{M}$ corresponding to $s(\mathcal{M})$ and using Lemma 2.6 yields

$$\max\left\{\omega_1(\mathcal{M}), \sup_{\lambda \in \sigma_D(\mathcal{M})\setminus\{\lambda_0\}} \operatorname{Re}\lambda\right\} = \sup_{\lambda \in \sigma_D(\mathcal{M})\setminus\{\lambda_0\}} \operatorname{Re}\lambda < \operatorname{Re}\lambda_0\,.$$

Then, the operator $\mathcal{M}$ satisfies all the conditions of Proposition 2.2 and thus results of this section can be summarized in the form of the following condition.

Condition 1. Assume that the assumptions (**A**1)-(**A**6) hold true. Moreover, assume that

$$\int_0^{\overline{x}} \frac{q(x)}{g(x)} \exp\left(-\int_0^x \frac{\mu(s) + \frac{1}{2}k_f(s)}{g(s)}\, ds\right) dx > 1\,,$$

then the zero stationary solution of the flocculation equation is unstable.

2.3.2 Stability of the trivial stationary solution

In this section we will prove that under certain condition on model parameters we can ensure that the spectral bound of $\mathcal{M}$ is strictly negative. Since the positivity arguments that we used in the previous section cannot guarantee negativity of $s(\mathcal{M})$, we use a direct approach to prove that growth bound of $\mathcal{M}$ is strictly negative, $\omega_0(\mathcal{M}) < 0$. To achieve our goal we use the following version of the well-known Lumer-Philips theorem (see for instance (Engel & Nagel, 2000, §2, Corollary 3.6) and Belleni-Morante & McBride (1998, Theorem 2.22)).

Theorem 2.9. *(Lumer-Philips) Let a linear operator $\mathcal{A}$ on a Banach space $(\mathcal{X}, \|\cdot\|)$ the following are equivalent:*

1. *$\mathcal{A}$ is closed, densely defined. Furthermore, $\mathcal{A} - \lambda I$ is surjective for some $\lambda > 0$ (and hence for all $\lambda > 0$) and there exists a real number ω such that $\mathcal{A} - \omega I$ is dissipative, i.e.,*

$$\|f - \lambda(\mathcal{A} - \omega I)f\| \geq \|f\| \quad \text{for all } \lambda > 0 \text{ and } f \in \mathcal{D}(\mathcal{A})\,.$$

2. *Then, $(\mathcal{A}, \mathcal{D}(\mathcal{A}))$ generates a strongly continuous quasicontractive semigroup $(T(t))_{t\geq 0}$ satisfying*

$$\|T(t)\| \leq e^{\omega t} \quad \text{for } t \geq 0\,.$$

In the following lemma, we show the operator satisfies the first part of the Lumer-Philips theorem. Particularly, we establish that there exist a strictly negative real number $w < 0$ such that the operator $\mathcal{M} - \omega I$ is dissipative.

Lemma 2.10. *Assume that the assumptions (**A**1)-(**A**6) hold true. Then the linear operator $\mathcal{M}$ defined in (2.17) is closed, densely defined operator on the Banach space $L^1(I)$, and for sufficiently large $\lambda > 0$ the operator $\mathcal{M} - \lambda I : \mathcal{D}(\mathcal{M}) \mapsto L^1(I)$ is surjective. Furthermore, if*

$$\mu(x) - q(x) - \frac{1}{2}k_f(x) > 0 \tag{2.20}$$

for all $x \in I$, then there exists $\alpha > 0$ such that the semigroup $(T(t))_{t\geq 0}$ generated by $\mathcal{M}$ satisfies the estimate

$$\|T(t)\|_1 \leq e^{-\alpha t} \text{ for all } t \geq 0\,.$$

Proof. Since the operator $\mathcal{M}$ generates a strongly continuous semigroup (Lemma 2.4), the first argument of the lemma is an immediate consequence of the Generation Theorem of (Engel & Nagel, 2000, §2.3). We now prove that there exist $\alpha > 0$ such that $\mathcal{M} + \alpha I$ is dissipative. For a given $f \in \mathcal{D}(\mathcal{M}) = \mathcal{D}(\mathcal{L})$ and some $h \in H$ and $\lambda > 0$ we have

$$f - \lambda(\mathcal{M} + \alpha I)f = h\,.$$

Consequently, multiplying both sides by the sign function of f yields

$$\begin{aligned}
|f(x)| &= f(x)\ \mathrm{sgn}\,(f(x)) \\
&= -\lambda\,[g(x)f(x)]'\ \mathrm{sgn}\,(f(x))\ dx - \lambda\left[\frac{1}{2}k_f(x) + \mu(x)\right] f(x)\ \mathrm{sgn}\,(f(x)) \\
&\quad + \lambda\ \mathrm{sgn}\,(f(x)) \int_x^{\overline{x}} \Gamma(x;\,y) k_f(y) f(y)\,dy\,dx + \lambda\alpha f(x) + h(x)\ \mathrm{sgn}\,(f(x))\ , \qquad (2.21)
\end{aligned}$$

where function $\mathrm{sgn}(f(x))$ is defined as usual with $\mathrm{sgn}(0) = 0$. For a given $f \in \mathcal{D}(\mathcal{M})$ the set of points for which f does not vanish can be written as a finite union of disjoint open sets $I_j = (a_j,\, b_j)$, i.e., $f(x) \neq 0$ for all $x \in \cup_{j=1}^{n} I_j = (0,\, \overline{x})$. [2] On each interval I_j the function f can be either strictly positive or strictly negative. Moreover, on the boundaries we have $f(a_j) = 0$ and $f(b_j) = 0$ unless $a_j = 0$ or $b_j = x_1$. Then, integrating both sides of (2.21) on a given interval $I_j = (a_j,\, b_j)$ we have

$$\begin{aligned}
\int_{a_j}^{b_j} |f(x)|\ dx \leq -\lambda g(b_j)\,|f(b_j)| + \lambda g(a_j)\,|f(a_j)| - \lambda \int_{a_j}^{b_j} \left[-\alpha + \frac{1}{2}k_f(x) + \mu(x)\right] |f(x)|\ dx \\
+ \lambda \int_{a_j}^{b_j} \int_x^{\overline{x}} \Gamma(x;\,y) k_f(y)\,|f(y)|\ dy + \int_{a_j}^{b_j} |h(x)|\ dx\,. \qquad (2.22)
\end{aligned}$$

[2] See also (Banks & Kappel, 1989) and (Farkas & Hagen, 2010) for similar partitioning in dissipativity proofs

Consequently, by summing (2.22) for $j = 1, \ldots, n$ we get

$$\begin{aligned}
\int_0^{\overline{x}} |f(x)|\, dx &\leq -\lambda g(x_1)\, |f(x_1)| + \lambda g(0)\, |f(0)| - \lambda \int_0^{\overline{x}} \left[-\alpha + \frac{1}{2} k_f(x) + \mu(x) \right] |f(x)|\, dx \\
&\quad + \lambda \int_0^{\overline{x}} \int_x^{\overline{x}} \Gamma(x;\, y) k_f(y)\, |f(y)|\, dy\, dx + \int_0^{\overline{x}} |h(x)|\, dx \\
&\leq -\lambda \int_0^{\overline{x}} \left[-\alpha - q(x) + \frac{1}{2} k_f(x) + \mu(x) \right] |f(x)|\, dx \\
&\quad + \lambda \int_0^{\overline{x}} k_f(y)\, |f(y)| \underbrace{\int_0^{y} \Gamma(x;\, y)\, dx}_{=1}\, dy + \int_0^{\overline{x}} |h(x)|\, dx \\
&= -\lambda \int_0^{\overline{x}} \left[-\alpha - q(x) - \frac{1}{2} k_f(x) + \mu(x) \right] |f(x)|\, dx + \int_0^{\overline{x}} |h(x)|\, dx\,.
\end{aligned}$$

Hence, provided that we have

$$-\alpha - q(x) - \frac{1}{2} k_f(x) + \mu(x) > 0 \tag{2.23}$$

for all $x \in I$, it follows that

$$\|f\|_1 \leq \|h\|_1 = \|f - \lambda(\mathcal{M} + \alpha I) f\|_1\,.$$

In fact, if (2.20) holds true, then there exists $\alpha > 0$ such that $\mathcal{M} + \alpha I$ is dissipative. Consequently, the result follows immediately from the Lumer-Philips theorem. □

As a direct consequence of Proposition 2.2 and the above lemma, we summarize the results of this section in form of the following condition.

Condition 2. Assume that the assumptions (**A**1)-(**A**6) hold true. Moreover, assume that

$$q(x) + \frac{1}{2} k_f(x) - \mu(x) < 0$$

for all $x \in I$, then the zero stationary solution of the flocculation equation is locally exponentially stable.

2.4 Linearized instability and stability criteria for non-trivial steady states

In this section we present linearized stability results for the non-trivial stationary solution $u_* \neq 0$. We first derive conditions for instability (Section 2.4.1) and then derive conditions for linear stability (Section 2.4.2).

2.4.1 Linearized instability

Recall that, from Proposition 2.2, instability of the non-trivial stationary solution depends on the spectral properties of the operator $\mathcal{L}$. Specifically, the spectrum of $\mathcal{L}$ contains at least one point $\lambda_0 \in \sigma(\mathcal{L})$ satisfying the instability condition (2.9). Towards this end (as we did in Section 2.3.1), we first show that the operator $\mathcal{L}$ has a positive spectral radius.

Lemma 2.11. *Assume that the positivity conditions (2.15)-(2.16) hold. Moreover, if the model parameters satisfy the following condition*

$$\int_0^{\overline{x}} \frac{q(x)}{g(x)} \exp\left(- \int_0^x \frac{\mu(s) + \frac{1}{2}k_f(s) + \int_0^{\overline{x}-s} k_a(s,\, y) u_*(y)\, dy}{g(s)}\, ds \right) dx > 1\,, \tag{2.24}$$

then the operator $\mathcal{L}$ has a positive spectral radius.

Proof. Recall that the operator $\mathcal{L}$ can be written as the sum of the operators $\mathcal{L}_1$, $\mathcal{L}_2$ and $\mathcal{L}_3$. Moreover, in Lemma 2.7 we have shown that the operator $\mathcal{L}_1$ generates a positive semigroup and the positivity assumptions (2.15) and (2.16) ensure the positivity of the operator $\mathcal{L}_2 + \mathcal{L}_3$. Therefore, from Corollary 1.11 of Engel & Nagel (2000, §6) it follows that the spectral radius of $\mathcal{L}$ is always greater than the spectral radius of the operator $\mathcal{L}_1$, i.e.,

$$s(\mathcal{L}_1) \leq s(\mathcal{L}_1 + \mathcal{L}_2 + \mathcal{L}_3) = s(\mathcal{L})\,. \tag{2.25}$$

Conversely, provided that the condition (2.24) holds, the arguments of Farkas & Hagen (2007, Theorem 5.1) can be used to show that the spectral radius of the operator $\mathcal{L}_1$ is strictly positive. This result, combined with the inequality (2.25) implies that the spectral radius of $\mathcal{L}$ is strictly positive. □

We are now ready to present the main result of this section in the form of the following condition.

Condition 3. Under the main assumptions (**A**1)-(**A**6) and the positivity conditions (2.15)-(2.16) the non-trivial steady state solution of the nonlinear evolution equation defined in (1.1) is unstable if

$$\int_0^{\overline{x}} \frac{q(x)}{g(x)} \exp\left(- \int_0^x \frac{\mu(s) + \frac{1}{2} k_f(s) + \int_0^{\overline{x}-s} k_a(s,\, y) u_*(y)\, dy}{g(s)}\, ds \right) dx > 1\,. \tag{2.26}$$

Proof. Recall that from the proof of Lemma 2.11 it follows that

$$s(\mathcal{L}_1) \leq s(\mathcal{L})\,,$$

where the operators $\mathcal{L}_1$ and $\mathcal{L}$ are defined in (2.11). Note that Farkas & Hagen (2007) have shown that the operator $\mathcal{L}_1$ has a positive spectral radius provided that the condition (2.26) holds true. Consequently, if the condition (2.26) holds true, it follows that the operator $\mathcal{L}$ has a positive spectral radius. Then from Proposition 2.6 and Remark 2.8 it follows that $s(\mathcal{L}) \in \sigma_D(\mathcal{L})$. Moreover, Proposition 2.6 together with (Webb, 1985, Remark 4.8) imply that α-growth bound of $\mathcal{L}$ is equal to negative infinity, $\omega_1(\mathcal{L}) = -\infty$. Therefore, in Proposition 2.2, choosing λ_0 equal to the eigenvalue corresponding to $s(\mathcal{L})$ yields

$$\max\left\{ \omega_1(\mathcal{L}), \sup_{\lambda \in \sigma_D(\mathcal{L}) \setminus \{\lambda_0\}} \operatorname{Re} \lambda \right\} = \sup_{\lambda \in \sigma_D(\mathcal{L}) \setminus \{\lambda_0\}} \operatorname{Re} \lambda < \operatorname{Re} \lambda_0\,,$$

and implies that the non-trivial stationary solution p_* of the nonlinear evolution equation defined in (1.1) is unstable. □

Remark 2.12. Let $S \subset L^1(I)$ be the set of non-trivial stationary solutions and S_1 (subset of S) denote the set of non-trivial stationary solutions existence of which guaranteed by Theorem 2.1. For a stationary solution $u_* \in S_1$ the modeling terms need to satisfy the conditions (**C**1) and (**C**2). Consequently, plugging $x = 0$ into (**C**2) yields the inequality

$$\int_0^{\overline{x}} \frac{q(x)}{g(x)}\, dx \leq 1\,.$$

Conversely, the instability condition (2.26) implies that

$$1 < \int_0^{\overline{x}} \frac{q(x)}{g(x)} \exp\left(- \int_0^x \frac{\mu(s) + \frac{1}{2}k_f(s) + \int_0^{\overline{x}-s} k_a(s,\, y) u_*(y)\, dy}{g(s)}\, ds \right) dx \leq \int_0^{\overline{x}} \frac{q(x)}{g(x)}\, dx\,,$$

which contradicts the existence condition (**C**2). This in turn implies that stationary solutions in the set S_1 do not satisfy the instability condition. However, we note that S_1 is only subset of S, and thus the results of this subsection areonly valid for non-trivial stationary solutions in the set $S \backslash S_1$.

2.4.2 Linearized stability

In Section 2.4.1 we have shown that the spectrum of the operator $\mathcal{L}$ is not empty. This result, together with Proposition 2.7 and Remark 2.8 imply that the spectral radius of $\mathcal{L}$ is one of the eigenvalues of the operator $\mathcal{L}$, so it is sufficient to show that all the eigenvalues of $\mathcal{L}$ have a negative real part. However, to the best of our knowledge, the eigenvalue problem

$$\mathcal{L}[\phi] = \lambda \phi$$

does not have an explicit solution. This forces us to utilize the positive perturbation method of Farkas & Hinow (2012) to locate the dominant eigenvalue of $\mathcal{L}$. This method relies on the fact that compact perturbations do not change the essential spectrum of a semigroup. Towards this end we will perturb the operator $\mathcal{L} = \mathcal{L}_1 + \mathcal{L}_2 + \mathcal{L}_3$ (the operators $\mathcal{L}_1$, $\mathcal{L}_2$ and $\mathcal{L}_3$ are defined in (2.13)-(2.14)) by a positive compact operator so that we can identify the point spectrum of the resulting operator.

Lemma 2.13. *Let us define the operator* $\mathcal{C}$ as

$$\mathcal{C}[f](x) = c_1 \int_0^{\overline{x}} f(y)\, dy,$$

where $c_1 = \|k_a \cdot u_*\|_\infty + \|\Gamma \cdot k_f\|_\infty$. *Then the operator* $\mathcal{C} - \mathcal{L}_2 - \mathcal{L}_3$ *is positive and compact.*

Proof. It is easy to see that $\mathcal{C} - \mathcal{L}_2 - \mathcal{L}_3$ *is a positive operator, i.e.,*

$$\mathcal{C}[f](x) - \mathcal{L}_2[f](x) - \mathcal{L}_3[f](x) \geq \int_0^x \left[\|k_a \cdot u_*\|_\infty - k_a(x-y,\, y)u_*(x-y)\right] f(y)\, dy \\ + \int_x^{\overline{x}} \left[\|\Gamma \cdot k_f\|_\infty - \Gamma(x;\, y)k_f(y)\right] f(y)\, dy \geq 0 \quad \forall f \in \left(L^1(I)\right)_+ .$$

Conversely, $\mathcal{C}$ is a bounded linear functional, hence it is compact. Then the compactness of $\mathcal{C} - \mathcal{L}_2 - \mathcal{L}_3$ follows from compactness of the operators $\mathcal{L}_2$ and $\mathcal{L}_3$ (see Lemma 2.5). □

Now define the perturbed operator $\mathcal{P}$ as $\mathcal{P} := \mathcal{L} + \mathcal{C} - \mathcal{L}_2 - \mathcal{L}_3 = \mathcal{L}_1 + \mathcal{C}$. Then the eigenvalue problem for the operator $\mathcal{P}$ reads as

$$\lambda f - \mathcal{P}[f] = \lambda f - \mathcal{L}_1[f] - \mathcal{C}[f] = 0\,. \tag{2.27}$$

This equation can be solved implicitly as

$$f(x) = U_1 \frac{1}{T(\lambda,\, x)g(x)} + U_2 \frac{c_1}{g(x)T(\lambda,\, x)} \int_0^x T(\lambda,\, s)\, ds\,, \tag{2.28}$$

where

$$U_1 = \int_0^{\overline{x}} q(y)f(y)\, dy, \qquad U_2 = \int_0^{\overline{x}} f(y)\, dy$$

and

$$T(\lambda,\, x) = \exp\left(\int_0^x \frac{\lambda + A(y)}{g(y)}\, dy\right) .$$

Integrating the equation (2.28) on I yields one equation for solving for U_1 and U_2. Moreover, multiplying the equation (2.28) by $q(x)$ and integrating over the interval I we obtain the second equation for solving for U_1 and U_2. Consequently, these two equations can be summarized in the following linear system,

$$\begin{cases} U_1 A_{11}(\lambda) + U_2\left(A_{12}(\lambda) - 1\right) = 0 \\ U_1(A_{21}(\lambda) - 1) + U_2 A_{22}(\lambda) = 0 \end{cases}, \tag{2.29}$$

where

$$A_{11}(\lambda) = \int_0^{\overline{x}} \frac{1}{T(\lambda,\, x)g(x)}\, dx, \quad A_{12}(\lambda) = \int_0^{\overline{x}} \frac{c_1}{g(x)T(\lambda,\, x)} \int_0^x T(\lambda,\, s)\, ds\, dx\,,$$
$$A_{21}(\lambda) = \int_0^{\overline{x}} \frac{q(x)}{T(\lambda,\, x)g(x)}\, dx, \quad A_{22}(\lambda) = \int_0^{\overline{x}} \frac{c_1 q(x)}{g(x)T(\lambda,\, x)} \int_0^x T(\lambda,\, s)\, ds\, dx\,.$$

If the eigenvalue problem (2.27) has a non-zero solution, then there is non-zero vector $(U_1,\, U_2)$ satisfying the linear system (2.29). On the other hand, if there is non-zero vector $(U_1,\, U_2)$ satisfying the linear system (2.29), then the eigenvalue problem has a non-zero solution. Hence $\lambda \in \mathbb{C}$ is an eigenvalue value of the operator $\mathcal{P}$ if and only if

$$K(\lambda) = \det \begin{pmatrix} A_{11}(\lambda) & A_{12}(\lambda) - 1 \\ A_{21}(\lambda) - 1 & A_{22}(\lambda) \end{pmatrix} = A_{11}(\lambda)A_{22}(\lambda) - (1 - A_{12}(\lambda))\,(1 - A_{21}(\lambda)) = 0\,. \quad (2.30)$$

In structured population dynamics the function K is often referred as a characteristic function of eigenvalues of an operator, and similar characteristic functions have been derived in (Prüss, 1983b; Farkas & Hagen, 2007; Farkas, 2005; Farkas & Hinow, 2012; Farkas & Hagen, 2007). The main advantage of having the characteristic function K is the task of locating the dominant eigenvalue value of the operator $\mathcal{L}$ reduces to locating the roots of the function K. Hence, in the following lemma we show that under certain conditions on the model parameters all the roots of the characteristic function K lie in the left half of the complex plane.

Lemma 2.14. *Under the conditions*

$$A_{12}(0) < 1, \qquad A_{21}(0) < 1 \quad (2.31)$$

and

$$K(0) < 0 \quad (2.32)$$

the function K does not have any roots with non-negative real part. Furthermore, the function K has at least one negative real root.

Proof. It is straightforward to see that

$$A_{11}(\lambda) = A_{12}(\lambda) = A_{21}(\lambda) = A_{22}(\lambda) = 0 \text{ as } \lambda \to \infty\,,$$

so

$$\lim_{\lambda\to\infty} K(\lambda) = -1\,.$$

Moreover, observe that for $i = 1, 2$ and $j = 1, 2$ the functions $A_{ij} : \mathbb{R} \to \mathbb{R}_+$ are non-increasing, i.e.,

$$\partial_\lambda A_{ij}(\lambda) \leq 0\,.$$

Consequently, for $\lambda \geq 0$ from (2.31) we have

$$1 - A_{12}(\lambda) \geq 1 - A_{12}(0) > 0$$

and

$$1 - A_{21}(\lambda) \geq 1 - A_{21}(0) > 0\,.$$

Conversely, differentiating $K(\lambda)$ for $\lambda \geq 0$ yields

$$K' = A'_{11}A_{22} + A_{11}A'_{22} + A'_{12}\underbrace{(1 - A_{21})}_{>0} + A'_{21}\underbrace{(1 - A_{12})}_{>0} \leq 0\,.$$

Thus the function K restricted to real numbers is non-increasing. This in turn together with the condition (2.32) implies that the function K does not have any positive real root.

Now for the sake of a contradiction, assume that there is $\lambda_1 = a - b\mathrm{i} \in \mathbb{C}$ with $a \geq 0$ and $b \neq 0$ such that

$$K(\lambda_1) = 0\,. \tag{2.33}$$

Let us define

$$G(x) = \int_0^x \frac{1}{g(y)}\,dy\,,$$

then for $\lambda = a - b\mathrm{i}$ we have

$$A_{11}(\lambda_1) = \int_0^{\overline{x}} \frac{\cos\left[bG(x)\right]}{T(a,\, x)g(x)}\, dx + \mathrm{i} \int_0^{\overline{x}} \frac{\sin\left[bG(x)\right]}{T(a,\, x)g(x)}\, dx\,.$$

This in turn implies that

$$-\, A_{11}(a) \leq \mathrm{Re}\ A_{11}(\lambda_1) \leq A_{11}(a)\,. \tag{2.34}$$

Analogous arguments yields similar inequalities for A_{12}, A_{21} and A_{22}. On the other hand, if (2.33) holds true then using (2.34) it follows that

$$\begin{aligned} A_{11}(a)A_{12}(a) &= |A_{11}(\lambda_1)A_{12}(\lambda_1)| = |(1 - A_{12}(\lambda_1))\,(1 - A_{21}(\lambda_1))| \\ &\geq |1 - \mathrm{Re}\ A_{12}(\lambda_1)|\,|1 - \mathrm{Re}\ A_{21}(\lambda_1)| \\ &\geq (1 - A_{12}(a))\,(1 - A_{21}(a)) \geq 0 \end{aligned} \tag{2.35}$$

Since $K(\lambda)$ is non-increasing for $\lambda \geq 0$, from (2.32) we have

$$K(a) \leq K(0) < 0\,. \tag{2.36}$$

The equation (2.36) is equivalent to

$$A_{11}(a)A_{12}(a) < (1 - A_{12}(a))\,(1 - A_{21}(a))\ ,$$

which obviously contradicts the equation (2.35). Hence, the function cannot have a complex root with a non-negative real part.

To establish the last statement of the lemma, observe that the function $1 - A_{12}(\lambda)$ is continuous and non-decreasing with

$$\lim_{\lambda \to -\infty} 1 - A_{12}(\lambda) = -\infty\,.$$

Conversely, from the condition (2.31) we have $1 - A_{12}(\lambda) > 0$ for $\lambda \geq 0$. Thus by Intermediate Value Theorem there is $\lambda_0 < 0$ such that $1 - A_{12}(\lambda_0) = 0$. Consequently, evaluating K at $\lambda = \lambda_0$

yields

$$K(\lambda_0) = A_{11}(\lambda_0)A_{22}(\lambda_0) - (1 - A_{12}(\lambda_0))\,(1 - A_{21}(\lambda_0)) = A_{11}(\lambda_0)A_{22}(\lambda_0) \geq 0\,.$$

Hence, the function K has at least one negative real root, which completes the proof of the lemma. □

With the above lemma in hand, we can now state the main result of this subsection in the form of the following condition.

Condition 4. Suppose that the conditions

$$K(0) = A_{11}(0)A_{22}(0) - (1 - A_{12}(0))\,(1 - A_{21}(0)) < 0\,,$$

$$A_{12}(0) = \left(\|k_a \cdot u_*\|_\infty + \|\Gamma \cdot k_f\|_\infty\right) \int_0^{\overline{x}} \frac{1}{g(x)} \int_0^x \exp\left(-\int_s^x \frac{A(s)}{g(s)}\right) ds\, dx < 1$$

and

$$A_{21}(0) = \int_0^{\overline{x}} \frac{q(x)}{g(x)} \exp\left(-\int_0^x \frac{A(s)}{g(s)}\, ds\right) dx < 1$$

hold true. Then, the non-trivial steady state solution u_* is linearly exponentially stable.

Proof. Lemma 2.14 implies that the operator $\mathcal{L}_1 + \mathcal{C}$ has negative spectral radius,

$$s(\mathcal{L}_1 + \mathcal{C}) < 0\,.$$

Conversely, from Engel & Nagel (2000, §6, Corollary 1.11), Proposition 2.7 and Lemma 2.13 it follows that

$$s(\mathcal{L}) = s(\mathcal{L}_1 + \mathcal{L}_2 + \mathcal{L}_3) \leq s(\mathcal{L}_1 + \mathcal{L}_2 + \mathcal{L}_3 + \mathcal{C} - \mathcal{L}_2 - \mathcal{L}_3) = s(\mathcal{L}_1 + \mathcal{C}) < 0\,.$$

Consequently, from Engel & Nagel (2000, §6, Theorem 1.15) it follows that

$$\omega_0(\mathcal{L}) = s(\mathcal{L}) < 0\,.$$

Hence, Proposition 2.2 yields that the non-trivial steady state solution u_* is linearly asymptotically stable. □

2.5 Concluding Remarks

Our primary motivation in this chapter is to investigate the ultimate behavior of solutions of a generalized size-structured flocculation model. The model accounts for a broad range of biological phenomena (necessary for survival of a community of microorganism in a suspension) including growth, aggregation, fragmentation, removal due to predation, and gravitational sedimentation. Moreover, the number of cells that erode from a floc and enter the single cell population is modeled with McKendrick-von Foerster type renewal boundary equation. Although it has been shown that the model has a unique positive solution, to the best of our knowledge, the large time behavior of those solutions has not been studied. Therefore, in this chapter we showed that under relatively weak restrictions the flocculation model possesses a non-trivial stationary solution (in addition to the trivial stationary solution).

We used the principle of linearized stability for nonlinear evolution equations to linearize the problem around the stationary solution. This allowed us to infer stability of the stationary solutions by the spectral properties of the linearized problem. We then used the rich theory developed for semigroups, to derive the stability and instability conditions for the zero stationary solution. Lastly, we used compactness and positivity arguments to derive conditions for local stability of the non-trivial stationary solutions.

Lastly, even though we showed that the flocculation model has at least one non-trivial stationary solution, our analysis does not state these stationary solutions explicitly. The nonlinearity introduced to the model by Smoluchowski coagulation equations, makes the task of finding explicit stationary solutions challenging even for constant model parameters. On the other hand, when only Smoluchowski coagulation equation is considered, it has been shown that the model has closed form self-similar solutions for constant and additive aggregation kernels (Menon & Pego, 2004; Wattis, 2006). Perhaps, under some conditions on the initial distribution and model parameters, solutions of the flocculation model also converge to self-similar profiles. Hence, as a future research, we plan to further investigate self-similar solutions of the flocculation model.

Chapter 3

Numerical Framework for stability analysis of steady states of general evolution equations[1]

Many natural phenomena can be formulated as the differential law of the development (evolution) in time of a physical system. The resulting differential equation combined with boundary conditions affecting the system are called *evolution equations*. Evolution equations are a popular framework for studying the dynamics of biological populations. For example, they have proven useful in understanding the dynamics of biological invasions (Schreiber & Ryan, 2011), bacterial flocculation in activated sludge tanks (Biggs & Lant, 2002), and the spread of parasites and diseases (Gourley et al., 2008). Since many biological populations converge to a time-independent state, many researchers have used theoretical tools to investigate long-term behavior of these models. Analytical and fixed point methods have been used to show the existence of stationary solutions to size-structured population models (Mirzaev & Bortz, 2015b; Farkas & Hinow, 2012) and semigroup theoretic methods have been used to investigate the stability of these stationary solutions (Farkas & Hagen, 2007; Mirzaev & Bortz, 2015a; Banasiak, 2011). For many models in the literature, the principle of linearized stability (Webb, 1985; Kato, 1995) can be used to show that the spectral

[1]This chapter has been published:
I. Mirzaev & D. M. Bortz, (2017). "A numerical framework for computing steady states of structured population models and their stability", *Mathematical Biosciences and Engineering*, 14, no.4, (February 2017)

properties of the infinitesimal generator (IG) of the linearized semigroup determines the stability or instability of a stationary solution. Moreover, using compactness arguments, spectral properties of the infinitesimal generator can be determined from the point spectrum of the IG, which in turn can be written as the roots of a characteristic equation.

Despite this theoretical development, the derived existence and stability conditions are oftentimes rather complex, and accordingly the biological interpretation of these conditions can be challenging. To overcome this difficulty several numerical methods for stability analysis of structured population models have been developed (Breda et al., 2004; Engelborghs et al., 2002; Kirkilionis et al., 2001; De Roos et al., 2010). For instance, Diekmann et al. (Kirkilionis et al., 2001; Diekmann et al., 2003; De Roos et al., 2010) present a numerical method for equilibrium and stability analysis of physiologically structured population models (PSPM) or life history models, where individuals are characterized by a (finite) set of physiological characteristics (traits such as age, size, sex, energy reserves). In this method a PSPM is first written as a system of integral equations coupled with each other via interaction (or feedback) variables. Consequently, equilibria and stability boundary of the resulting integral equations are numerically approximated using curve tracing methods. Later, De Roos (2008) presented the modification of the curve tracing approach to compute the demographic characteristics (such as population growth rate, reproductive value, etc) of a linear PSPM. For a fast and accurate software for theoretical analysis of PSPMs we refer interested reader to a software package by De Roos (2014). An alternative method for stability analysis of physiologically structured population models, developed by Breda and coworkers (Breda et al., 2013, 2005; Breda, 2006), uses a pseudospectral approach to compute eigenvalues of a discretized infinitesimal generator. This method (also known as infinitesimal generator (IG) approach) has been employed to produce bifurcation diagrams and stability regions of many different linear evolution equations arising in structured population modeling (Breda et al., 2005, 2006, 2009). Unfortunately, not all structured population models fit into the framework of PSPMs and thus there is a need for a more general numerical framework for asymptotic analysis of structured population models.

In this chapter we develop a numerical framework to guide theoretical analysis of structured population models. We demonstrate that our methodology can be used for numerical computation and stability analysis of positive stationary solutions of both linear and nonlinear size-structured population models. Moreover, we illustrate the utility of our framework to produce approximate

existence and stability regions for steady states of size-structured population models. We also provide an open source Python program used for the numerical simulations in our GitHub repository (Mirzaev, 2015). Although, the examples presented in this chapter are size-structured population models, in Section 3.1, we show that the framework is applicable to more general evolution equations.

The main idea behind the numerical framework is first to write a structured population model in the form of an evolution equation and then use the well-known Trotter-Kato Theorem (Trotter, 1958; Kato, 1959) to approximate the infinitesimal generator of the evolution equation on a finite dimensional space. This in turn allows one to approximate solutions (or spectrum) of the evolution equation with the solution (or spectrum) of system of differential equations. Consequently, we approximate the stationary solutions of an actual model with stationary solutions of the approximate infinitesimal generator on a finite dimensional space. Approximate local stability of the approximate steady states are then computed from the spectrum of the Jacobian of ODE system evaluated at this steady states. Our method is similar to the IG approach in (Breda et al., 2005, 2006, 2009), in a sense that we also approximate infinitesimal generator and analyze the spectrum of the resulting operator to produce existence and stability regions. However, in contrast to IG approach, our framework also computes actual steady states and is easily applied to nonlinear evolution equations arising in structured population dynamics.

The rest of the chapter is structured as follows. We describe the theoretical development of our framework for general evolution equations in Section 3.1.1. Note that readers with more biological background can skip Section 3.1.1 and directly jump into the application of the framework in Section 3.1.3. In Section 3.1.3, we illustrate the convergence of the approximation method by applying it to linear Sinko-Streifer model, for which the exact form of the stationary solutions is known. Moreover, in Section 3.1.2, we show that approximate local stability conditions for a stationary solution can be derived from the spectral properties of the approximate infinitesimal generator. To further illustrate the utility of our approach, in Section 3.2, we apply our framework to a nonlinear size-structured population model (also known as population balance equations in the engineering literature) described in (Banasiak & Lamb, 2009; Bortz et al., 2008). Finally, we conclude with some remarks and a summary of our work in Section 3.3.

3.1 Numerical Framework

In this section, we demonstrate our numerical methodology for general evolution equations. We first present the numerical scheme used to approximate the infinitesimal generator of a semigroup. Subsequently, in Section 3.1.3, we illustrate the convergence of our approach by applying it to linear Sinko-Streifer equations, for which exact stationary solutions are known.

3.1.1 Infinitesimal generator approximation

Given a Banach space $\mathcal{X}$, consider an abstract evolution equation,

$$u_t = \mathcal{F}(u), \qquad u(0, \bullet) = u_0 \in \mathcal{X}\,, \tag{3.1}$$

where $\mathcal{F} : \mathcal{D}(\mathcal{F}) \subseteq \mathcal{X} \to \mathcal{X}$ is some operator defined on its domain $\mathcal{D}(\mathcal{F})$ and u_0 is an initial condition at time $t = 0$. Note that any boundary condition belonging to a given partial differential equation can be included in the domain $\mathcal{D}(\mathcal{F})$. The solution to (3.1) can be related to the initial state u_0 by some transition operator $T(t)$ so that

$$u(t,\, x) = T(t)u_0(x)\,.$$

The transition operator $T(t)$ is said to be a strongly continuous semigroup (or simply C_0 -semigroup) if satisfies the following three conditions:

1. $T(s)T(t) = T(s + t)$ for all $s,\, t \geq 0$
2. $T(0) = I$, the identity operator on $\mathcal{X}$
3. For each fixed $u_0 \in \mathcal{X}$,
$$\lim_{t \to 0^+} \|T(t)u_0 - u_0\| = 0\,.$$

Moreover, showing that the operator $\mathcal{F}$ generates a C_0-semigroup is equivalent to establishing well-posedness of the abstract evolution equation given in (3.1). In general, finding the explicit form of the transition operator is challenging. Hence, approximation methods, e.g. Yosida approximants, are used to study a more complicated evolution equation and the semigroups they generate. One

of the famous approximation theorems is due to Trotter (1958) and Kato (Kato, 1959) (see (Kato, 1976) for the classical literature on the approximation of generators of semigroups). The goal is to construct approximating generators $\mathcal{F}_n$ on the approximate spaces $\mathcal{X}_n$ such that C_0-semigroups $T_n(\cdot)$ generated by $\mathcal{F}_n$ approximate the C_0-semigroup $T(t)$ generated by $\mathcal{F}$. Although there are multiple ways to approximate the infinitesimal generator $\mathcal{F}$, for our purposes we use the approximation scheme based on Galerkin-type projection of the state space $\mathcal{X}$ (Banks & Kappel, 1989; Ito & Kappel, 1998; Ackleh & Fitzpatrick, 1997). For the convenience of readers, we will summarize the approximation scheme here.

Let $\mathcal{X}_n$, $n = 1, 2, \ldots$ be a sequence of subspaces of $\mathcal{X}$ with $\dim(\mathcal{X}_n) = n$ and define projections $\pi_n : \mathcal{X} \to \mathcal{X}_n$ and canonical injections $\iota_n : \mathcal{X}_n \to \mathcal{X}$. Assume that the projections π_n are bounded, i.e., there exists $\tilde{M} > 0$ such that

$$\|\pi_n\| \leq \tilde{M} \tag{A1}$$

for all $n = 1, \ldots, n$. Moreover, assume that

$$\lim_{n\to\infty} \pi_n v = v \tag{A2}$$

for all $v \in \mathcal{X}$. Consequently, for each subspace $\mathcal{X}_n$ we choose basis elements $\{\beta_i^n\}_{i=1}^n$ such that each element v of subspace $\mathcal{X}_n$ can be written in the form $v = \sum_{i=1}^n \alpha_i \beta_i^n$. Moreover, for each subspace $\mathcal{X}_n$ we define the bijective mappings $p_n : \mathcal{X}_n \to \mathbb{R}^n$ by

$$p_n v = (\alpha_1, \cdots, \alpha_n)^T$$

and the norm on $\mathbb{R}^n$ by

$$\|v\|_{\mathbb{R}^n} = \left\|p_n^{-1} v\right\|_{\mathcal{X}} .$$

Consequently, we define bounded linear operators $P_n : \mathcal{X} \to \mathbb{R}^n$ and $E_n : \mathbb{R}^n \to \mathcal{X}$ by

$$P_n v = p_n \pi_n v, \quad v \in \mathcal{X} \tag{3.2}$$

and

$$E_n z = \iota_n p_n^{-1} z, \quad z \in \mathbb{R}^n , \tag{3.3}$$

respectively. Finally, we define approximate operators $\mathcal{F}_n$ on $\mathbb{R}^n$ by

$$\mathcal{F}_n(z) = P_n \mathcal{F}(E_n z) \tag{3.4}$$

for all $z \in \mathbb{R}^n$.

Accordingly, the Trotter-Kato Theorem states that the semigroup generated by the discrete operator $\mathcal{F}_n$ converges to the semigroup generated by the infinitesimal generator $\mathcal{F}$. For the convenience of the reader, we state the theorem here and refer readers to (Ito & Kappel, 1998) for a proof.

Theorem. *(Trotter-Kato) Assume that (**A**1) and (**A**2) are satisfied. Let $(T(t))_{t\geq 0}$ and $(T_n(t))_{t\geq 0}$, $n \in \mathbb{N}$, be strongly continuous semigroups on $\mathcal{X}$ and $\mathbb{R}^n$ with generators $\mathcal{F}$ and $\mathcal{F}_n$, respectively. Furthermore, assume that they satisfy the estimate*

$$\|T(t)\|_{\mathcal{X}}, \|T_n(t)\|_{\mathbb{R}^n} \leq M e^{wt} \qquad \text{for all } t \geq 0,\, n \in \mathbb{N},$$

for some constants $M \geq 1$, $w \in \mathbb{R}$. Then the following are equivalent:

1. *There exists a $\lambda_0 \in \rho(\mathcal{F}) \cap \bigcap_{i=1}^{n} \rho(\mathcal{F}_i)$ such that for all $v \in \mathcal{X}$*

$$\left\| E_n (\lambda_0 I_n - \mathcal{F}_n)^{-1} P_n v - (\lambda_0 I - \mathcal{F})^{-1} v \right\|_{\mathcal{X}} \to 0 \quad \text{as } n \to \infty.$$

2. *For all $v \in \mathcal{X}$ and $t \geq 0$,*

$$\|E_n T_n(t) P_n v - T(t) v\|_{\mathcal{X}} \to 0$$

as $n \to \infty$, uniformly on compact t intervals.

In general, one establishes the first statement for a Trotter-Kato approximation and then uses the second statement to approximate an abstract evolution equation on a finite dimensional space. In their paper, Ito and Kappel (Ito & Kappel, 1998) present the standard ways to establish the first statement of the theorem (see also (Banks & Kappel, 1989; Ackleh & Fitzpatrick, 1997; Ackleh, 1997)). Therefore, here we assume that for a particular problem the first statement in the theorem has already been established and thus the evolution equation in (3.1) can be approximated by the

following system of ODEs,

$$u_n'(t) = \mathcal{F}_n\left(u_n(t)\right), \quad u_n(0) = P_n u(0, \bullet)\,. \tag{3.5}$$

Consequently, the solution of the IVP is mapped onto the infinite dimensional Banach space $\mathcal{X}$ and one has the following convergence

$$\lim_{n\to\infty} \|E_n u_n(t) - u\|_{\mathcal{X}} = 0 \tag{3.6}$$

for t in compact intervals.

In general, finding explicit stationary solutions of abstract evolution equations is a challenging task. Conversely, many efficient root finding methods have been developed for finding steady states of a system of ODEs. For large-scale nonlinear systems, many efficient methods have been developed as well. Hence, we propose a numerical framework that utilizes those efficient root finding methods to approximate steady state solutions of general evolution equations. The idea is to use an efficient and accurate root finding method to approximate a stationary solution of the evolution equation (3.1) with the stationary solutions of the IVP in (3.5). Thus, as a consequence of the Trotter-Kato Theorem, the steady states of (3.5) converge to the steady states of (3.1) as $n \to \infty$.

3.1.2 Stability of stationary solutions

Studying the asymptotic behavior of solutions is a fundamental tool for exploring the evolution equations which arise in the mathematical modeling of real world phenomena. To this end, many mathematical methods have been developed to describe long-term behavior of evolution equations. For instance, for long-time behavior of linear evolution equations, linear semigroup theoretic methods can be used to formulate physically interpretable conditions. Furthermore, for nonlinear evolution equations, the principle of linearized stability can be used to relate the spectrum of the linearized infinitesimal generator to the local stability or instability of the stationary solution. Nevertheless, investigating the spectrum of the linearized infinitesimal generator is cumbersome and requires advanced functional analysis techniques. In contrast to general evolution equations, the asymptotic behavior of ordinary differential equations are determined by the eigenvalues of the Jacobian and

well-studied. Hence, in this section we demonstrate that the approximation scheme, presented in Section 3.1.1, can also be used to give some insights about the stability of stationary solutions of the general evolution equations.

Stability results discussed in this section are not in a traditional Lyapunov sense. In particular, since stationary solutions discussed in this chapter are only approximations to actual stationary solutions, the stability results only hold for finite time intervals. Therefore, we refer to this kind of stability as *approximate local stability* of stationary solutions as this stability is deduced from numerical approximation of an evolution equation. In mathematical terms, the local numerical stability of a stationary solution is defined as follows.

Definition 3.1. Stationary solution u_* of an abstract evolution (3.1) is called *approximately locally stable*, if for every closed finite time interval $[0,\, t_f]$ and $\epsilon > 0$, there exists $\delta > 0$ such that a unique solution of (3.1), $u(t,\, x)$, with initial condition u_0 fulfilling $\|u_0 - u_*\|_{\mathcal{X}} < \delta$ satisfies

$$\|u(t,\, \cdot) - u_*\|_{\mathcal{X}} < \epsilon \tag{3.7}$$

for all $t \in [0,\, t_f]$.

Having the required definition in hand, we now prove the following stability result for general evolution equations.

Corollary 3.2. *Let u_* denote a stationary solution of the abstract evolution (3.1) and $J_A(u_n)$ denote the Jacobian of the approximate system of ODEs defined in (3.5). If for all sufficiently large n the eigenvalues of $J_A(P_n u_*)$ are strictly negative, then u^* is approximately locally stable in the sense of Definition 3.1.*

Proof. Since the infinitesimal generator approximation scheme, presented in Section 3.1.1, is convergent, for every given $\epsilon > 0$ and finite time interval $[0,\, t_f]$ there exist $n_\epsilon \in \mathbb{N}$ such that for $n \geq n_\epsilon$,

$$\|u(t,\, \cdot) - E_n u_n(t)\|_{\mathcal{X}} < \epsilon/2 \tag{3.8}$$

for all $t \in [0,\, t_f]$ (where the bounded linear function E_n is defined as in (3.3)). Moreover, the eigenvalues of $J_A(P_n u_*)$ are strictly negative for all sufficiently large n. This in turn implies that

$P_M u_*$ is a locally asymptotically stable solution of (3.5) for some $M \geq n_\epsilon$. That is, for given $\epsilon > 0$ there is $\delta > 0$ such that

$$\|u_M(t,\cdot) - P_M u_*\|_{\mathbb{R}^M} = \|E_M u_M(t,\cdot) - u_*\|_{\mathcal{X}} < \epsilon/2 \tag{3.9}$$

for all $t > 0$ and for all u_0 such that $\|P_M u_0 - P_M u_*)\|_{\mathbb{R}^M} = \|u_0 - u_*\|_{\mathcal{X}} < \delta$ (see for instance (Arnold, 1992, §23)). Consequently, combining (3.8) and (3.9) yields

$$\|u(t,\cdot) - u_*\|_{\mathcal{X}} \leq \|u(t,\cdot) - E_M u_M(t,\cdot)\|_{\mathcal{X}} + \|E_M u_M(t,\cdot) - u_*\|_{\mathcal{X}} < \epsilon$$

for all $t \in [0,\, t_f]$ and for all u_0 such that $\|u_0 - u_*\|_{\mathcal{X}} < \delta$. □

We note that although the stability result of Corollary 3.2 holds for arbitrarily large finite time intervals, the Corollary does not guarantee *Lyapunov* stability of stationary solutions.

3.1.3 Numerical convergence results

To verify convergence of the proposed approximation scheme, we apply the framework to the linear Sinko-Streifer model (Sinko & Streifer, 1967) for which an exact form of the stationary solution is available. The model describes the dynamics of single species populations and takes into account the physiological characteristics of animals of different sizes (and/or ages). The mathematical model reads as

$$u_t = \mathcal{G}(u) = -(gu)_x - \mu u, \quad t \geq 0, \quad 0 \leq x \leq \overline{x} < \infty \tag{3.10}$$

with a McKendrick-von Foerster type renewal boundary condition at $x = 0$

$$g(0)u(t,\,0) = \int_0^{\overline{x}} q(y)u(t,\,y)\,dy$$

and initial condition

$$u(0,\,x) = u_0(x)\,.$$

The variable $u(t,\,x)$ denotes the population density at time t with size class x. The population is assumed to have a minimum and a maximum size 0 and $\overline{x} < \infty$, respectively. The function

$g(x)$ represents the average growth rate of the size class x and the coefficient $\mu(\bullet)$ represents a size-dependent removal rate due to death or predation. The renewal function $q(\bullet)$ represents the number of new individuals entering the population due to birth.

We note that this boundary condition could also be used to model the surface erosion of flocs, where single cells are eroded off the floc and enter single cell population. The well-posedness and stability of equilibrium solutions of the Sinko-Streifer equations has been extensively studied by many researchers using a wide variety of mathematical conditions (Gurtin & MacCamy, 1974, 1979; Prüss, 1983b,a; Diekmann et al., 1984; Banks & Kappel, 1989). For numerical simulation of the model, a convergent numerical scheme has been proposed in (Banks & Kappel, 1989), and inverse problems for estimation of the parameters of the model have been discussed in (Banks et al., 1987; Banks & Kunisch, 1989; Fitzpatrick, 1993).

Setting the right side of the equation (3.10) to zero and integrating over the size on $(0,\, x)$ yields the exact stationary solution

$$u_*(x) = \frac{1}{g(x)} \exp\left(- \int_0^x \frac{\mu(s)}{g(s)}\, ds \right) \int_0^{\overline{x}} q(y) u_*(y)\, dy\,. \tag{3.11}$$

Multiplying both sides of (3.11) by $q(x)$ integrating over the size on $(0,\, \overline{x})$, we obtain a necessary condition for existence of a stationary solution,

$$1 = \int_0^{\overline{x}} \frac{q(x)}{g(x)} \exp\left(- \int_0^x \frac{\mu(s)}{g(s)}\, ds \right)\, dx\,. \tag{3.12}$$

The convergence of the approximation scheme presented in Section 3.1.1 for Sinko-Streifer models has already been established in (Banks & Kappel, 1989). Using the basis functions for n-dimensional subspace $\mathcal{X}_n$ of the state space $\mathcal{X} = L^1(0,\, \overline{x})$ are defined as

$$\beta_i^n(x) = \begin{cases} 1; & x_{i-1}^n < x \le x_i^n\,;\; i = 1, \ldots, n \\ 0; & \text{otherwise} \end{cases}$$

for positive integer n with $\{x_i^n\}_{i=0}^n$ a uniform partition of $[0, \overline{x}]$, and $\Delta x = x_j^n - x_{j-1}^n$ for all j. The

functions β^n form an orthogonal basis for the approximate solution space

$$\mathcal{X}_n = \left\{ h \in \mathcal{X} \mid h = \sum_{i=1}^{n} \alpha_i \beta_i^n,\ \alpha_i \in \mathbb{R} \right\},$$

and accordingly, we define the orthogonal projections $\pi_n : \mathcal{X} \to \mathcal{X}_n$

$$\pi_n h(x) = \sum_{j=1}^{n} \alpha_j \beta_j^n(x), \qquad \text{where } \alpha_j = \frac{1}{\Delta x} \int_{x_{j-1}^n}^{x_j^n} h(x)\, dx.$$

Moreover, since the evolution equation defined in (3.10) is a linear partial differential equation, the approximate operator $\mathcal{G}_n$ on $\mathbb{R}^n$ is given by the following $n \times n$ matrix

$$\mathcal{G}_n = \begin{pmatrix} -\frac{1}{\Delta x} g(x_1^n) - \mu(x_1^n) + q(x_1^n) & q(x_2^n) & \cdots & q(x_{n-1}^n) & q(x_n^n) \\ \frac{1}{\Delta x} g(x_1^n) & -\frac{1}{\Delta x} g(x_2^n) - \mu(x_2^n) & 0 & \cdots & 0 \\ 0 & \frac{1}{\Delta x} g(x_2^n) & \ddots & \ddots & \vdots \\ \vdots & \ddots & \frac{1}{\Delta x} g(x_{n-2}^n) & -\frac{1}{\Delta x} g(x_{n-1}^n) - \mu(x_{n-1}^n) & 0 \\ 0 & \cdots & 0 & \frac{1}{\Delta x} g(x_{n-1}^n) & -\frac{1}{\Delta x} g(x_n^n) - \mu(x_n^n) \end{pmatrix}. \tag{3.13}$$

At this point, one can use numerical techniques to calculate zeros of the linear system

$$\mathcal{G}_n u_n = 0\,. \tag{3.14}$$

For the purpose of illustration, we set the model rates to

$$q(x) = a(x+1), \quad g(x) = b(x+1), \quad \mu(x) = c\,. \tag{3.15}$$

Plugging this rates into the necessary condition (3.12) yields

$$a = \begin{cases} \frac{\ln 2}{b} & b = c \\ (b-c)/(2^{1-c/b} - 1) & b \neq c \end{cases}.$$

For $b = c$ this is a curve in 3D coordinate system and when $b \neq c$ the surface is illustrated in Figure 3.1a. To illustrate the utility of our approach, we used the numerical scheme described in this section to generate existence and stability regions for Sinko-Streifer model. Particularly, the

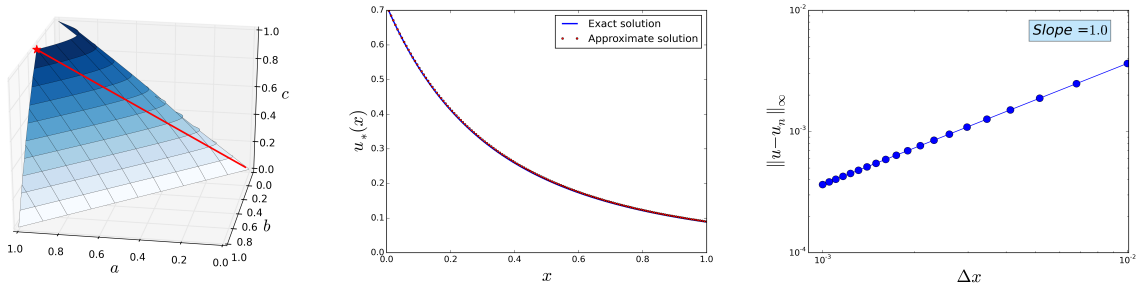

(a) (b) (c)

Figure 3.1: Results of the numerical simulations. a) a, b, c values satisfying the necessary condition (3.12), form a 3D surface (blue surface). Steady states of the Sinko-Streifer model only exist on the red line b) Comparison of exact stationary solution (for the point marked with red star in Figure 3.1a) with approximate stationary solution for $n = 100$. c) Absolute error between exact stationary solution and approximate stationary solution decays linearly as the dimension of approximate subspaces $\mathcal{X}_n$ increase.

interval $(a, b, c) \in [0, 1] \times [0, 1] \times [0, 1]$ is discretized with $\Delta a = \Delta b = \Delta c = 0.01$. Consequently, we checked for the existence of a positive steady state at each of these discrete points. Since the approximate operator $\mathcal{G}_n$ is an $n \times n$ matrix, we can check if $\mathcal{G}_n$ is a singular matrix using standard tools. The resulting existence region is depicted in Figure 3.1a forming a nontrivial three-dimensional curve (red) on the surface defined by the necessary condition for existence of the steady states. Moreover, the existence and stability regions of the Sinko-Streifer model coincide for the chosen model rates in (3.15).

For the purpose of illustration, we arbitrarily choose $b = 0.5$ and $a = c = 1$ (marked with a red star in Figure 3.1a) as for these values a positive steady state of the Sinko-Streifer model exists. Figure 3.1b indicates that even for $n = 100$ the fit between approximate and actual stationary solution is satisfactory (the infinity norm of the error is 0.004). Moreover, Figure 3.1c illustrates that as the dimension of the approximate space $\mathcal{X}_n$ increases the absolute error between the exact stationary solution and the approximate stationary solution decreases. Furthermore, the numerical algorithm has a linear convergence rate. This is due to the fact that we chose zeroth order functions as basis functions for approximate subspaces. In general, if one desires a higher order convergence for Galerkin-type approximations, choosing higher order basis functions gives higher convergence rate (Kappel & Kunisch, 1981).

3.2 Application to nonlinear population balance equation

In aerosol physics and environmental sciences, studying the *flocculation* of particles is widespread. The process of flocculation involves disperse particles in suspension combining into aggregates (i.e., a floc) and separating.

3.2.1 Numerical implementation and results

For the numerical implementation we adopt the scheme developed in Section 3.1.1. Therefore, the approximate formulation of (1.1) becomes the following system of n nonlinear ODEs for $u_n = (\alpha_1, \cdots, \alpha_n)^T \in \mathbb{R}^n$:

$$\dot{u}_n = \mathcal{F}_n(u_n) = \mathcal{G}_n u_n + P_n \mathcal{A}(E_n u_n) + P_n \mathcal{B}(E_n u_n), \tag{3.16}$$

$$u_n(0, x) = P_n u_0(x)\,, \tag{3.17}$$

where the matrix $\mathcal{G}_n$ is defined as in Section 3.1.3,

$$P_n\mathcal{A}(E_n u_n) = \begin{pmatrix} -\alpha_1 \sum_{j=1}^{n-1} k_a(x_1^n,\, x_j^n)\alpha_j \Delta x \\ \frac{1}{2} k_a(x_1^n,\, x_1^n)\alpha_1\alpha_1 \Delta x - \alpha_2 \sum_{j=1}^{n-2} k_a(x_2^n,\, x_j^n)\alpha_j \Delta x \\ \vdots \\ \frac{1}{2}\sum_{j=1}^{n-2} k_a(x_j^n,\, x_{n-1-j}^n)\alpha_j\alpha_{n-1-j}\Delta x - \alpha_{n-1} k_a(x_{n-1}^n,\, x_1^n)\alpha_1 \Delta x \\ \frac{1}{2}\sum_{j=1}^{n-1} k_a(x_j^n,\, x_{n-j}^n)\alpha_j\alpha_{n-j}\Delta x \end{pmatrix}$$

and

$$P_n\mathcal{B}(E_n u_n) = \begin{pmatrix} \sum_{j=2}^{n} \Gamma(x_1^n;\, x_j^n) k_f(x_j^n)\alpha_j \Delta x - \frac{1}{2} k_f(x_1^n)\alpha_1 \\ \sum_{j=3}^{n} \Gamma(x_2^n;\, x_j^n) k_f(x_j^n)\alpha_j \Delta x - \frac{1}{2} k_f(x_2^n)\alpha_2 \\ \vdots \\ \Gamma(x_{n-1}^n;\, x_n^n) k_f(x_n^n)\alpha_n \Delta x - \frac{1}{2} k_f(x_{n-1}^n)\alpha_{n-1} \\ -\frac{1}{2} k_f(x_n^n)\alpha_n \end{pmatrix}.$$

The convergence of the approximate scheme (3.16)-(3.17) has been established by Ackleh (1997). Therefore, the stationary solutions of the microbial flocculation model (1.1) can be systematically

approximated by the stationary solutions of the system of nonlinear ODEs given in (3.16). We used Powell's hybrid root finding method (Powell, 1970) as implemented in Python 2.7.10 [2] to find zeros of the steady state equation (see available code at (Mirzaev, 2015)). For faster convergence rate, we provided the solver with the exact Jacobian of $\mathcal{F}_n(u_n)$ (see Section 3.1.2, Eqn (3.18) for the formulation of the Jacobian). For the purpose of illustration, for a post-fragmentation density function we chose the well-known Beta distribution[3] with $\alpha = \beta = 2$,

$$\Gamma(x,\, y) = \mathbb{1}_{[0,\, y]}(x)\frac{6x(y-x)}{y^3}\,,$$

where $\mathbb{1}_I$ is the indicator function on the interval I. The aggregation kernel was chosen to describe flow within laminar shear field (i.e., *orthokinetic* aggregation)

$$k_a(x,\, y) = \left(x^{1/3} + y^{1/3}\right)^3$$

Other model rates were chosen arbitrarily as

$$q(x) = a(x+1), \quad g(x) = b(x+1) \quad \mu(x) = cx \quad k_f(x) = x\,,$$

where a, b and c are some positive real numbers.

The main advantage of this approximation scheme (3.16)-(3.17) is that it can be initialized very fast using Toeplitz matrices (Matveev et al., 2015). Fast initialization of the discretization scheme allows one to check the existence of the steady states at many discrete points efficiently. This in turn allows for the generation of the existence and stability regions of the steady states of the PBE in (1.1). To illustrate the existence regions of the steady states of the PBE, we discretized the intervals $a \in [0,\, 15]\,, b \in [0,\, 1]$ and $c \in [0,\, 5]$ with $\Delta a = \Delta b = \Delta c = 0.1$. We note that for faster convergence the root finding method needs an initial seed close to the steady state solution. Since we have no information about the existing steady state, we seed the root finding method with 10

[2] `scipy.optimize.fsolve`

[3] Although normal and log-normal distributions are mostly used in the literature, Byrne et al. (2011) have provided evidence that the Beta density function describes the fragmentation of small bacterial flocs.

different uniform initial guesses i.e.,

$$\left\{u_0(x) = 2^i \,|\, i = 0, 1, \ldots, 9\right\} ,$$

before we conclude a positive steady state does not exist for a given point (a, b, c). Consequently, we checked for the existence of a positive steady state at each of these discrete points. As depicted in Figure 3.2a, approximate existence region of positive steady states of the PBE forms a three dimensional wedge like region. Moreover, in Figures 3.2b-3.2d, to deduce stability of each steady state solution, we checked the spectrum of the Jacobian matrix evaluated at each steady state. Particularly, if the real part of rightmost eigenvalue of the Jacobian matrix is negative, the steady state is identified as locally stable (blue region). Conversely, if the real part of the rightmost eigenvalue of the Jacobian matrix is positive the steady state is identified as unstable (red region). One can observe that growth (b) and removal (c) rates can balance the smaller renewal rates (a), and thus locally stable steady states exist. However, as the renewal rate gets larger steady states first become unstable and then cease to exist (yellow region). This is also illustrated in Figure 3.3b, where steady states start diverging for the larger renewal rates (a).

Figure 3.3a illustrates an example stationary solution for $b = 0.5$, $a = c = 1$. To confirm that the function depicted in Figure 3.4 is indeed a locally stable steady state, we simulated the system of ODEs in (3.16)-(3.17) for $t \in [0,\, 10]$ with a collection of arbitrary initial conditions (Figure 3.4a) close to the steady state solution. One can observe in Figure 3.4 that the stationary solution is indeed locally stable and thus initial conditions, Figure 3.4, converge to the steady state depicted in Figure 3.4b. As depicted in Figures 3.4c and 3.4d, convergence is also reflected in the evolution of the total number of flocs (zeroth moment),

$$M_0(t) = \int_0^{\overline{x}} u(t,\, x)\, dx \approx \sum_{i=1}^{n} \int_{x_{i-1}^n}^{x_i^n} \alpha_i \beta_i^n(x)\, dx = \Delta x \sum_{i=1}^{n} \alpha_i \,,$$

and total mass of the flocs (first moment),

$$M_1(t) = \int_0^{\overline{x}} x u(t,\, x)\, dx \approx \sum_{i=1}^{n} \int_{x_{i-1}^n}^{x_i^n} \alpha_i x \beta_i^n(x)\, dx = \frac{\Delta x}{2} \sum_{i=1}^{n} \alpha_i \left(x_i^n + x_{i-1}^n\right) .$$

Moreover, to confirm that the steady state solution is not changing with increasing dimension

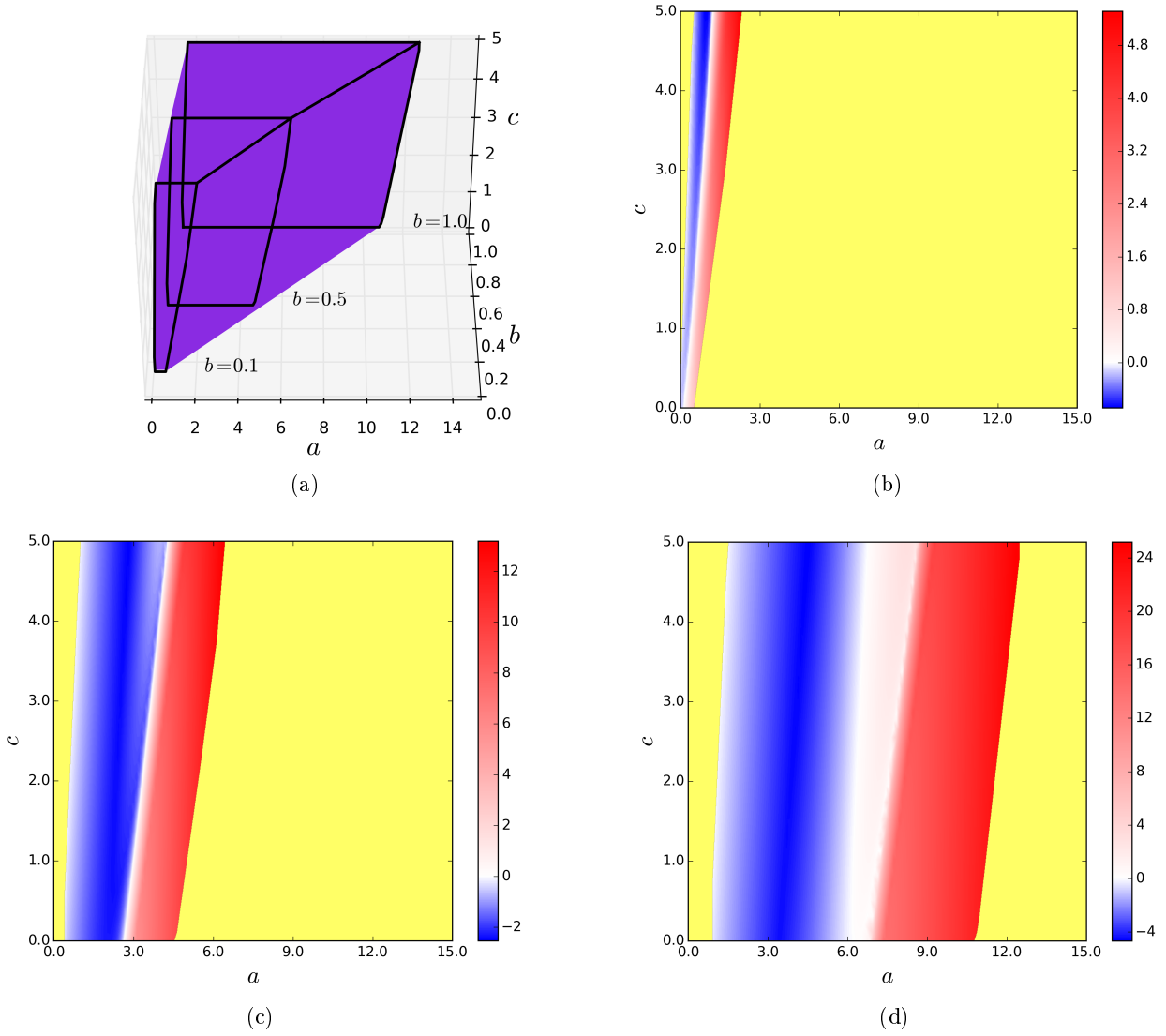

Figure 3.2: Existence and stability regions for the steady states of the PBE a) Existence region for the steady states of the PBE forms a wedge like shape. b) Stability region for $b = 0.1$, $a \in [0, 15]$ and $c \in [0, 5]$. c) Stability region for $b = 0.5$, $a \in [0, 15]$ and $c \in [0, 5]$. d) Stability region for $b = 1.0$, $a \in [0, 15]$ and $c \in [0, 5]$. Color bar represents the real part of rightmost eigenvalue of the Jacobian matrix evaluated at each steady state. Yellow regions represents the region for which a positive steady state does not exists.

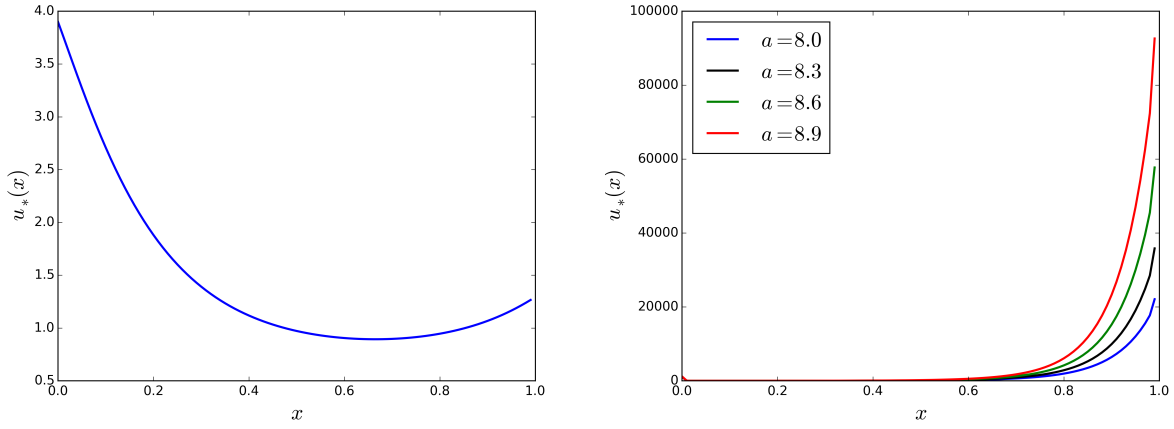

(a) (b)

Figure 3.3: a) An example steady-state solution of the PBE for $b = 0.5$, $a = c = 1$. b) Steady states for increasing renewal rate and $b = c = 1$

of approximate spaces $\mathcal{X}_n$, we simulated our numerical scheme for different values of n. Figure 3.5a illustrates that stationary solutions converge to exact stationary solution of (1.1) as $n \to \infty$. Furthermore, one can observe, in Figure (3.5)b that difference between approximate steady states for different values of n is considerably small.

3.2.2 Conditions for numerical stability of positive steady states

In this section, we derive conditions for *approximate* local stability of the stationary solution of the nonlinear population balance equation defined in (1.1). In particular, we impose conditions on the model rates of the population balance equation for which the first statement of Corollary 3.2 holds. Towards this end, we use the well-known Gershgorin theorem for locating eigenvalues of a matrix. The Gershgorin theorem states that each eigenvalue of A lies in one of the the circular areas, called Gershgorin disks, in the complex plane that is centered at the ith diagonal element and whose radius is R_i,

$$\{z \in \mathbb{C} : |z - a_{ii}| \leq R_i\} ,$$

where

$$R_i = \sum_{j=1, j\neq i}^{n} |a_{ji}| .$$

Since the approximate system for the microbial flocculation model is nonlinear, we linearize the

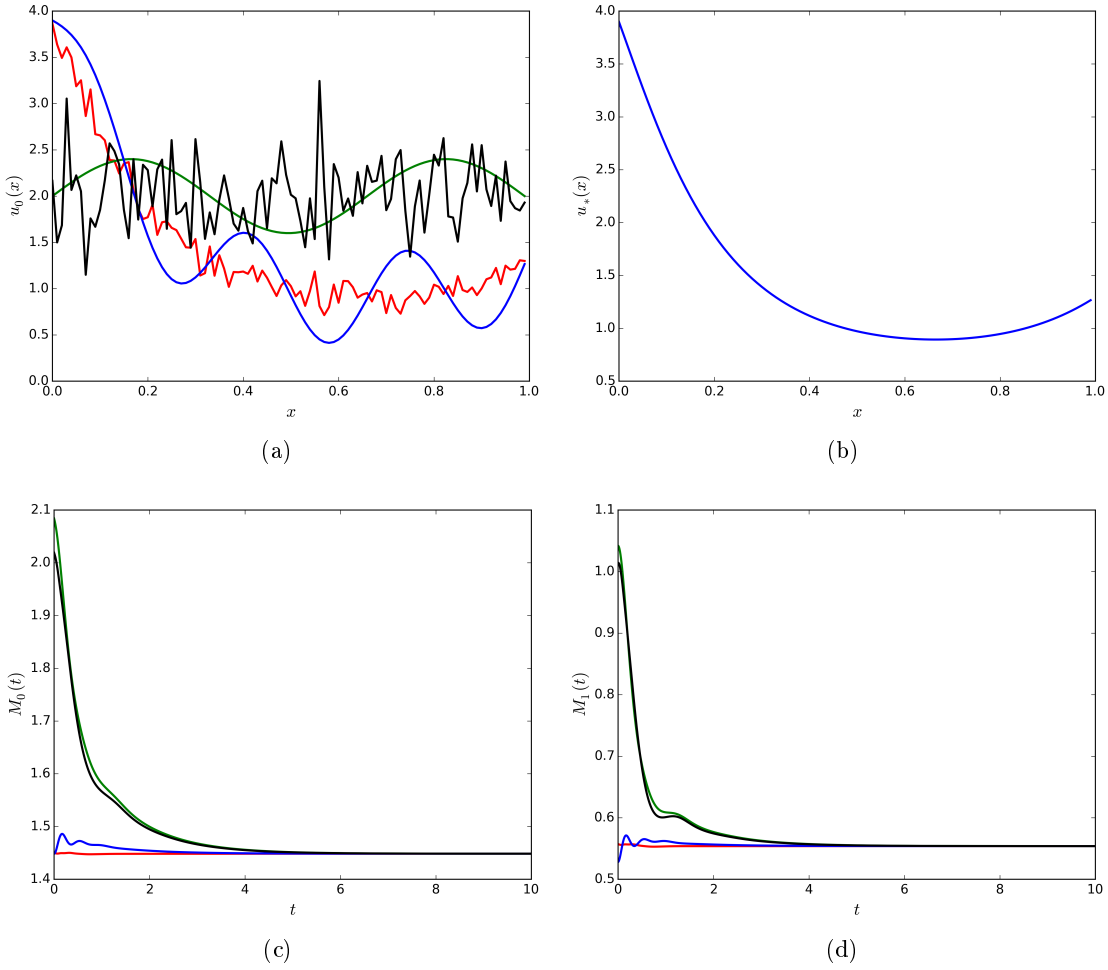

Figure 3.4: Time evolution of the flocculation model with arbitrary initial conditions. a) Four different initial conditions are chosen close to the steady state. b) Solution of the PBE for those initial conditions at $t = 10$. c) Evolution of the total number $M_0(t)$ of the flocs for $t \in [0, 10]$. d) Evolution of the total mass $M_1(t)$ of the flocs for $t \in [0, 10]$.

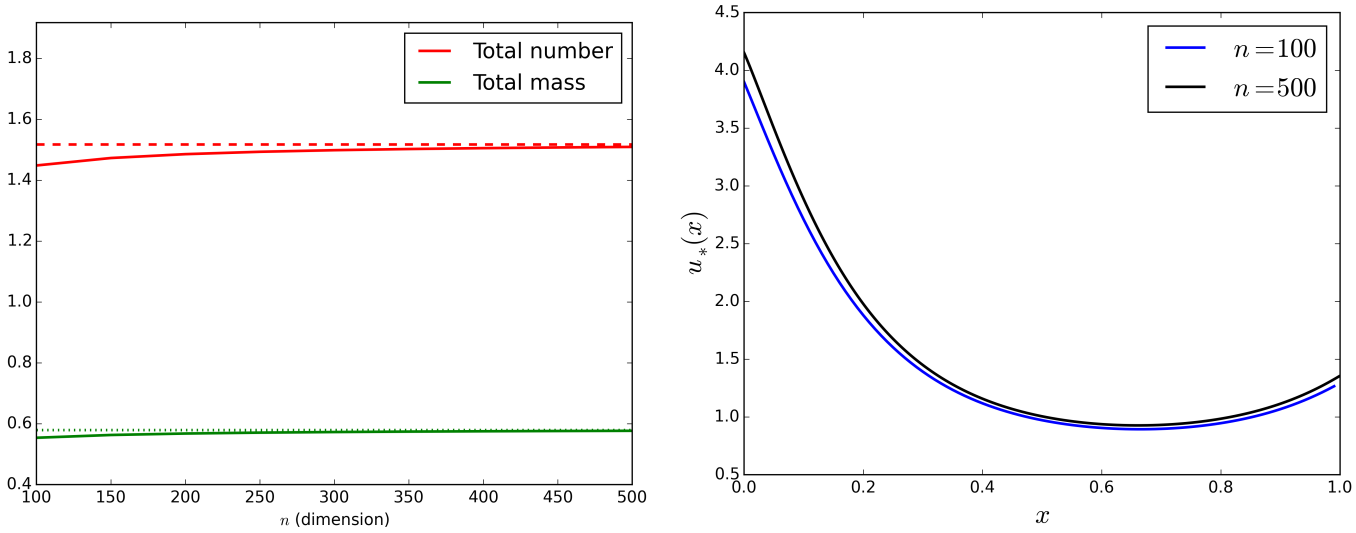

(a) (b)

Figure 3.5: Change in zeroth and first moments with increasing dimension of the approximate space $\mathcal{X}_n$. a) Change in the total number and the total mass of the flocs with respect to increasing dimension n. Dashed red lines and dotted green lines corresponds to the total number and the total mass of the flocs of the steady state for $n = 1000$, respectively. b) Steady state solution for $n = 100$ and $n = 500$.

system around its stationary solutions. Let $u_* \in L^1(0, \overline{x})$ be a stationary solution of (1.1) and denote the projection of the stationary solution u_* onto $\mathbb{R}^n$ by $\alpha = P_n u_* = [\alpha_1, \cdots, \alpha_n]^T$, then the Jacobian of the approximate operator $\mathcal{F}_n$ defined in (3.16) can be written as

$$J_{\mathcal{F}}(\alpha) = \mathcal{G}_n + J_{\mathcal{A}}(\alpha) + J_{\mathcal{B}}(\alpha)\,, \tag{3.18}$$

where $\mathcal{G}_n$ is defined in (3.13),

$$J_{\mathcal{A}}(\alpha) = \begin{pmatrix} -\alpha_1 k_a(x_1^n,\, x_1^n)\Delta x & -\alpha_1 k_a(x_1^n,\, x_2^n)\Delta x & \cdots & -\alpha_1 k_a(x_1^n,\, x_{n-1}^n)\Delta x & 0 \\ -\alpha_2 k_a(x_2^n,\, x_1^n)\Delta x & \cdots & -\alpha_2 k_a(x_2^n,\, x_{n-2}^n)\Delta x & 0 & 0 \\ \vdots & \vdots & \ddots & \vdots & \vdots \\ -\alpha_{N-1} k_a(x_{n-1}^n,\, x_1^n)\Delta x & 0 & \cdots & 0 & 0 \\ 0 & 0 & \cdots & 0 & 0 \end{pmatrix}$$

$$+ \begin{pmatrix} -\sum_{j=1}^{n-1} k_a(x_1^n,\, x_j^n)\alpha_j \Delta x & 0 & \cdots & 0 & 0 \\ \alpha_1 k_a(x_1^n,\, x_1^n)\Delta x & -\sum_{j=1}^{n-2} k_a(x_2^n,\, x_j^n)\alpha_j \Delta x & 0 & \cdots & 0 \\ \alpha_2 k_a(x_1^n,\, x_2^n)\Delta x & \alpha_1 k_a(x_2^n,\, x_1^n)\Delta x & \ddots & 0 & \vdots \\ \vdots & \vdots & \ddots & -\sum_{j=1}^{1} k_a(x_{n-1}^n,\, x_j^n)\alpha_j \Delta x & 0 \\ \alpha_{n-1} k_a(x_1^n,\, x_{n-1}^n)\Delta x & \alpha_{n-2} k_a(x_2^n,\, x_{n-2}^n)\Delta x & \cdots & \alpha_1 k_a(x_{n-1}^n,\, x_1^n)\Delta x & 0 \end{pmatrix},$$

and

$$J_{\mathcal{B}}(\alpha) = \begin{pmatrix} -\frac{1}{2}k_f(x_1^n) & \Gamma(x_1^n; x_2^n)k_f(x_2^n)\Delta x & \Gamma(x_1^n; x_3^n)k_f(x_3^n)\Delta x & \cdots & \Gamma(x_1^n; x_n^n)k_f(x_n^n)\Delta x \\ 0 & -\frac{1}{2}k_f(x_2^n) & \Gamma(x_2^n; x_3^n)k_f(x_3^n)\Delta x & \cdots & \Gamma(x_2^n; x_n^n)k_f(x_n^n)\Delta x \\ \vdots & 0 & \ddots & \ddots & \vdots \\ 0 & \cdots & 0 & -\frac{1}{2}k_f(x_{n-1}^n) & \Gamma(x_{n-1}^n; x_n^n)k_f(x_n^n)\Delta x \\ 0 & 0 & \cdots & 0 & -\frac{1}{2}k_f(x_n^n) \end{pmatrix}$$

To bound the eigenvalues of $J_{\mathcal{F}}(\alpha)$ we use Gershgorin theorem. Consequently, the centers and the radii of Gershgorin disks are given by

$$a_{ii} = -\frac{1}{\Delta x} g(x_i^n) - \mu(x_i^n) - \frac{1}{2}k_f(x_i^n) - \alpha_i k_a(x_i^n,\, x_i^n)\Delta x - \sum_{j=1}^{n-i} k_a(x_i^n,\, x_j^n)\alpha_j \Delta x$$

and

$$R_i \leq \frac{1}{\Delta x} g(x_i^n) + q(x_i^n) + \sum_{j=1}^{i-1} \Gamma(x_j^n; x_i^n)k_f(x_i^n)\Delta x + \sum_{j=1}^{n-i} \alpha_j k_a(x_j^n,\, x_i^n)\Delta x + \sum_{j=1,\, j\neq i}^{n-i} \alpha_j k_a(x_i^n,\, x_j^n)\Delta x\,,$$

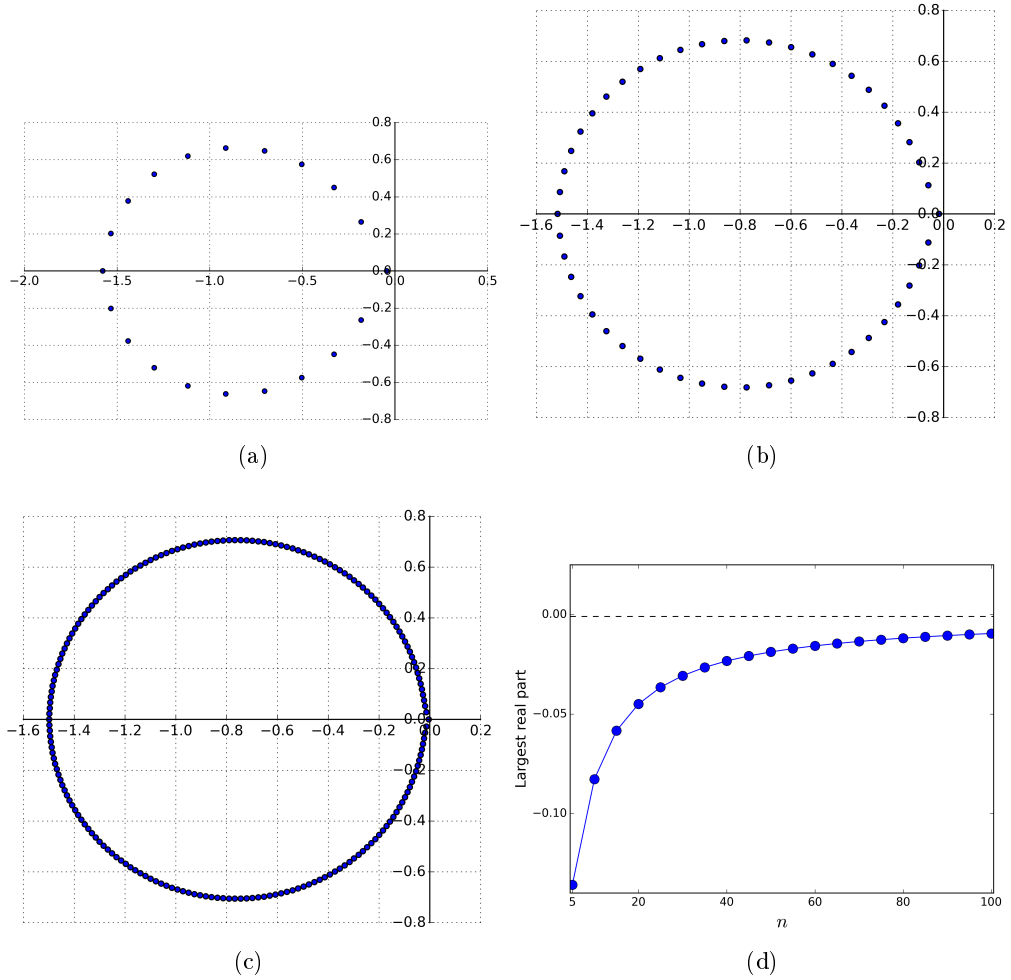

Figure 3.6: Eigenvalues of the Jacobian $J_{\mathcal{F}}(\alpha)$ multiplied by Δx for the steady state illustrated in Figure 3.3a. a) Eigenvalues of the Jacobian plotted in the complex plane for $n = 20$. b) Eigenvalues of the Jacobian plotted in the complex plane for $n = 50$. c) Eigenvalues of the Jacobian plotted in the complex plane for $n = 200$. d) Change in the rightmost eigenvalue for increasing n. Dashed black line corresponds to the rightmost eigenvalue of the Jacobian for $n = 1000$.

respectively. Consequently, if we can show that

$$|a_{ii}| > R_i \qquad \text{for each } i \in \{1, \ldots, n\} \,, \tag{3.19}$$

then each of the Gershgorin disks lie strictly on the left side of the complex plane. To this end, inequality (3.19) can be simplified as

$$\mu(x_i^n) + \frac{1}{2}k_f(x_i^n) > q(x_i^n) + \sum_{j=1}^{i-1} \Gamma(x_j^n; x_i^n) k_f(x_i^n) \Delta x + \sum_{j=1}^{n-i} \alpha_j k_a(x_j^n,\, x_i^n) \Delta x \tag{3.20}$$

for each $i \in \{1, \cdots, n\}$. Accordingly, taking the limit of (3.20) as $n \to \infty$ yields

$$\mu(x) + \frac{1}{2}k_f(x) > q(x) + \int_0^x \Gamma(y,\, x) k_f(x)\, dy + \int_0^{\overline{x}-x} k_a(x,\, y) u_*(y)\, dy \tag{3.21}$$

for all $x \in [0,\, \overline{x}]$ and together with the number conservation requirement (1.5) implies

$$q(x) + \frac{1}{2}k_f(x) - \mu(x) + \int_0^{\overline{x}-x} k_a(x,\, y) u_*(y)\, dy < 0$$

for all $x \in [0,\, \overline{x}]$. Conversely, note that the integral approximations in (3.20) are right Riemann sums. Therefore, if the functions $\Gamma(y,\, x)$ and $k_a(x,\, y)u_*(y)$ are decreasing in y then integral approximations in (3.20) are underestimation of the integrals in (3.21). Thus, the inequality stated in (3.21) ensures that the eigenvalues of the Jacobian $J_{\mathcal{F}}(\alpha)$ are strictly negative for all sufficiently large n. Now, we are in a position to summarize the results of this section in the following proposition.

Proposition 3.3. *Let u_* be a stationary solution of the microbial flocculation model (1.1). Moreover, if*

$$q(x) + \frac{1}{2}k_f(x) - \mu(x) + \int_0^{\overline{x}-x} k_a(x,\, y) u_*(y)\, dy < 0 \tag{3.22}$$

for all $x \in [0,\, \overline{x}]$ and

$$\partial_y \left(k_a(x,\, y) u_*(y)\right) \leq 0 \text{ and } \partial_y \Gamma(y,\, x) \leq 0 \tag{3.23}$$

for all $x \in [0,\, \overline{x}]$ and $y \in [0,\, \overline{x}]$, then stationary solution u_* is approximately locally stable in the

sense of Definition 3.1.

To illustrate the utility of the framework developed in this section we applied our approach to the model rates given in Section 3.2.1 for generation of Figure 3.3a. The Beta distribution used for the post-fragmentation function Γ is not monotonically decreasing, and thus it does not satisfy the conditions of Proposition 3.3. However, Figure 3.6a-c illustrates that the model rates satisfy the conditions of Corollary 3.2. In fact, Figure 3.6d depicts that for the steady state illustrated in Figure 3.3a the eigenvalues of $J_{\mathcal{F}}(P_n u_*)$ have strictly negative real part for $n \geq 5$. Therefore, as it has already been established in Figure 3.4, this steady state solution is locally asymptotically stable in the sense of Corollary 3.2.

3.3 Concluding remarks

Our primary motivation in this chapter was to show that available numerical tools in the literature can facilitate theoretical analysis of evolution equations. Towards this end we developed a numerical framework for theoretical analysis of evolution equations arising in population dynamical models. The main idea behind this framework is to approximate generators of semigroups of evolution equations and use numerical tools to study stability of steady states of evolution equations. We demonstrated the utility of our approach by applying the numerical framework to both linear and nonlinear size-structured population models. In particular, we generated approximate existence and stability regions of the steady states of both models (which can be difficult to obtain by using conventional analytical tools). We showed that our numerical framework can also be used to gain insight about the approximate local stability (see Definition 3.1) of stationary solutions. Furthermore, code used for the numerical simulations can be obtained from our GitHub repository under the open source MIT License (MIT) (Mirzaev, 2015).

Although the stability inequality in (3.7) holds for arbitrarily large finite time intervals, behavior of the solutions as $t \to \infty$ is unclear. Hence, we note that the local stability of the stationary solutions specified in Corollary 3.2 is not in a usual Lyapunov sense. In order to prove Lyapunov stability of stationary solutions using the approximation scheme presented in Section 3.1.1, one has to prove uniform convergence of the approximation scheme for all $t \geq 0$. Hence, as a future plan we wish to utilize the numerical framework presented here to establish Lyapunov stability of stationary

solutions of general evolution equations.

Chapter 4

Efficient numerical approximation of non-trivial stationary solutions

In Chapter 3 we developed a numerical framework for numerical computation and stability analysis of positive stationary solutions of size-structured population models. However, the employed numerical scheme was only first order accurate and thus required large approximation dimension for a reasonable accuracy. Therefore, in this chapter, we wish to improve on the numerical scheme of Chapter 3. In particular, we develop several efficient and high-precision numerical schemes to approximate stationary solutions of the microbial flocculation equations. All the codes employed for the numerical simulations of this chapter can be found in my GitHub repository (Mirzaev, 2017). We also note that the results of this chapter have not been published yet and are merely explorations of numerical issues encountered in the approximation of the stationary solutions of the microbial flocculation equations.

Recall that at steady state the microbial flocculation equations reduce to first order integro-differential equation

$$\begin{aligned}\partial_x(gu_*) = \frac{1}{2}\int_0^x k_a(x-y,\, y)u_*(x-y)u_*(y)\,dy - u_*(x)\int_0^{\overline{x}-x} k_a(x,\, y)u_*(y)\,dy \\ + \int_x^{\overline{x}} \Gamma(x;\, y)k_f(y)u_*(y)\,dy - \frac{1}{2}k_f(x)u_*(x) - \mu(x)u_*(x)\end{aligned} \tag{4.1}$$

with a boundary condition

$$g(0)u_*(0) = \int_0^{\overline{x}} q(x)u_*(x)dx\,.$$

This in turn can be expressed in the form of a boundary value problem.

$$\frac{du_*}{dx} = F(x,\, u_*), \qquad u_*(0) = \int_0^{\overline{x}} q(x)u_*(x)dx/g(0)\,. \tag{4.2}$$

If we set

$$\int_0^{\overline{x}} q(x)u_*(x)dx = 1$$

and adjust the renewal rate to the obtained steady state as in Chapter 2, we get an initial value problem

$$\frac{du_*}{dx} = F(x,\, u_*), \qquad u_*(0) = 1/g(0)\,. \tag{4.3}$$

Using Picard's Existence Theorem for IVPs, one can show that the IVP (4.3) has a unique solution for a suitably chosen interval around the initial condition. Therefore, the above IVP is well-posed. Note that we still need results of Chapter 2 for the existence of a positive stationary solution since Picard's Existence Theorem does not guarantee positivity of solutions of (4.3).

The solutions of the IVP (4.3) can be approximated using various numerical schemes such as finite difference, finite element, and spectral methods. One of the straightforward ways to approximate solutions of IVPs is using finite difference methods. Hence, in Section 4.1, we present a numerical scheme based on finite difference method. We compare accuracy and rate of convergence of several multistep Finite Difference methods up to order four.

In Section 4.2, we develop another numerical scheme to approximate the solutions of the IVP (4.3). The numerical scheme is based on spectral collocation method and thus yields very accurate results even for small approximation dimensions. We exploit spectral accuracy of the method for the numerical spectral analysis. In particular, we illustrate that the eigenvalues of the Fréchet derivative (2.10) evaluated at the stationary solutions can be approximated using spectral collocation method. This in turn allows to heuristically deduce local stability of numerically computed steady states. Furthermore, in Section 4.3, we explore the stationary solutions of the model for various biologically relevant parameters and give valuable insights for the efficient removal of suspended particles.

Unless otherwise stated, all the model rates and parameters used for the simulations in this

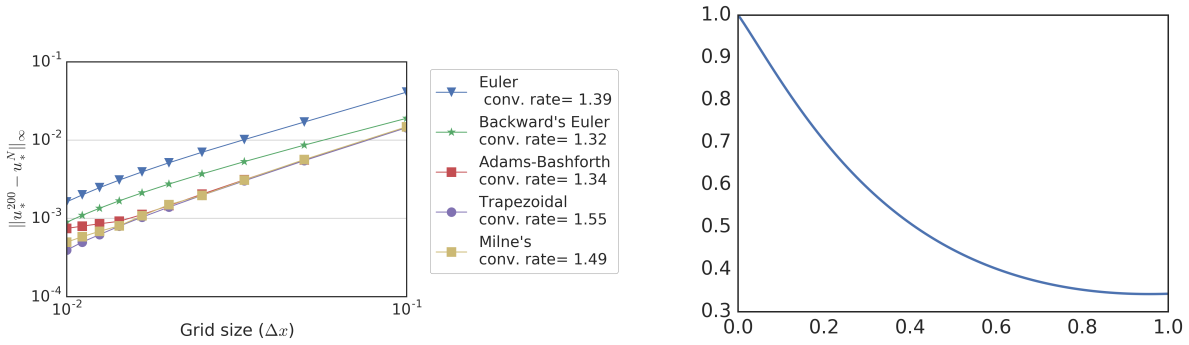

(a) (b)

Figure 4.1: Results of numerical simulation of Finite Difference methods. a) Rate of convergence (compared to $u_*^{200}(x)$) for different Finite Difference Methods. a) Steady state solution for $C_g = 1$ and $\dot{\gamma} = 1$ using Trapezoidal method.

chapter are given in Appendix A.

4.1 Finite Difference Methods

This initial value problem can be easily approximate using *Euler's method*

$$u_{n+1} = u_n + \Delta x F(x_n, u_n)\,. \tag{4.4}$$

Integrals in the IVP can be approximated using a second order Trapezoidal method

$$\int_0^{\overline{x}} f(s)\,ds \approx \frac{\Delta x}{2} \sum_{i=0}^{N-1} \left(f(x_{i+1}) + f(x_i)\right)\,,$$

Therefore, the resulting system is implicit and thus has to be solved using a root finding algorithm, e.g., Newton's algorithm. In principle, since the IVP (4.3) is a well-posed, the root finding algorithm should converge to the unique solution of IVP provided that the algorithm is seeded sufficiently close to the solution of the IVP.

Euler's method can be easily modified to the first order *Backward Euler method*,

$$u_{n+1} = u_n + \Delta x F(x_{n+1}, u_{n+1})\,. \tag{4.5}$$

the second order *Trapezoidal Method*,

$$u_{n+1} = u_n + \frac{\Delta x}{2}\left(F(x_n,\, u_n) + F(x_{n+1},\, u_{n+1})\right)\,, \tag{4.6}$$

the third order *Adams-Bashforth method*

$$u_{n+1} = u_n + \frac{\Delta x}{12}\left(23F(x_n,\, u_n) - 16F(x_{n-1},\, u_{n-1}) + 5F(x_{n-2},\, u_{n-2})\right)\,, \tag{4.7}$$

and the fourth order *Milne's Method*,

$$u_{n+1} = u_{n-1} + \frac{\Delta x}{3}\left(F(x_{n-1},\, u_{n-1}) + 4F(x_n,\, u_n) + F(x_{n+1},\, u_{n+1})\right)\,, \tag{4.8}$$

The rate of convergences of the above methods are illustrated in Figure (4.1a). Backward Euler method and Trapezoidal method perform better compared to Euler's Method. However, increasing the order of the method to third order with Adams-Bashforth and fourth order with Milne's method did not improve the rate of convergence and accuracy. In fact, both Adams-Bashforth and Milne's methods marginally underperformed Trapezoidal method. An example steady state solution for $C_g = 1$ and $\dot{\gamma} = 1$, computed using Trapezoidal method, is depicted in Figure 4.1b.

Although the Trapezoidal method, the best of the five methods listed above, has convergence rate of 1.55, it achieves three digit precision (10^{-3}) only after $N = 70$. In the subsequent section, we show that this rate of convergence and accuracy can be significantly improved using spectral collocation methods.

4.2 Spectral collocation method

In this section, we develop a numerical scheme to approximate non-trivial stationary solutions of the general size-structured flocculation model, (1.1). The approximation scheme is based on spectral collocation method. Spectral collocation method, also known as pseudospectral methods, is a subclass of Galerkin spectral methods (Fornberg, 1998; Trefethen, 2000). Spectral methods have higher accuracy compared to Finite difference and Finite Element methods and thus have widespread use for the numerical simulation of partial differential equations. The main idea behind the method is to express numerical solutions as a finite expansion of some set of basis functions

on a number of points on the domain (i.e., collocation points). Convergence of the approximations depend only on the smoothness of the solutions and thus the method can attain high precision even with a few grid points.

We approximate the stationary solution $u_*(x)$ as linear combination of Nth degree polynomials $\{\phi_j(x)\}_{j=0}^N$, i.e.,

$$[I_N u_*](x) = \sum_{j=0}^{N} u_*(x_j)\phi_j(x)\,,$$

for some collocation points $\{x_j\}_{j=0}^N \subset I$. Furthermore, we require that this approximation is exact at collocation points, i.e.,

$$\phi_j(x_k) = \begin{cases} 1 & \text{if } j = k \\ 0 & \text{otherwise} \end{cases}.$$

The polynomials $\{\phi_j(x)\}_{j=0}^N$ satisfying the above requirements are called cardinal functions. Straightforward way to compute such polynomials is using Lagrangian interpolation, i.e.,

$$\phi_j(x) = \frac{\pi(x)}{\pi'(x_j)(x - x_j)}\,, \tag{4.9}$$

where $\pi(x) = \Pi_{j=0}^N (x - x_j)$. Consequently, derivative can be computed as

$$\frac{d}{dx}[I_N u_*](x) = \sum_{j=0}^{N} u_*(x_j)\phi_j'(x)\,.$$

This in turn implies that derivative at x_i can be computed as linear combination of $\{u_*(x_j)\}_{j=0}^N$. Plugging in collocation points into above equation yields the differentiation matrix $[D]_{i,j} = \phi_j'(x_i)$. Entries of D can be computed explicitly as

$$D_{ij} = \frac{\pi'(x_i)}{\pi'(x_j)(x_i - x_j)}$$

for off-diagonal entries $i \neq j$ and

$$D_{jj} = \sum_{k=0,\, k\neq j}^{N} \frac{1}{x_j - x_k}$$

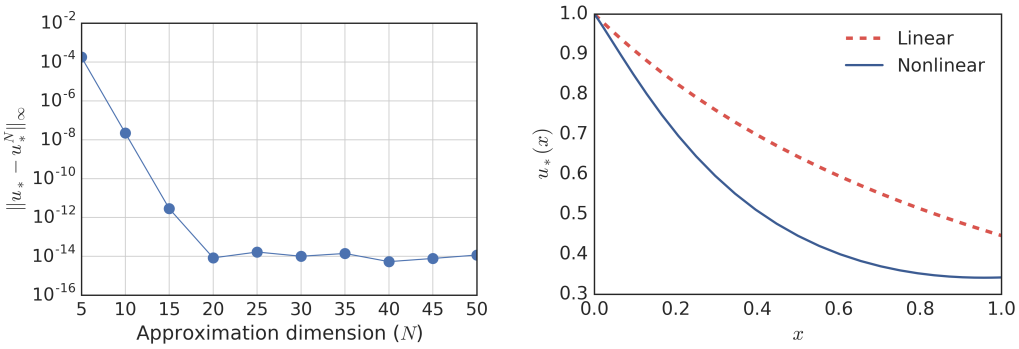

(a) (b)

Figure 4.2: a) Error in approximation of the steady states of linear Sinko-Streifer. Compared to existing analytical solution. b) Example steady state solutions for linear Sinko-Streifer equations and nonlinear microbial flocculation equations

for diagonal entries. Let $\vec{u}$ denote the vector

$$\begin{bmatrix} u_*(x_0) & \cdots & u_*(x_N) \end{bmatrix}^T,$$

then derivatives at collocation points are given by

$$\begin{bmatrix} u'_*(x) & \cdots & u'_*(x_N) \end{bmatrix}^T = D\vec{u}\,.$$

When a smooth function is interpolated by polynomials in N equally space points, the approximations sometimes fail to converge as $N \to \infty$, which is also known as *Runge phenomenon*. Moreover, when using uniform gird points, the elements of the differentiation matrix not only fail to converge but they get worse and diverge as $N \to \infty$. For the spectral collocation methods, it is a general consensus to cluster the grid points roughly quadratically toward the endpoints of the interval (Fornberg, 1998). Therefore, for collocation points we use unevenly space grid points. Unless, otherwise specified, we employ non-uniform shifted Chebyshev-Gauss-Lobatto grid points,

$$x_j = \left(1 - \cos\left(\frac{j\pi}{N}\right)\right)\frac{\overline{x}}{2} \qquad \forall i = 0, 1, \ldots, N\,. \tag{4.10}$$

Points $\left\{\cos\left(\frac{j\pi}{N}\right)\right\}_{j=0}^{N}$ are in fact extrema of Nth Chebyshev polynomial on the interval $-1 \leq x \leq 1$.

At this point we can approximate steady states of Sinko-Streifer model presented in Section

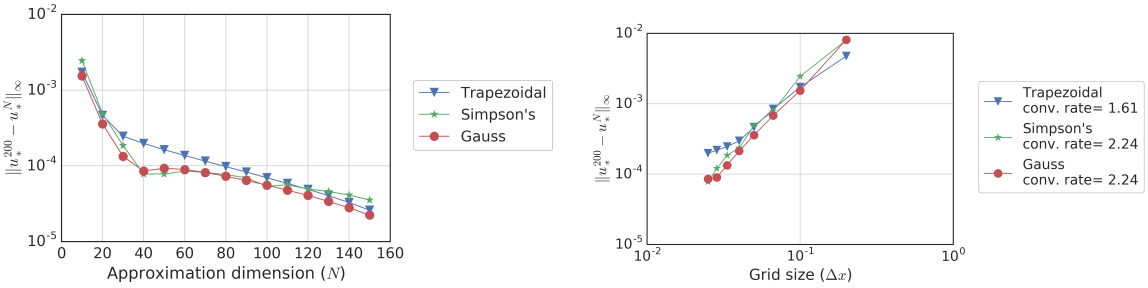

(a) (b)

Figure 4.3: Comparison of integral approximations. a) Absolute error compared to approximate solution for $N = 200$. b) Rate of convergence of the methods for $N \leq 50$.

(3.1.3). Recall that for this model the analytical stationary solution can be calculated exactly (see Mirzaev & Bortz (2017) for the derivation) as

$$u_*(x) = \frac{1}{g(x)} \exp\left(- \int_0^x \frac{\mu(s)}{g(s)}\, ds \right) . \tag{4.11}$$

In Figure 4.2a, we compared numerical approximations of the stationary solution to exact solution given in (4.11). The absolute error decreases exponentially fast for increasing approximation dimension N. Numerical approximation attains machine precision for $N \geq 20$. Moreover, an example steady state solution of Sinko-Streifer model is given in Figure 4.2b.

For the numerical approximations of the steady state of the microbial flocculation model (1.1)For integral approximations we tried three different integration methods on non-uniform grids. Namely, Trapezoidal rule

$$\int_0^{\overline{x}} f(s)\, ds \approx \frac{1}{2} \sum_{i=0}^{N-1} (x_{i+1} - x_i)\, (f(x_{i+1}) + f(x_i)) \ ,$$

Simpson's rule as implemented in `scipy.integrate.simps` and Gaussian quadrature

$$\int_0^{\overline{x}} f(s)\, ds \approx \sum_{i=0}^{N} w_i f(x_i)\, .$$

We require Gaussian quadrature to be exact for chosen cardinal functions $\{\phi_i(x)\}_{i=0}^N$, which yields weights

$$w_i = \int_0^{\overline{x}} \phi_i(s)\, ds\, .$$

Moreover, in the evaluation of the integrals in (1.3) one has to evaluate $[I_N u_*](x)$ at non-

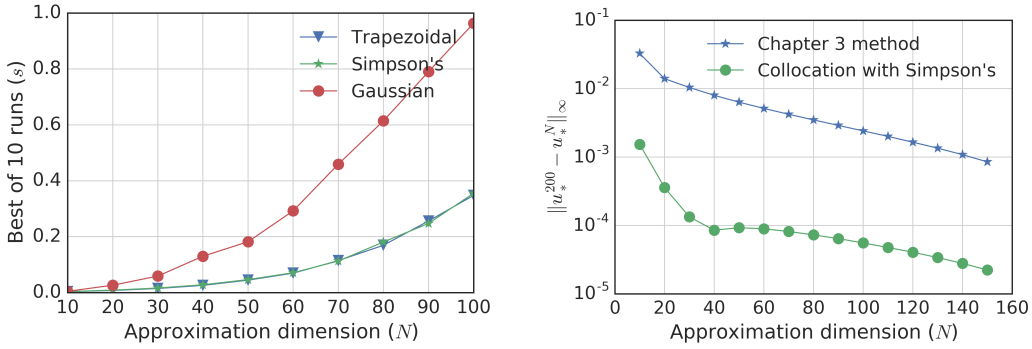

(a) (b)

Figure 4.4: a) Computation times for the numerical schemes with different integral approximation methods b) Error comparison of the previous method developed in Chapter 3 with the improved method developed here.

collocation points, i.e.,

$$[I_N u_*]\,(x_k - x_i) = \sum_{j=0}^{N} u_*(x_j)\phi_j(x_k - x_i)\,. \tag{4.12}$$

Once $\phi_j(x_k - x_i)$ are calculated explicitly using (4.9), the approximations at non-collocation points (4.12) can be evaluated as linear combination of entries of $\vec{p}$. For efficient implementation the elements $\phi_j(x_k - x_i)$ can be initialized as entries of three dimensional array, i.e.,

$$[\Phi]_{k,i,j} = \begin{cases} \phi_j(x_k - x_i) & \text{if } k \geq i \\ 0 & \text{otherwise} \end{cases}.$$

Consequently, approximation for (4.12) can be obtained as

$$[I_N u_*]\,(x_k - x_i) = \sum_{j=0}^{N} [\Phi]_{k,i,j}\vec{u}_j\,,$$

which is simply dot product of three dimensional array Φ with the vector $\vec{u}$.

Furthermore, we have plotted computation times required for the execution of each method with respect to approximation dimension N. The approximations based on Trapezoidal and Simpson's rule perform similarly on computation times. However, the approximation based on Gaussian Quadrature becomes very inefficient with the increasing approximation dimension N.

Spectral collocation methods are very sensitive to the node distribution. Consequently, in Figure

4.5, we have compared the precision of the schemes for unevenly space grid points with different clustering at the ends of the interval. Node distributions were selected from a well-known one-parameter family of node density functions,

$$\mu_\gamma(x) = \frac{c_\gamma}{(1-x^2)^\gamma}\,,$$

where $\gamma < 1$ and $c_\gamma = \pi^{-1/2}\Gamma(1.5-\gamma)/\Gamma(1-\gamma)$ (Fornberg, 1998). Consequently, nodes $\{x_j\}_{j=0}^N$ were generated satisfying

$$\frac{j}{N} = \int_{-1}^{x_j} \mu_\gamma(x)\,dx\,.$$

Note that for $\gamma = 0$ this density function generates evenly spaced grids and for $\gamma = 0.5$ it generates Chebyshev-Gauss-Lobatto grid points given in (4.10). All the grid points are in the interval $[-1,\,1]$ and thus were mapped to the interval $[0,\,\overline{x}]$ using an affine map,

$$x \to (x+1)\frac{\overline{x}}{2}\,.$$

Figures 4.5a and 4.5b illustrate that both numerical schemes with Simpson's rule and Gaussian quadrature favor node distributions close to $\gamma = 0.5$. Node distribution with $\gamma = 0.5$ roughly corresponds to quadratic clustering of the nodes towards the ends of the interval, which is consistent with the results in the literature (Fornberg, 1998; Trefethen, 2000).

Furthermore, in Figure 4.6, we tested out the numerical schemes on different quadratically clustered node distributions. For our purposes, we have considered the following grids: zeros of Nth order Chebyshev polynomial, extrema of Nth order Chebyshev polynomial, zeros of Nth order Legendre polynomial and extrema of Nth order Legendre polynomial. Figures 4.6a and 4.6b illustrate that both numerical schemes with Simpson's rule and Gaussian quadrature perform qualitatively the same on different grid points. Different choices of node distributions affect initial convergence of both schemes significantly. However, for large N both numerical schemes attain about the same precision.

Overall, Spectral Collocation method developed in this section have at least quadratic rate of convergence and achieve much higher precision compared to Finite Difference methods developed in Section 4.1. In particular, Spectral Collocation method with Simpson's rule for quadrature is

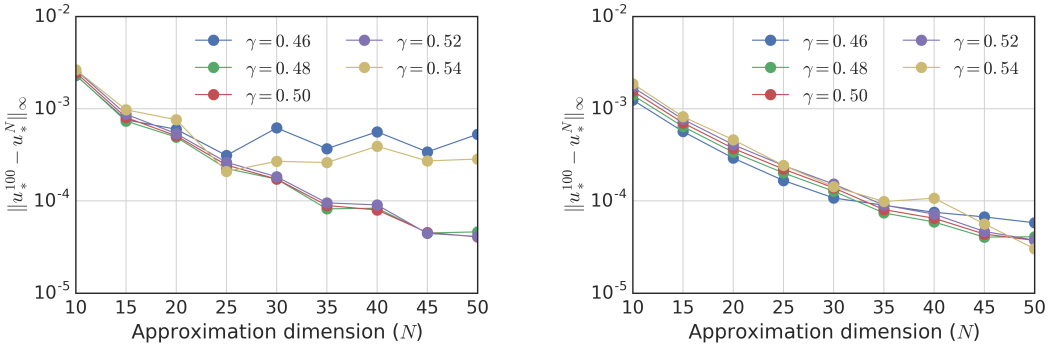

(a) (b)

Figure 4.5: Error comparison for unevenly spaced grid points with different density. a) Numerical scheme with Simpson's rule b) Numerical scheme with Gaussian quadrature

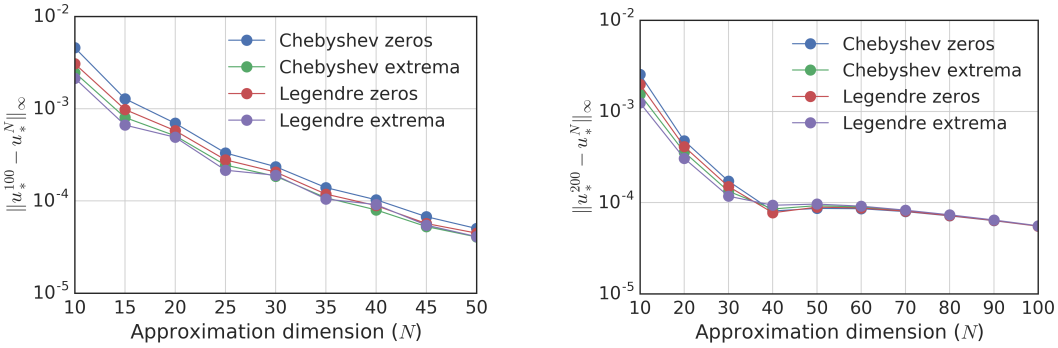

(a) (b)

Figure 4.6: Error comparison for different unevenly spaced grid points. a) Numerical scheme with Simpson's rule b) Numerical scheme with Gaussian quadrature

accurate and takes considerably less computation time. Therefore, in the subsequent sections, we will only employ this method for steady state approximations.

Furthermore, as illustrated in Figure 4.4b, the best numerical scheme of this chapter is much more accurate compared to the numerical scheme utilized in Chapter 3. Particularly, the numerical scheme of this chapter achieves three digit precision for $N \geq 20$, which is achieved by the numerical scheme of the previous chapter for only $N \geq 140$.

4.3 Numerical Exploration of Steady States

In this section, we explore the stationary solutions of the model for various biologically relevant parameters and give valuable insights for the efficient removal of suspended particles.

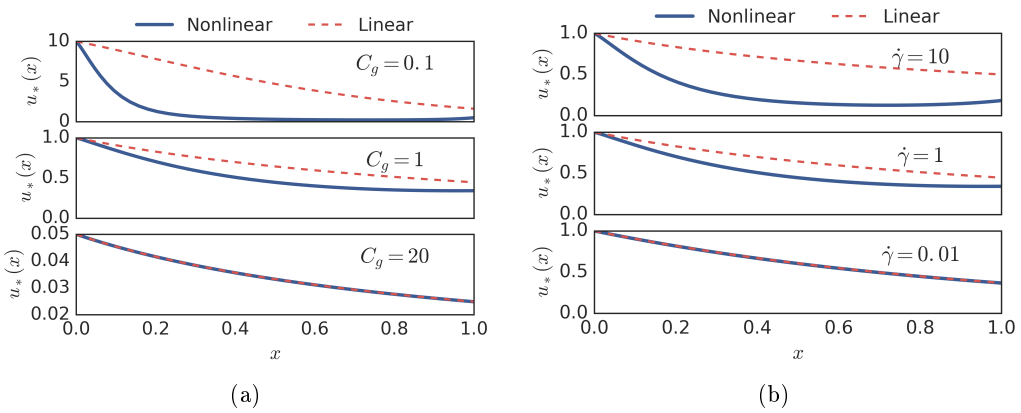

(a) (b)

Figure 4.7: Results of some numerical simulations. Dashed red and solid blue lines correspond to the stationary of the linear Sinko-Streifer and the nonlinear microbial flocculation equations, respectively. a) Steady state solutions for increasing growth rate b) Steady state solutions for decreasing shear rate

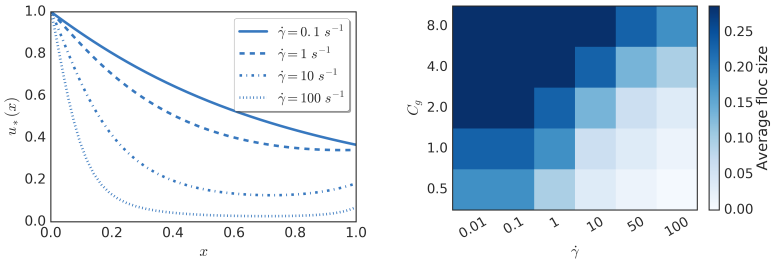

(a) (b)

Figure 4.8: Effect of the shear rate on the average floc size and the renewal rate. a) Increasing the shear rate results in stationary distributions with smaller average floc size. b) For each given growth rate of a microbial floc, increasing the shear rate decreases the average floc size.

Stationary solutions of the linear and nonlinear case for several different values of C_g are depicted in Figure 4.7a. It is interesting to note that for increasing values of C_g the growth dominates and thus stationary solution of the nonlinear case approaches the stationary solutions of the linear case. Analogously, as one could expect, results in Figure 4.7b indicate that as $\dot{\gamma} \to 0$ the stationary solutions of the microbial flocculation model converge to that of essentially linear Sinko-Streifer model.

Thorough control of floc formation is crucial for proper operation of bioreactors used in fermentation industry and waste water treatment. For efficient removal of suspended particles, it is usually desirable to have larger and denser flocs that settle faster under gravitational forces. Therefore, in Figures 4.8a and 4.8b, we investigated the effects of the shear rate on the average floc size. One can

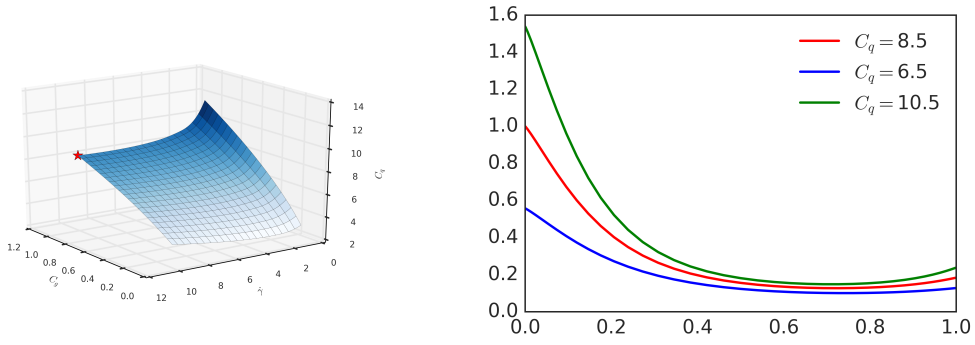

(a) (b)

Figure 4.9: Effect of growth and shear rates on the renewal rate, C_q. a) Renewal rates form a smooth surface. Marked red star corresponds to the point $C_g = 1$, $\dot{\gamma} = 1$ and $C_q = 8.5$ b) Steady states for marked red star and some points below and above the marked point.

observe in Figure 4.8a that increasing the shear rate results in increased fragmentation of the flocs and thus drives the stationary distribution into the smaller size range, which is also consistent with the results of (Flesch et al., 1999). Moreover, results in Figure 4.8b indicate that for each given growth rate of a microbial floc one can adjust the shear rate to yield an optimal average floc size.

As it is stated in Theorem 2.1, for the existence of a positive stationary solution the renewal rate has to be modified according to equation (2.4). Consequently, in Figure 4.9a, for different growth and shear rates we computed the renewal rate C_q based on the equation (6.2). Computed renewal rates lie on a smooth three-dimensional surface. Moreover, the results indicate that the renewal rate is directly proportional to both growth and shear rates.

The numerical algorithm described in this chapter can be easily modified to find steady states of the boundary value problem in (4.2). In this general case, the results of Chapter 2 do not guarantee the existence of a positive steady state. However, Figure 4.9b depicts that positive steady states exist for the points not lying on the surface illustrated in Figure 4.9a. This in turn suggests well-posedness of the boundary value problem given in (4.2) for sufficiently smooth model rates. Therefore, as the future plan, we wish to further investigate well-posedness of this boundary value problem.

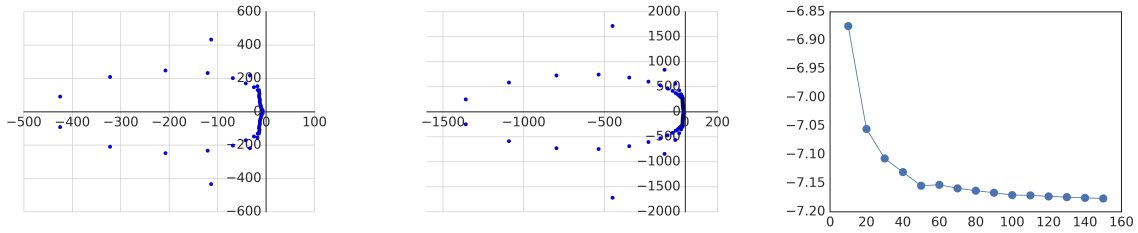

(a) (b) (c)

Figure 4.10: Spectrum of the linearized operator for $C_g = 1$ and $\dot{\gamma} = 10$ a) Spectrum approximation for $N = 50$. b) Spectrum approximation for $N = 100$. c) Convergence of the leading eigenvalues.

4.4 Numerical spectral analysis

In Chapter 2, using the principle of linearized stability, we showed that the local stability of a stationary solution of the microbial flocculation equations depends on the spectrum of the Fréchet derivative of the (1.1) evaluated at the stationary solutions. However, defining the spectrum of an operator is rather cumbersome using analytical techniques. Moreover, stability criteria found depend on the existence of analytical stationary solutions. This in turn makes derived stability criteria hard to validate. Therefore, in this section, we illustrate that the eigenvalues of the Fréchet derivative evaluated at the stationary solutions can be approximated using numerical techniques. This in turn allows deducing local stability of numerically computed steady states.

The Fréchet derivative of the nonlinear operator $\mathcal{F}$ in the equation (1.1) evaluated at a steady state solution u_* is given explicitly by

$$\mathcal{L}[h](x) = D\mathcal{F}(u_*)[h](x) = -\partial_x(g(x)h(x)) - A(x)h(x) + \int_x^{\overline{x}} \Gamma(x;\, y)k_f(y)h(y)\, dy \\ - \int_0^{\overline{x}-x} E(x,\, y)h(y)\, dy + \int_0^x E(x-y,\, y)h(y)\, dy\,, \tag{4.13}$$

where

$$E(x,\, y) = k_a(x,\, y)u_*(x)$$

and

$$A(x) = \frac{1}{2}k_f(x) + \mu(x) + \int_0^{\overline{x}-x} E(y,\, x)\, dy\,.$$

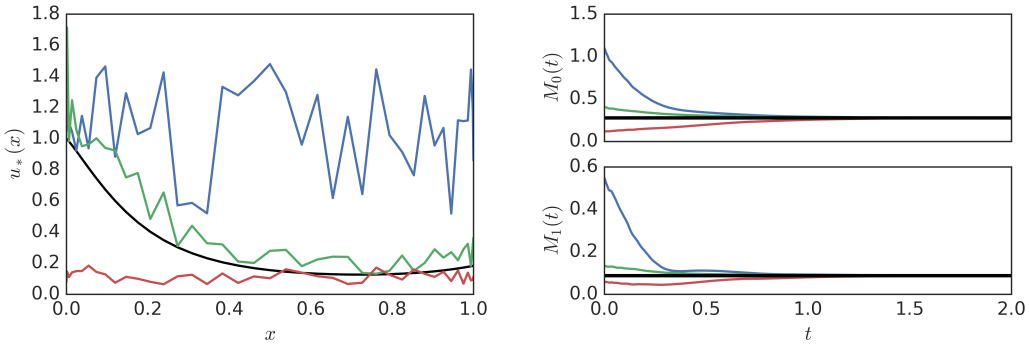

(a) (b)

Figure 4.11: Numerical simulations of the microbial flocculation equations for $C_g = 1$ and $\dot{\gamma} = 10$. a) Initial size distributions. Solid black line represents the steady state solution for $C_g = 1$ and $\dot{\gamma} = 10$. b) Transient behavior of the zeroth and the first moment of the solution.

Hereby, we refer to the operator (4.13) simply as linearized operator.

Spectral methods are powerful tools for the numerical approximation of nonlinear differential and integral eigenvalue problems. We approximate the linearized operator using the pseudospectral method developed in Section 4.2. The eigenvalues of the resulting matrix approximate part of the spectrum of the operator (4.13). The spectral accuracy of the method allows one to work with low-dimensional approximations and still relish efficient performance of the available software packages.

Figures 4.10a and 4.10b illustrate approximate spectrum, $N = 50$ and $N = 100$, of the linearized operator for $C_g = 1$ and $\dot{\gamma} = 10$. Although those two spectral approximations differ qualitatively, Figure 4.10c depicts fast convergence of the leading eigenvalue of the linearized operator.

In Figure 4.11, we numerically simulated the microbial flocculation equation (1.1) for different initial conditions. In particular, we used the approximation scheme described in Section 4.2 for discretization of size x and applied the method of lines to integrate the resulting system of ODEs. We used growth and shear rates $C_g = 1$ and $\dot{\gamma} = 10$, respectively. Recall that the leading eigenvalue of the steady state for this parameters converges to ≈ -7.2. For all the initial conditions given in Figure 4.11a the solutions converged to the stationary solutions represented by a solid black line. As depicted in Figure 4.11b, local stability of the stationary solution is also reflected in the evolution

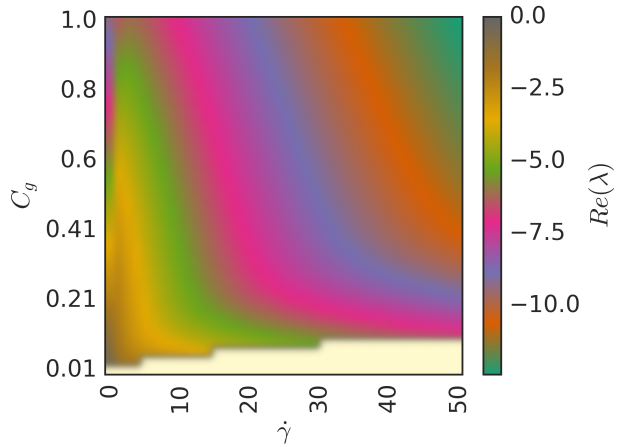

Figure 4.12: Leading eigenvalues of the linearized operator for different growth and shear rates ($N = 50$). Yellow region represents the parameter combinations for which a positive stationary solution has not been found.

of the total number of flocs (zeroth moment),

$$M_0(t) = \int_0^{\overline{x}} p(t,\, x)\, dx\,,$$

and total mass of the flocs (first moment),

$$M_1(t) = \int_0^{\overline{x}} xp(t,\, x)\, dx\,.$$

In Figure 4.12, we computed the leading eigenvalues of the linearized operator for different growth and shear rates. Yellow region represents the parameter combinations for which a positive stationary solution has not been found. For small growth rates increasing the shear rate yields no steady state. Conversely, for larger growth rates increasing the shear rate yields steady states with leading eigenvalues further to the left in the complex plane. Furthermore, for the small growth and shear rates, the leading eigenvalues of the steady states are significantly close to zero. Consequently, in Figure 4.13, we have simulated the microbial flocculation equations for $C_g = 0.1$ and $\dot{\gamma} = 5$. As illustrated in Figure 4.13a, the leading eigenvalue of this steady state converges to ≈ -3.13. One can observe in Figure 4.13c that for the green initial size distribution, chosen sufficiently close to the steady state (solid black line), zeroth and first moments converge to the moments of the steady state. However, for other initial size distributions, chosen marginally further to the steady state,

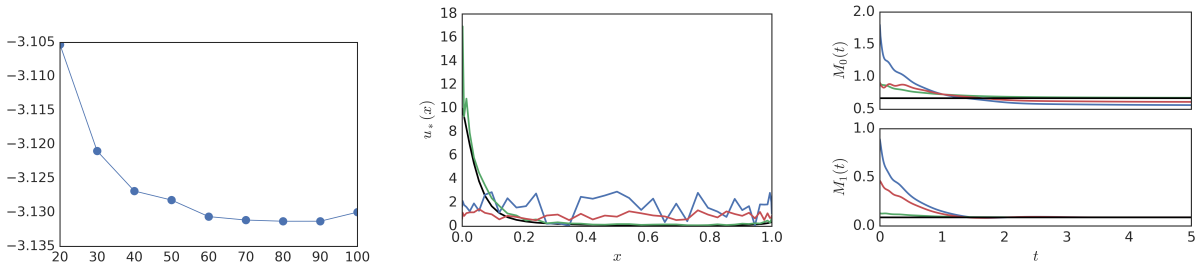

(a) (b) (c)

Figure 4.13: Numerical simulations of the microbial flocculation equations for $C_g = 0.1$ and $\dot{\gamma} = 5$. a) Convergence of the leading eigenvalue b) Initial size distributions. Solid black line represents the steady state solution for $C_g = 0.1$ and $\dot{\gamma} = 5$. c) Transient behavior of the zeroth and the first moment of the solution.

the zeroth moment is converging to the moment of some other steady state. This in turn suggests existence of multiple locally stable stationary solutions. Hence, we conjecture that the leading eigenvalue of the linearized operator (4.13) defines the basin of attraction of the steady state and thus wish to investigate this behavior further.

4.5 Concluding remarks

We developed numerical schemes based on finite difference and spectral collocation methods to approximate nontrivial stationary solutions of the microbial flocculation equations. Trapezoidal method on evenly spaced grid yielded the most accurate results. Moreover, we found that employing higher order finite difference methods did not improve the accuracy of the numerical scheme. Consequently, in Section 4.2, we developed a numerical scheme based on spectral collocation method. We implemented several different integral approximations. Our findings indicate that the spectral collocation method with Simpson's rule for integral approximation yields fast and precise approximations with an at least quadratic rate of convergence. Moreover, we tested the algorithm on several different unevenly spaced grid points. Although different grids affect initial convergence of the numerical schemes, for large N the numerical schemes attain about the same accuracy.

In Section 4.4 we exploit high precision of the approximation scheme developed for the numerical spectral analysis. In particular, we illustrated that the eigenvalues of the Fréchet derivative evaluated at the stationary solutions can be accurately approximated using numerical techniques

of this chapter. This in turn allowed us to heuristically deduce local stability of positive steady states of the microbial flocculation equations. Furthermore, using our numerical scheme we were only able to find locally stable non-trivial stationary solutions. Perhaps, the positive steady states of the microbial flocculation equations satisfying

$$g(0)p(0) = \int_0^{\overline{x}} q(y)u_*(y)\,dy = 1\,,$$

existence of which is guaranteed by Theorem 2.1, are always locally stable. Hence, as a future research, we plan to further investigate the stability of non-trivial steady states of the microbial flocculation equations.

Furthermore, in Section 4.3, we numerically investigated physically relevant parameter ranges. In particular, we studied the effects of the shear rate on the average floc size. Our results, consistent with the results in the literature (Flesch et al., 1999; Spicer et al., 1998; Spicer, 1997), indicate that increasing the shear rate of the stirring tank results in increased fragmentation and thus decreases the steady-state average floc size.

Chapter 5

An Inverse Problem for a Class of Conditional Probability Measure-Dependent Evolution Equations[1]

In this chapter, we examine an inverse problem involving a general conditional probability measure-dependent partial differential equation (PDE) arising in structured population modeling. We consider a general abstract evolution equation with solution b on a Banach space H, defined on an interval $Q \subset \mathbb{R}^+ \cup \{0\}$, depending on the conditional probability measure F:

$$b_t = g(b, F) \tag{5.1}$$

$$b(0, x) = b_0(x) \qquad \forall x \in Q \tag{5.2}$$

for $t \in T = [0, t_f]$ with $t_f < \infty$.

Although estimation of conditional probability measures in statistics is common (Dagan, 1982;

[1]This chapter has been published:
I. Mirzaev, E.C. Byrne & D.M. Bortz. "An Inverse Problem for a Class of Conditional Probability Measure-Dependent Evolution Equations", *Inverse Problems*, 32, no. 9 (July 2016)
Note that a preliminary version of some of the results in this chapter appeared in the dissertation of Dr. Erin Byrne. Those results have been substantially revised and extended and are detailed in this publication.

Hall et al., 2004; Krishnaswamy et al., 2014; Iori et al., 2015), results on the estimation of probability distributions within the context of size-structured models are not widespread. Banks et al. (Banks & Fitzpatrick, 1991; Banks et al., 1999) formulated a Sinko-Streifer model such that growth rates vary probabilistically across individuals of the population and presented inverse problem techniques for estimation of this growth distribution using aggregate population data. Banks & Bihari (2001) developed an inverse problem framework for identifying a single probability measure in general measure-dependent dynamical systems. Later, Banks & Bortz (2005) extended this framework to a class of dynamical systems with distributed temporal delays and countable number of probability measures. All these inverse problem techniques are based on a Prohorov metric framework, for reviews of which we refer readers to (Banks et al., 2012; Banks & Thompson, 2015).

Our study of the class of models in (5.1)-(5.2) is motivated by our interest in fragmentation phenomena, which arise in a wide variety of areas including algal populations (Banasiak & Lamb, 2009; Ackleh & Fitzpatrick, 1997; Ackleh, 1997), cancer metastases (DeVita et al., 2008; Ilana et al., 2006; Wyckoff et al., 2000), and mining (Gamma & Jimeno, 1993; Persson et al., 1994). The most prominent approach to model fragmentation is based on structured population equations, which can be traced back to the works of Smoluchowski (van Smoluchowski, 1917, 1916) and Becker & Döring (1935). The solutions of the forward problem of structured population models has been extensively studied in over the years, and the mathematical techniques for their analysis are highly developed. For the review of these mathematical techniques we refer interested readers to the books by Webb (1985) and Metz & Diekmann (1986). For the applications of the theory in an engineering context we recommend the book by Ramkrishna (2000).

Inverse problems for structured population models have also received a substantial interest in recent years (Gyllenberg et al., 2002; Pilant & Rundell, 1991; Engl et al., 1994; Perthame & Zubelli, 2007). Efficient methodologies for the estimation of growth and mortality rates in physiologically structured Sinko & Streifer (1967) equation has been developed and used to measure the lethal effects of pesticides in insect populations (Banks et al., 2008, 2007a). Estimation of the model rates in a size-structured Bell and Anderson model (Bell & Anderson, 1967), describing the dynamics of proliferation and death processes of a population of cells, has also been widely investigated. Perthame et al. (Perthame & Zubelli, 2007; Doumic et al., 2009) developed an inverse problem methodology for determining the cell division (birth) rate from the measured stable size distribution

of the population. Their approach is based on a novel regularization technique relying on generalized relative entropy estimates (Michel et al., 2005). Later, this methodology was further extended to recover fragmentation rates in growth-fragmentation equations by Doumic et al. (Doumic & Tine, 2012; Bourgeron et al., 2014). For the same model, Luzyanina et al. (Luzyanina et al., 2008, 2006, 2007) formulated a numerical method, based on a maximum likelihood approach, for the robust identification of the cell division rates from CFSE (a type of cell division tracking dye) histogram time-series data. Moreover, several improvements and extensions of this numerical approach has been suggested in (Banks et al., 2010b).

Bortz et al. (2008) developed a size-structured partial differential equation (PDE) model for bacterial *flocculation*, the process whereby flocs, i.e., aggregates, in suspension adhere and separate. For the breakage term in that PDE model, the fragmentation of each parent particle will generate child particles according to a *post-fragmentation conditional probability distribution*. In the literature, it is widespread to assume that this distribution is normally distributed for all parent floc size (Lu & Spielman, 1985; Pandya & Spielman, 1982). However, Byrne et al. (2011) focused only on the fragmentation and developed a microscale mathematical model which contradicts this result and predicted that the distribution is non-normal and conditionally dependent on parent size. Thus it is clear that there is a need for a methodology to identify this conditional distribution from available data.

Building upon the work in (Banks & Bortz, 2005), in this chapter we present and investigate an inverse problem for estimating the *conditional* probability measures in size-structured population models from size-distribution measurements. In Section 5.1, we formulate the inverse problem as a least squares problem for the probability measure estimation. We use the Prohorov metric (convergence in which is equivalent to weak convergence of measures) in a functional-analytic setting and show existence and consistency of the estimators for the least squares problem. Consequently, in Section 5.2, we develop an approximation approach for computational implementation and prove convergence of this approximate inverse problem. We show the convergence of solutions of the approximate inverse problem to solutions of the original inverse problem. In Section 5.3, we illustrate that the flocculation dynamics of bacterial aggregates in suspension as one realization of a system satisfying the hypotheses in our framework. Furthermore, we present numerical examples to demonstrate the feasibility of our inverse methodology for artificial data sets.

5.1 Least squares problem for estimation of conditional probability distributions

In this section, we consider the inverse problem for inferring a conditional probability distribution from aggregate population data. First, in Section 5.1.1, we formulate the inverse problem as a least squares problem for the probability measure estimation. Consequently, in Section 5.1.2, we will develop the theoretical results needed to prove the existence and consistency of the estimates of the least squares problem. Accordingly, we will state some assumptions which are motivated by the features of the validating data.

5.1.1 Theoretical framework for the least squares problem

Let $\mathscr{P}(Q)$ be the space of all probability distributions on $(Q, \mathscr{A})$, where $\mathscr{A}$ is the Borel σ-algebra on Q. Since we are primarily concerned with the systems with unknown conditional probability measures, we restrict the space of probability distributions to those that can be solutions to our inverse problem. Towards this end, we define *regular conditional probability* measures $F : Q \times Q \to [0, 1]$ such that $F(\cdot, y)$ is a probability measure in $\mathscr{P}(Q)$ for all $y \in Q$. We then define our space of solutions to the inverse problem $\mathscr{F}(Q \times Q)$ as the set of all conditional probability measures defined on Q, i.e, $F \in \mathscr{F}(Q \times Q)$ if and only if $F(\cdot, y) \in \mathscr{P}(Q)$ for all $y \in Q$.

We define a metric on the space $\mathscr{F}$ to create a metric topology, and we accomplish this by making use of the well-known Prohorov metric (see Billingsley (1968) for a full description). Convergence in the Prohorov metric is equivalent to weak convergence of measures and we direct the interested reader to (Gibbs & Su, 2002) for a summary of its relationship to a variety of other metrics on probability measures. For $F, \tilde{F} \in \mathscr{F}$ and fixed y, we use the Prohorov metric ρ_{proh} to denote the distance $\rho_{\text{proh}}(F(\cdot, y), \tilde{F}(\cdot, y))$ between the measures. We extend this concept to define the metric ρ on the space $\mathscr{F}(Q \times Q)$ by taking the supremum of ρ_{proh} over all $y \in Q$,

$$\rho(F, \tilde{F}) = \sup_{y \in Q} \rho_{\text{proh}}(F(\cdot, y), \tilde{F}(\cdot, y)) \,.$$

The most widely available, high-fidelity data for flocculating particles are in the form of particle size histograms from, e.g., from flow-cytometers, Coulter counters, etc. Accordingly, we will define

our inverse problem with the goal of comparing with histograms of floc sizes. Let $n_j(t_i)$ represent the number of flocculated biomasses with volume between x_j and x_{j+1} at time t_i. We assume that the data is generated by an actual post-fragmentation probability distribution. In other words, $\mathbf{n}^d$ is representable as the partial zeroth moment of the solution

$$n_{ji}^d = \int_{x_{j-1}}^{x_j} b(t_i,\, x; F_0)\, dx + \mathcal{E}_{ji} \tag{5.3}$$

for some *true* conditional probability-measure $F_0 \in \mathscr{F}$. The random variables $\mathcal{E}_{ji}$ represent measurement noise. We also assume, as it is commonly assumed, that the random variables $\mathcal{E}_{ji}$ are independent, identically distributed, with mean $E[\mathcal{E}_{ji}] = 0$ and variance

$$Var[\mathcal{E}_{ji}] = \sigma^2 < \infty \tag{5.4}$$

(which is generally true for flow-cytometers (Darzynkiewicz et al., 1994)). Thus our inverse problem entails finding a minimizer $F \in \mathscr{F}$ of the least squares cost functional, defined as

$$J(F;\, \mathbf{n}^d) = \sum_{i=1}^{N_t} \sum_{j=1}^{N_x} \left(\int_{x_{j-1}}^{x_j} b(t_i, x; F)\, dx \;-\; n_{ji}^d \right)^2 , \tag{5.5}$$

where the data $\mathbf{n}^d \in \mathbb{R}^{N_x \times N_t}$ consists of the number of flocs in each of the N_x bins for floc volume at N_t time points. The superscript d denotes the dimension of the data, $d = N_x \times N_t$. The function b is the solution to (5.1)-(5.2) corresponding to the probability measure F.

For a given data $\mathbf{n}^d$, the cost functional J may not have a unique minimizer, thus we denote a corresponding solution set of probability distributions as $\mathscr{F}^*(\mathbf{n}^d)$. We then define the distance between two such sets of solutions, $\mathscr{F}^*(\mathbf{n}_1^{d_1})$ and $\mathscr{F}^*(\mathbf{n}_2^{d_2})$ (for data $\mathbf{n}_1^{d_1}$ and $\mathbf{n}_2^{d_2}$) to be the well-known Hausdorff distance (Kelley, 1955)

$$d_H(\mathscr{F}^*(\mathbf{n}_1^{d_1}),\, \mathscr{F}^*(\mathbf{n}_2^{d_2})) = \inf\{\rho(F,\, \tilde{F}) :\; F \in \mathscr{F}^*(\mathbf{n}_1^{d_1}),\; \tilde{F} \in \mathscr{F}^*(\mathbf{n}_2^{d_2})\}\,.$$

5.1.2 Existence and consistency of the least squares estimates

In this section we establish existence and consistency of the estimates of the least squares problem defined in (5.5). In particular, we will first show that for a given data set $\mathbf{n}^d$ with dimension d, the

least squares estimator defined in (5.5) has at least one minimizer. Next, we will investigate the behavior of minimizers of (5.5) as more data is collected. Specifically, we will show that the least squares estimator is consistent, i.e., as the dimension of data increases ($N_t \to \infty$ and $N_x \to \infty$) the minimizers of the estimator (5.5) converge to *true* probability measure F_0 generating the data $\mathbf{n}^d$.

5.1.2.1 Existence of the estimator.

In this section we prove that the cost functional defined in (5.5) possesses at least one minimizer. We use the well-known result that a continuous function on a compact metric space has a minimum. In particular, first we show that $(\mathscr{F}, \rho)$ is a compact metric space. Next, we establish continuous dependence of the solution b on the conditional probability measure F.

For much of the following analysis, we require the operator g to satisfy a Lipschitz-type condition. We detail that condition in the following.

Condition 5.1. Suppose that b and $\tilde{b}$ are solutions to the evolution equation (5.1)-(5.2). For fixed t, the function $g : H \times \mathscr{F} \to H$ must satisfy

$$\left\| g(b, F) - g(\tilde{b}, \tilde{F}) \right\| \leq C \left\| b - \tilde{b} \right\| + \mathscr{T}(F, \tilde{F}),$$

where $C > 0$, and $\mathscr{T}(F, \tilde{F})$ is some functional such that $|\mathscr{T}(F, \tilde{F})| < \infty$ and $\mathscr{T}(F, \tilde{F}) \to 0$ as $\rho(F, \tilde{F}) \to 0$.

We begin by proving that $(\mathscr{F}, \rho)$ is a compact metric space.

Lemma 5.2. *$(\mathscr{F}, \rho)$ is a compact metric space.*

Proof. Consider a Cauchy sequence $\{F_n\} \in \mathscr{F}$. Then $\forall\, \epsilon > 0$, $\exists\, N$ such that $\forall\, n, m \geq N$,

$$\sup_{y \in Q} \rho_{\text{proh}} \left(F_n(\cdot, y), F_m(\cdot, y) \right) < \epsilon.$$

It is easy to see we have a Cauchy sequence $\{F_n(\cdot, y)\} \in \mathscr{P}(Q)$ which converges uniformly in $y \in Q$. From results in (Banks & Thompson, 2015, Corollary 2.16), $\mathscr{P}(Q)$ is a compact metric space with respect to the Prohorov metric, and thus there exists $F(\cdot, y) \in \mathscr{P}(Q)$ such that

$\rho_{Proh}(F_n(\cdot, y), F(\cdot, y)) < \epsilon$ for all $n \geq N$. Thus

$$\sup_{y \in Q} \rho_{\text{proh}}\left(F_n(\cdot, y), F(\cdot, y)\right) < \epsilon$$

and $(\mathscr{F}, \rho)$ is a complete metric space. Analogously, we can show that $(\mathscr{F}, \rho)$ is sequentially compact. Therefore, we conclude that $(\mathscr{F}, \rho)$ is a compact metric space. □

Now that we have a compact metric space, it remains to show that the cost functional on that space is continuous with respect to the function F. It suffices to prove point-wise continuity.

Lemma 5.3. *If $t \in T$, $F \in \mathscr{F}$, and the operator g in (5.1) satisfies Condition 5.1, then the unique solution b to (5.1) is point-wise continuous at $F \in \mathscr{F}$. Moreover, since $\mathscr{F}$ is compact space the unique solution b is uniformly continuous on $\mathscr{F}$.*

Proof. For the function b to be point-wise continuous at F, we need to show that $\|b(t, \cdot; F_i) - b(t, \cdot; F)\| \to 0$ as $\rho(F_i, F) \to 0$ for $\{F_i\} \in \mathscr{F}$ and fixed t. We begin by re-writing (5.1) as an integral equation

$$b(t, x) = b_0(x) + \int_0^t g(b(s, x), F) ds\,.$$

For fixed t, consider b to be a function of F

$$b(t, x; F) = b_0(x) + \int_0^t g(b(s, x; F), F) ds\,.$$

By definition of solutions, we have

$$\|b(t, \cdot; F_i) - b(t, \cdot; F)\| \leq \int_0^t \|g(b(s, \cdot; F_i), F_i) - g(b(s, \cdot; F), F)\|\, ds\,.$$

Based on Condition 5.1, we obtain

$$\|b(t, \cdot; F_i) - b(t, \cdot; F)\| \leq C \int_0^t \|b(s, \cdot; F_i) - b(s, \cdot; F)\|\, ds + \mathcal{T}(F_i, F)\,,$$

where we define $\mathcal{T}(F_i, F) = \int_0^{t_f} \mathscr{T}(F_i, F) ds$, independent of t. An application of Gronwall's in-

equality yields

$$\|b(t,\cdot;F_i) - b(t,\cdot;F)\| \leq \mathcal{T}(F_i,F)\, e^{\int_0^t C\, ds} \leq \mathcal{T}(F_i,F)\, e^{C\, t_f} \to 0$$

since we know that $\mathcal{T}(F_i,F) \to 0$ as $F_i \to F$ in $(\mathscr{F},\, \rho)$. Thus the solutions b are point-wise continuous at $F \in \mathscr{F}$. □

We use the results of the above two lemmas to establish existence of a solution to our inverse problem.

Theorem 5.4. *There exists a solution to the inverse problem as described in (5.5).*

Proof. It is well known that a continuous function on a compact set obtains both a maximum and a minimum. We have shown $(\mathscr{F},\rho)$ is compact, and from Lemma 5.3, for fixed $t \in T$, we have that $F \mapsto b(t,\cdot;F)$ is continuous. Since J is continuous with respect to F,we can conclude there exist minimizers for J. □

5.1.2.2 Consistency of the estimator.

In previous section we have proven that for a given data there exists minimizers of the least squares cost functional defined in (5.5). In this section we will investigate the behavior of the least squares estimators as the number of observations increase. In particular, the estimator is said to be *consistent* if the estimators for the data $\mathbf{n}^d$ converge to *true* probability measure F_0 as $N_t \to \infty$ and $N_x \to \infty$. Consistency of the estimators of the least squares problems are well-studied in statistics and the results of this section follow closely the theoretical results of Banks & Thompson (2012) and Banks & Fitzpatrick (1990). Hence, as in (Banks & Thompson, 2012, Theorem 4.3) and (Banks & Fitzpatrick, 1990, Corallary 3.2), we will make the following two assumptions required for the convergence of the estimators to the unique *true* probability measure F_0.

(**A**1) Let us denote the space of positive functions $T \times Q \mapsto \mathbb{R}^+$, which are bounded and Riemann integrable by $\mathscr{R}\,(T \times Q,\, \mathbb{R}^+)$. Then, the model function $b(t,x;\,\cdot) \,:\, \mathscr{F} \to \mathscr{R}\,(T \times Q,\, \mathbb{R}^+)$ is continuous on $(\mathscr{F},\, \rho)$.

(**A**2) The functional

$$J_0(F) = \sigma^2 + \int_T \int_Q \left(b(t,x;F) - b(t,x;F_0)\right)^2 \, dx\, dt$$

is uniquely (up to L^1 norm) minimized at $F_0 \in \mathscr{F}$. Here σ^2 is variance of the measurement noise defined in (5.4).

Assumption (**A**2) is often referred to as *identifiability* condition (or output least squares identifiability (Chavent, 1979)) and addresses the question of whether the least squares inverse problem (5.5) has a unique solution for given data set. Establishing identifiability conditions is generally mathematically challenging and depends to a great extent on the model involved. Chavent (1979) presented general sufficient conditions for identifiability of parameters when the parameter space is finite dimensional, which require additional smoothness on the model function b. In some cases, non-identifiability of parameters can be eliminated by reducing the dimensionality of the parameter space (Carrera & Neuman, 1986) or by adding a regularization term to the cost functional J (Cooley, 1982). For further details about the identifiability of parameters in inverse problems, we refer readers to a review articles by Yeh (1986) and Miao et al. (2011).

In this chapter, we will not develop any detailed rules about the identifiability of the parameters. However, a few general conclusions can be drawn. For instance, from continuity arguments of Theorem (5.3) it follows that the function $J_0 : \mathscr{F} \to \mathbb{R}^+$, defined in assumption (**A**2), is continuous with respect to Prohorov metric. Therefore, the function J_0 has at least one minimizer on $(\mathscr{F}, \rho)$. Moreover, it is easy to see that the function J_0 is minimized at F_0. Suppose that there is another minimizer F_1 of J_0 such that $\rho\,(F_1, F_0) \neq 0$. Then

$$\int_T \int_Q \left(b(t,x;F_1) - b(t,x;F_0)\right)^2 \, dx\, dt = 0\,.$$

This in turn implies that

$$b(t,x;F_1) = b(t,x;F_0)$$

almost everywhere on $(t, x) \in T \times Q$, which is very strict condition to fulfill for significantly different F_1 and F_0. Furthermore, the value of $b(t_1, x; F)$ at time t_1 for fixed $F \in \mathscr{F}$ depends on the profile of $b(t, x; F)$ for $t \in [0, t_1)$ and thus by choosing the observation interval $T = [0, t_f]$ sufficiently large one can ensure uniqueness of the minimizer of the function J_0.

Having the required assumptions in hand, we now present the following theorem about the consistency of the estimators of the least squares cost functional (5.5).

Theorem 5.5. *Under assumptions (**A**1) and (**A**2)*

$$d_H\left(\mathscr{F}^*(\mathbf{n}^d),\, F_0\right) \to 0$$

as $N_t \to \infty$ *and* $N_x \to \infty$.

Proof. The specific details of this proof are nearly identical to a similar theorem in (Banks & Thompson, 2012) and so here we simply provide an overview. Briefly, one first shows that $J(F;\, \mathbf{n}^d)$ converges to $J_0(F)$ for each $F \in \mathscr{F}$ as $N_t \to \infty$ and $N_x \to \infty$. Then, using the fact that $J_0(F)$ is uniquely (up to the metric ρ) minimized at F_0, one can show that for each sequence $\left\{F^d \in \mathscr{F}^*(\mathbf{n}^d)\right\}$ the distance $\rho\left(F^d,\, F_0\right)$ converges to zero as $N_t \to \infty$ and $N_x \to \infty$, which yields the result. □

5.2 Approximate Inverse Problem

Since the original problem involves minimizing over the infinite dimensional space $\mathscr{F}$, pursuing this optimization is challenging without some type of finite dimensional approximation. Thus we define some approximation spaces over which the optimization problem becomes computationally tractable. Similar to the partitioning presented in (Banks & Bortz, 2005), let $Q_M = \{q_j^M\}_{j=0}^M$ be partitions of $Q = [0, \overline{x}]$ for $M = 1, 2, \ldots$ and

$$Q_D = \bigcup_{M=1}^{\infty} Q_M \tag{5.6}$$

where the sequences are chosen such that Q_D is dense in Q.

For positive integers M, L, let the approximation space be defined as

$$\begin{aligned}\mathscr{F}^{ML} \;=\; \Bigg\{ & F \in \mathscr{F} \mid \forall \Omega \subseteq Q, \quad F(\Omega, y) = \sum_{m=1}^{M} p_{\ell m} \Delta_{q_m^M}(\Omega)\, \mathbb{1}_{(q_{\ell-1}^L,\, q_\ell^L]}(y), \\ & q_m^M \in Q_M,\, q_\ell^L \in Q_L,\, p_{ij} \geq 0,\, \sum_{m=1}^{\ell} p_{\ell m} = 1,\, \ell = 1, 2, \ldots, L \Bigg\},\end{aligned}$$

where Δ_q is the Dirac measure with atom $x = q$ defined for all $\Omega \subseteq Q$ as

$$\Delta_q(\Omega) = \begin{cases} 1 & q \in \Omega \\ 0; & q \notin \Omega \end{cases} .$$

The function $\mathbb{1}_A$ is the indicator function on the interval A.

Next, define the space $\mathscr{F}_D$ as

$$\mathscr{F}_D = \bigcup_{M,L=1}^{\infty} \mathscr{F}^{ML}.$$

Consequently, since Q is a complete, separable metric space, and by Theorem 3.1 in (Banks & Bihari, 2001) and properties of the sup norm, $\mathscr{F}_D$ is dense in $\mathscr{F}$ in the ρ metric. Therefore we can directly conclude that any measure $F \in \mathscr{F}$ can be approximated by a sequence $\{F_{M_jL_k}\}$, $F_{M_jL_k} \in \mathscr{F}^{M_jL_k}$ such that as M_j, $L_k \to \infty$, $\rho(F_{M_jL_k}, F) \to 0$.

Similar to the discussion concerning Theorem 4.1 in (Banks & Bihari, 2001), we now state the theorem regarding the continuous dependence of the inverse problem upon the given data, as well as stability under approximation of the inverse problem solution space $\mathscr{F}$.

Theorem 5.6. *Let $Q = [0, \overline{x}]$, assume that for fixed $t \in T$, $x \in Q$, $F \mapsto b(t, x, F)$ is continuous on $\mathscr{F}$, and let Q_D be a countable dense subset of Q as defined in (5.6). Suppose that $\mathscr{F}^{*ML}(\mathbf{n}^d)$ is the set of minimizers for $J(F; \mathbf{n}^d)$ over $F \in \mathscr{F}^{ML}$ corresponding to the data $\mathbf{n}^d$. Then, $d_H(\mathscr{F}^{*ML}(\mathbf{n}^d), F_0) \to 0$ as M, L, N_t, $N_x \to \infty$.*

Proof. Suppose that $\mathscr{F}^*(\mathbf{n}^d)$ is the set of minimizers for $J(F; \mathbf{n}^d)$ over $F \in \mathscr{F}$ corresponding to the data $\mathbf{n}^d$. Using continuous dependence of solutions on F, compactness of $(\mathscr{F}, \rho)$, and the density of $\mathscr{F}_D$ in $\mathscr{F}$, the arguments follow precisely those for Theorem 4.1 in (Banks & Bihari, 2001). In particular, one would argue in the present context that any sequence $F_d^{*ML} \in \mathscr{F}^{*ML}(\mathbf{n}^d)$ has a subsequence $F_{d_k}^{*M_jL_i}$ that converges to a $\tilde{F} \in \mathscr{F}^*(\mathbf{n}^d)$. Therefore, we can claim that

$$d_H\left(\mathscr{F}^{*ML}(\mathbf{n}^d), \mathscr{F}^*(\mathbf{n}^d)\right) \to 0 \tag{5.7}$$

as M, L, N_t, $N_x \to \infty$. Conversely, a simple application of the triangle inequality yields that

$$d_H(\mathscr{F}^{*ML}(\mathbf{n}^d), F_0) \leq d_H\left(\mathscr{F}^{*ML}(\mathbf{n}^d), \mathscr{F}^*(\mathbf{n}^d)\right) + d_H\left(\mathscr{F}^*(\mathbf{n}^d), F_0\right) .$$

This is in turn, from (5.7) and Theorem 5.5, implies that $d_H(\mathscr{F}^{*ML}(\mathbf{n}^d), F_0)$ converges to zero as M, L, N_t, $N_x \to \infty$. □

Since we do not have direct access to an analytical solution to (5.1), our efforts are focused on finding a minimizer $F \in \mathscr{F}$ of the approximate least squares cost functional

$$J^N(F, \mathbf{n}^d) = \sum_{i=1}^{N_t} \sum_{j=1}^{N_x} \left(\int_{x_{j-1}}^{x_j} b^N(t_i, x_j; F) dx - n_{ji}^d \right)^2 . \tag{5.8}$$

Here, N_t is the number of data observations, N_x is the number of data bins for floc volume, and b^N is the semi-discrete approximation to b. In Section 5.3, we will define a uniformly (in time) convergent discretization scheme and its corresponding approximation space $H^N \subset H$. The discretized version of (5.8) is represented by

$$b_t^N = g^N(b^N, F) \tag{5.9}$$

$$b^N(0, x) = b_0^N(x) \tag{5.10}$$

where $g^N : H^N \times \mathscr{F} \to H^N$ denotes the discretized version of g. We will need that g^N exhibits a type of local Lipschitz continuity and accordingly define the following condition.

Condition 5.7. Suppose that the discretization given in (5.9)-(5.10) is a convergent scheme. Let (b^N, F), $(\tilde{b}^N, \tilde{F}) \in H^N \times \mathscr{F}$. For fixed t, the function $g^N : H^N \times \mathscr{F} \to H^N$ must satisfy

$$\left\| g^N(b^N, F) - g^N(\tilde{b}^N, \tilde{F}) \right\| \leq C_N \left\| b^N - \tilde{b}^N \right\| + \mathscr{T}^N(F, \tilde{F}),$$

where $C_N > 0$, and $\mathscr{T}^N(F, \tilde{F})$ is some function such that $|\mathscr{T}^N(F, \tilde{F})| < \infty$ and $\mathscr{T}^N(F, \tilde{F}) \to 0$ as $\rho(F, \tilde{F}) \to 0$.

General *method stability* (Banks & Kunisch, 1989) requires $b^N(t, x; F_i) \to b(t, x; F)$ as $F_i \to F$ in the ρ metric and as $N \to \infty$; we will now prove this.

Lemma 5.8. *Let $t \in T$, $F \in \mathscr{F}$, and $\{F_i\} \in \mathscr{F}$ such that $\lim_{i\to\infty} \rho(F_i, F) = 0$. For fixed N, if $b^N(t, x; F_i)$ is the solution to (5.19)-(5.20) and Condition 5.7 holds, then b^N is pointwise continuous at $F \in \mathscr{F}$.*

Proof. The proof of this lemma is identical to that for Lemma 5.3. We first recast (5.9) as an integral equation and then apply Condition 5.7 and Gronwall's inequality to obtain the desired result. □

Corollary 5.9. *Under Condition 5.7 and Lemma 5.8, we can conclude that* $\left\|b^N(t,\cdot;F_N) - b(t,\cdot;F)\right\| \to 0$ *as* $N \to \infty$ *uniformly in* t *on* I.

Proof. A standard application of the triangle inequality yields

$$\begin{aligned}\left\|b^N(t,\cdot;F_N) - b(t,\cdot;F)\right\| &\leq \left\|b^N(t,\cdot;F_N) - b^N(t,\cdot;F)\right\| \\ &\quad + \left\|b^N(t,\cdot;F) - b(t,\cdot;F)\right\| .\end{aligned}$$

The first term converges by Lemma 5.8, while the second term converges because the proposed numerical scheme is assumed to converge uniformly. □

With this corollary, we now consider the existence of a solution to the approximateleast squares cost functional in (5.8), as well as the solution's dependence on the given data $\mathbf{n}^d$.

Theorem 5.10. *Assume that there exists solutions to both the original and the approximate inverse problems in (5.5) and (5.8), respectively. For fixed data* $\mathbf{n}^d$*, there exist a subsequence of the estimators* $\{F_N\}_{N=1}^{\infty}$ *of (5.8) that converge to a solution of the original inverse problem (5.5).*

Proof. As noted above, $(\mathscr{F}, \rho)$ is compact. By Lemmas 5.3 and 5.8, we have that both $F \mapsto b(t,x;F)$ and $F \mapsto b^N(t,x;F)$, for fixed $t \in T$, are continuous with respect to F. We therefore know there exist minimizers in $\mathscr{F}$ to the original and approximate cost functionals J and J^N respectively.

Let $\{F_N^*\} \in \mathscr{F}$ be any sequence of solutions to (5.8) and $\{F_{N_k}^*\}$ a convergent (in ρ) subsequence of minimizers. Recall that minimizers are not necessarily unique, but one can always select a convergent subsequence of minimizers in $\mathscr{F}$. Denote the limit of this subsequence with F^*. By the minimizing properties of $F_{N_k}^* \in \mathscr{F}$, we then know that

$$J^{N_k}(F_{N_k}^*, \mathbf{n}^d) \leq J^{N_k}(F, \mathbf{n}^d) \qquad \text{for all } F \in \mathscr{F}. \tag{5.11}$$

By Corollary 5.9, we have the convergence of $b^N(t,x;F_N) \to b(t,x;F)$ and thus $J^N(F_N) \to J(F)$

as $N \to \infty$ when $\rho(F_N, F) \to 0$. Thus in the limit as $N_k \to \infty$, the inequality in (5.11) becomes

$$J(F^*, \mathbf{n}^d) \leq J(F, \mathbf{n}^d) \qquad \text{for all } F \in \mathscr{F}$$

with F^* providing a (not necessarily unique) minimizer of (5.5). □

Theorem 5.11. *Assume that for fixed $t \in T$, $F \mapsto b(t, x; F)$ is continuous on $\mathscr{F}$ in ρ, b^N is the approximate solution to the forward problem given (5.19)-(5.20), J^N is the approximation given in (5.8), and Q_D a countable dense subset of Q as defined in (5.6). Moreover, suppose that $\mathscr{F}_N^{*ML}(\mathbf{n}^d)$ is the set of minimizers for $J^N(F; \mathbf{n}^d)$ over $F \in \mathscr{F}^{ML}$ corresponding to the data $\mathbf{n}^d$. Similarly, suppose that $\mathscr{F}^*(\mathbf{n}^d)$ is the set of minimizers for $J(F; \mathbf{n}^d)$ over $F \in \mathscr{F}$ corresponding to the data $\mathbf{n}^d$. Then, $d_H(\mathscr{F}_N^{*ML}(\mathbf{n}^d), F_0) \to 0$ as N, M, L, N_t, $N_x \to \infty$.*

Proof. Observe that an application of a simple triangle inequality yields

$$d_H\left(\mathscr{F}_N^{*ML}(\mathbf{n}^d), F_0\right) \leq d_H\left(\mathscr{F}_N^{*ML}(\mathbf{n}^d), \mathscr{F}^{*ML}(\mathbf{n}^d)\right) + d_H\left(\mathscr{F}^{*ML}(\mathbf{n}^d), F_0\right).$$

Therefore, combining the arguments of Theorem 5.6 and Theorem 5.10, we readily obtain that $d_H\left(\mathscr{F}_N^{*ML}(\mathbf{n}^d), F_0\right)$ converges to zero as N, M, L, N_t, $N_x \to \infty$. □

With the results of these two theorems, we can claim that both that there exists a solution to the approximate inverse problem, defined in (5.8), and that it is continuously dependent on the given data. We have also established method stability under approximation of the state space and parameter space of our inverse problem. Therefore, we can conclude the existence and consistency of the estimators of the approximate least squares problem.

5.3 Application to flocculation equations

Modeling *flocculation*, a process whereby destabilized suspended particles (i.e., flocs) reversibly aggregate and fragment, has received considerably attention over the years (Han et al., 2003; Davis & Hunt, 1986; Adachi, 1995; Thomas et al., 1999). Flocculation is ubiquitous in many diverse areas such as water treatment, biofuel production, beer fermentation, etc. In modeling the dynamics of flocculation, four important mechanisms arise in a wide range of applications: aggregation,

fragmentation, proliferation and sedimentation. Mathematical modeling of flocculation is usually based on a size-structured population equations that take into account one or more of the above listed mechanisms.

The particular flocculation model we study here accounts for aggregation, fragmentation and sedimentation of the flocs. The equations for the flocculation model track the time-evolution of the particle size number and is given by the following integro-differential equation

$$b_t = \mathcal{A}[b] + \mathcal{B}[b] + \mathcal{R}[b], \tag{5.12}$$

$$b(0,\, x) = b_0(x), \tag{5.13}$$

where $b(t,\, x)\, dx$ is the number of aggregates with volumes in $[x,\, x + dx]$ at time t, and $\mathcal{A}$, $\mathcal{B}$ and $\mathcal{R}$ are the aggregation, breakage (fragmentation) and removal operators, respectively. We consider $x \in Q = [0,\, \overline{x}]$, where $\overline{x}$ is the maximum floc size and $t \in T = [0,\, t_f]$, $t_f < \infty$. As investigated in our previous work (Bortz et al., 2008; Mirzaev & Bortz, 2015b), the function space for both the initial condition $b_0(\cdot)$ and the solution $b(t,\, x)$ is $H = L^1(Q,\, \mathbb{R}^+)$, where $Q = [0,\, \overline{x}]$, $\overline{x} \in \mathbb{R}^+$ and $g : H \times \mathscr{F} \to H$.

The aggregation, fragmentation and removal operators are defined by:

$$\begin{aligned} \mathcal{A}[p](t,\, x) := {} & \frac{1}{2}\int_0^x k_a(x - y,\, y)p(t,\, x - y)p(t,\, y)\, dy \\ & - p(t,\, x)\int_0^{\overline{x}} k_a(x,\, y)p(t,\, y)\, dy\,, \end{aligned} \tag{5.14}$$

$$\mathcal{B}[p](t,\, x) := \int_x^{\overline{x}} \Gamma(x;\, y)k_f(y)p(t,\, y)\, dy - \frac{1}{2}k_f(x)p(t,\, x) \tag{5.15}$$

and

$$\mathcal{R}[p](t,\, x) := -\mu(x)p(t,\, x)\,. \tag{5.16}$$

The aggregation kernel, $k_a(x,\, y)$, describes the rate at which flocs of volume x and y combine to form a floc of volume $x + y$ and is a symmetric function satisfying $k_a(x,\, y) = 0$ for $x + y > \overline{x}$. The

fragmentation kernel $k_f(x)$ describes the rate at which a floc of volume x fragments. The function $\Gamma(x,\, y)$ is the post-fragmentation probability density function, for the conditional probability of producing a daughter floc of size x from a mother floc of size y. This probability density function is used to characterize the stochastic nature of floc fragmentation (e.g., see the discussions in (Han et al., 2003; Bortz et al., 2008; Byrne et al., 2011; Bäbler et al., 2008)).

The flocculation equations, presented in (5.12)-(5.20), are a generalization of many mathematical models appearing in the size-structured population modeling literature. The forward problem of the flocculation equations has also been the focus of considerable mathematical analysis. There is a significant literature on the existence and uniqueness of solutions to flocculation equations, see for example (White, 1980; Dacosta, 1995). Nevertheless, because of the nonlinear term introduced by the aggregation, derivation of analytical solutions for the flocculation equations has proven elusive except for some special cases (Aldous, 1999). However, many discretization schemes for numerical simulations of the PBEs have been proposed: the least squares spectral method (Dorao & Jakobsen, 2006b), the finite volume methods (Bourgade & Filbet, 2008) and the finite element method Nicmanis & Hounslow (1998). For a review of further mathematical results, we refer readers to the review article by Wattis (2006).

We now consider the application of our inverse methodology to the evolution equation defined in (5.12)-(5.13). For fixed $t \in T, b(t,\cdot) \in H$, $F \in \mathscr{F}$, consider the right side of (5.12), represented by (5.1),

$$g(b,\, F) = \mathcal{A}[b] + \mathcal{B}[b;\, F] + \mathcal{R}[b]\,, \tag{5.17}$$

where the conditional probability measure $F(\cdot,\, y)$ on $\Omega \subseteq Q$ and for fixed $y \in Q$ is defined as

$$F(\Omega,\, y) = \int_{\Omega} \Gamma(\xi, y)\, d\xi\,.$$

Note that $0 \leq F(\Omega,\, y) \leq 1$ for all $\Omega \subseteq Q$, since $\Gamma(\cdot, y)$ is a probability density function for each fixed y.

Setting $\Omega = [0,\, x]$ yields

$$F([0,\, x],\, y) = \int_0^x \Gamma(\xi, y)\, d\xi\,,$$

which is cumulative probability of getting flocs smaller than size x when a parent floc of size y

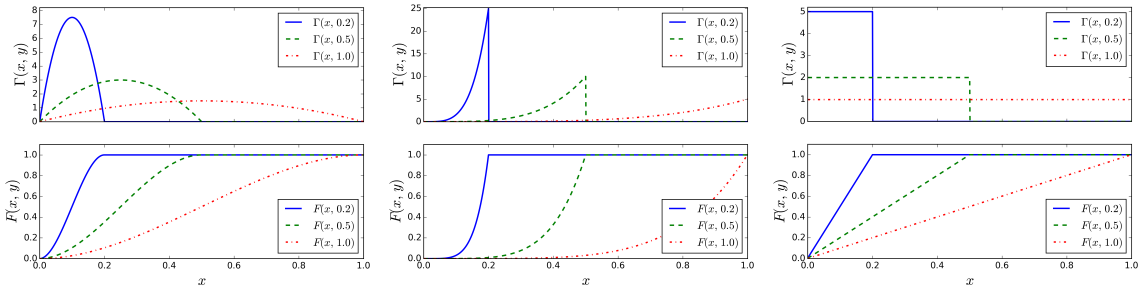

(a) (b) (c)

Figure 5.1: Relationship between post-fragmentation density functions $\Gamma(x, y)$ (top row) and cumulative density function $F(x, y)$ (bottom row) a) $\Gamma(x, y)$, Beta distribution with $\alpha = \beta = 2$. b) $\Gamma(x, y)$, Beta distribution with $\alpha = 5$ and $\beta = 1$. c) $\Gamma(x, y)$, uniform distribution in x for fixed y.

fragments. Hereafter, for convenience and in mild abuse of the notation, we refer to this quantity as cumulative density function (cdf) and denote it simply by $F(x, y)$. Note that a fragmentation cannot result in a daughter floc larger than the original floc, therefore $F(x, y) \equiv 1$ for $x \geq y$ and fixed $y \in Q$. Furthermore, one can infer the post-fragmentation density function $\Gamma(x, y)$ by numerical differentiation of the cdf $F(x, y)$. Figure 5.1 depicts the relationship between the cdf $F(x, y)$ and the post-fragmentation density function $\Gamma(x, y)$ for several different probability distributions.

Before we proceed to the inverse problem, we need to establish existence and uniqueness, i.e., well-posedness, of the solutions of the forward problem. Well-posedness of the forward problem for $\overline{x} < \infty$ and $t_f < \infty$ was first established by Ackleh & Fitzpatrick (1997) in an L^2-space setting and later by Banasiak & Lamb (2009) for $\overline{x} = \infty$ and $t_f = \infty$ in an L^1-space setting. For the sake of completeness, in the following lemma, we will summarize assumptions needed for the well-posedness for $\overline{x} < \infty$ and $t_f < \infty$ in L^1-space setting and refer readers to (Bortz et al., 2008, §3) for the proof.

Lemma 5.12. *Suppose that* k_f, $\mu \in L^\infty(Q)$, $k_a \in L^\infty(Q \times Q)$. *Moreover, assume that the post-fragmentation density function* $\Gamma(\cdot, y) \in L^1(Q)$ *for all* $y \in (0, \overline{x}]$ *and*

$$F(x, y) = \int_0^x \Gamma(\xi, y)\, d\xi = 1 \qquad \text{for all } x \geq y\,.$$

The evolution equation (5.12)-(5.13) is well-posed on $H = L^1(Q, \mathbb{R}^+)$ *and for any compact set*

$T = [0,\, t_f]$ and $b_0 \geq 0$, the classical solution of (5.12)-(5.13) satisfies

$$C_0 = \sup_{t \in T,\, x \in Q} |b(t,\, x)| < \infty\,. \tag{5.18}$$

Having the well-posedness of the forward problem, we now show that the solution $b(t,\, x,\, \cdot)$ is uniformly continuous on compact space $\mathscr{F}$. This in turn, from Theorem 5.4, proves the existence of minimizers for the least squares problem defined in (5.5). Towards this end, we establish the following lemma, which we will need later to show that g, defined in (5.17), satisfies the locally Lipschitz property of Condition 5.1.

Lemma 5.13. *The operator $\mathcal{A} + \mathcal{R}$ is locally Lipschitz*

$$\left\| \mathcal{A}[b] + \mathcal{R}[b] - \mathcal{A}[\tilde{b}] - \mathcal{R}[\tilde{b}] \right\| \leq C_1 \left\| b - \tilde{b} \right\|$$

where $C_1 = 3C_0 \left\| k_a \right\|_\infty + \left\| \mu \right\|_\infty$. Furthermore, the fragmentation operator $\mathcal{B}$ satisfies the locally Lipschitz property of Condition 5.1.

Proof. To show that $\mathcal{A} + \mathcal{R}$ is locally Lipschitz, first observe that

$$\begin{aligned}
\left\| \mathcal{A}[b] - \mathcal{A}[\tilde{b}] \right\| \;\leq\; & \frac{1}{2} \int_Q \left| \int_0^x k_a(x-y,\, y) b(x-y) b(y)\, dy \right. \\
& \left. - \int_0^x k_a(x-y,\, y) \tilde{b}(x-y) \tilde{b}(y)\, dy \right| dx \\
& + \int_Q \left| b(x) \int_Q k_a(x,\, y) b(y)\, dy - \tilde{b}(x) \int_Q k_a(x,\, y) \tilde{b}(y)\, dy \right| dx \\
\leq\; & \left\| k_a \right\|_\infty \left[\frac{1}{2} \int_Q \left| \int_0^x b(x-y) \left(b(y) - \tilde{b}(y) \right) dy \right| dx \right. \\
& + \frac{1}{2} \int_Q \left| \int_0^x \tilde{b}(y) \left(b(x-y) - \tilde{b}(x-y) \right) dy \right| dx \\
& + \int_Q \left| b(x) \int_Q \left(b(y) - \tilde{b}(y) \right) dy \right| dx \\
& \left. + \int_Q \left| \tilde{b}(x) \int_Q \left(b(y) - \tilde{b}(y) \right) dy \right| dx \right].
\end{aligned}$$

At this point, applying Young's inequality Adams & Fournier (2003, Theorem 2.24) for the first two

integrals yields the desired result

$$\begin{aligned}\left\|\mathcal{A}[b]-\mathcal{A}[\tilde{b}]\right\| &\leq \|k_a\|_\infty \left[\frac{1}{2}\|b\|\left\|b-\tilde{b}\right\|+\frac{1}{2}\left\|\tilde{b}\right\|\left\|b-\tilde{b}\right\|\right.\\ &\quad \left.+\|b\|\left\|b-\tilde{b}\right\|+\left\|\tilde{b}\right\|\left\|b-\tilde{b}\right\|\right]\\ &\leq 3C_0\|k_a\|_\infty\left\|b-\tilde{b}\right\|.\end{aligned}$$

For the second part of the lemma, examining the fragmentation term, we find

$$\begin{aligned}\left\|\mathcal{B}(b,F)-\mathcal{B}(\tilde{b},\tilde{F})\right\| &\leq \left\|\frac{1}{2}k_f(x)\left(\tilde{b}(t,\,x)-b(t,\,x)\right)\right\|\\ &\quad+\left\|\int_x^{\overline{x}}k_f(y)\left(b(t,\,y)\,\Gamma(x,y)-\tilde{b}(t,\,y)\,\tilde{\Gamma}(x,y)\right)dy\right\|\\ &\leq \frac{1}{2}C_{\text{frag}}\left\|b-\tilde{b}\right\|+C_{\text{frag}}\left\|\int_Q b(t,\,y)\left(\Gamma(x,y)-\tilde{\Gamma}(x,y)\right)dy\right\|\\ &\quad+C_{\text{frag}}\left\|\int_Q\left(b(t,\,y)-\tilde{b}(t,\,y)\right)\tilde{\Gamma}(x,y)\,dy\right\|\end{aligned}$$

where $C_{\text{frag}}=\|k_f\|_\infty$. The second term on the right hand side becomes

$$\begin{aligned}C_{\text{frag}}\left\|\int_Q b(t,\,y)\left(\Gamma(x,y)-\tilde{\Gamma}(x,y)\right)dy\right\| &\leq C_{\text{frag}}\int_Q\int_Q|b(t,\,y)|\left|\Gamma(x,y)-\tilde{\Gamma}(x,y)\right|dy\,dx\\ &\leq C_{\text{frag}}\int_Q|b(t,\,y)|\int_Q\left|\Gamma(x,y)dx-\tilde{\Gamma}(x,y)dx\right|dy\\ &\leq C_{\text{frag}}\int_Q|b(t,\,y)|\left(\int_Q\left|dF_y-d\tilde{F}_y\right|\right)dy\\ &\leq C_{\text{frag}}\sup_{y\in Q}\int_Q\left|dF_y-d\tilde{F}_y\right|\int_Q|b(t,\,y)|\,dy\\ &\leq C_{\text{frag}}\overline{x}C_0\sup_{y\in Q}\int_Q\left|dF_y-d\tilde{F}_y\right|,\end{aligned}$$

where dF_y denotes the Radon–Nikodym derivative of the measure $F(\cdot,\,y)$ and C_0 is the upper bound of the solutions defined in (5.18). Since $\int_Q\left|dF_y-d\tilde{F}_y\right|\to 0$ is equivalent to $\rho_{Proh}(F_y,\tilde{F}_y)\to 0$, we know that

$$\sup_{y\in Q}\int_Q\left|dF_y-d\tilde{F}_y\right|\to 0\quad\text{as}\quad\rho(F,\tilde{F})\to 0.$$

Therefore,

$$C_{\text{frag}}\left\|\int_Q b(y)\left(\Gamma(x,y)-\tilde{\Gamma}(x,y)\right)dy\right\|\to 0\quad\text{as}\quad\rho(F,\,\tilde{F})\to 0.$$

Similar analysis for the third term leads to the bound

$$C_{\text{frag}} \left\| \int_Q \left(b(y) - \tilde{b}(t,y) \right) \tilde{\Gamma}(x,y)\, dy \right\| \leq C_{\text{frag}} \overline{x} \left\| \Gamma \right\|_\infty \left\| b - \tilde{b} \right\|.$$

Combining these results we find the overall fragmentation term can be bounded by

$$\left\| \mathcal{B}(b,\phi) - \mathcal{B}(\tilde{b},\tilde{\phi}) \right\| \leq C_{\text{frag}} \left(\frac{1}{2} + \overline{x} \left\| \Gamma \right\|_\infty \right) \left\| b - \tilde{b} \right\| + \mathscr{T}(F,\, \tilde{F}).$$

At this point we are ready to make the following claim. □

Claim 5.14. The function g satisfies the locally Lipschitz property of Condition 5.1.

Proof. Consider

$$\begin{aligned} \left\| g(b,F) - g(\tilde{b},\tilde{F}) \right\| &= \left\| \mathcal{A}[b] - \mathcal{A}[\tilde{b}] + \mathcal{B}[b;F] - \mathcal{B}[\tilde{b};\tilde{F}] + \mathcal{R}[b] - \mathcal{R}[\tilde{b}] \right\| \\ &\leq \left\| \mathcal{A}[b] - \mathcal{A}[\tilde{b}] \right\| + \left\| \mathcal{B}[b;F] - \mathcal{B}[\tilde{b};\tilde{F}] \right\| + \left\| \mathcal{R}[b] - \mathcal{R}[\tilde{b}] \right\|. \end{aligned}$$

Using the Lipschitz constants from the fragmentation and aggregation terms,

$$\left\| g(b,\phi) - g(\tilde{b},\tilde{\phi}) \right\| \leq C \left\| b - \tilde{b} \right\| + \mathscr{T}(F,\, \tilde{F})$$

where $C = C_{\text{frag}} \left(\frac{1}{2} + \overline{x} \left\| \Gamma \right\|_\infty \right) + C_1$ and C_1 and C_{frag} are defined in Lemma 5.13. □

The above claim proves continuity and the existence of minimizers of the least squares functional J, defined in (5.5), on the space of admissible probability distributions. Furthermore, Lemma 5.12 establishes that the classical solution of (5.12)-(5.13) is bounded on $T \times Q$. Moreover, since the space of Riemann integrable functions are dense on $L^1(Q,\, \mathbb{R}^+)$, we can assume that the classical solution is also Riemann integrable. Therefore, the evolution equation (5.12)-(5.13) satisfies the consistency conditions of Theorem 5.5, and thus estimators of the least squares problem, defined in (5.5), are consistent for this flocculation model.

5.3.1 Numerical Implementation

In this section, we outline a discretization scheme for approximating the flocculation equations. We first form an approximation to H. We define basis elements

$$\beta_i^N(x) = \begin{cases} 1; & x_{i-1}^N \le x \le x_i^N \,;\, i = 1, \ldots, N \\ 0; & \text{otherwise} \end{cases}$$

for positive integer N and $\{x_i^N\}_{i=0}^N$ a uniform partition of $[0, \overline{x}] = [x_0^N, x_N^N]$, and $\Delta x = x_j^N - x_{j-1}^N$ for all j. The β^N functions form an orthogonal basis for the approximate solution space

$$H^N = \left\{ h \in H \mid h = \sum_{i=1}^N \alpha_i \beta_i^N,\ \alpha_i \in \mathbb{R} \right\},$$

and accordingly, we define the orthogonal projections $\pi^N : H \mapsto H^N$

$$\pi^N h = \sum_{j=1}^N \alpha_j \beta_j^N, \qquad \text{where } \alpha_j = \frac{1}{\Delta x} \int_{x_{j-1}^N}^{x_j^N} h(x)\, dx.$$

Thus our approximating formulations of (5.12), (5.13) becomes the following system of N ODEs for $b^N \in H^N$ and $F \in \mathscr{F}$:

$$b_t^N = \pi^N \left(\mathcal{A}[b^N] + \mathcal{B}[b^N; F] + \mathcal{R}[b^N] \right), \tag{5.19}$$

$$b^N(0, x) = \pi^N b_0(x)\,, \tag{5.20}$$

where

$$\pi^N \mathcal{A}[b^N] = \begin{pmatrix} -\alpha_1 \sum_{j=1}^{N-1} k_a(x_1,\, x_j)\alpha_j \Delta x \\ \frac{1}{2} k_a(x_1, x_1)\alpha_1\alpha_1 \Delta x - \alpha_2 \sum_{j=1}^{N-2} k_a(x_2,\, x_j)\alpha_j \Delta x \\ \vdots \\ \frac{1}{2} \sum_{j=1}^{N-2} k_a(x_j, x_{N-1-j})\alpha_j \alpha_{N-1-j} \Delta x - \alpha_{N-1} k_a(x_{N-1},\, x_1)\alpha_1 \Delta x \\ \frac{1}{2} \sum_{j=1}^{N-1} k_a(x_j, x_{N-j})\alpha_j \alpha_{N-j} \Delta x \end{pmatrix}$$

and

$$\pi^N\left(\mathcal{B}[b^N;F]+\mathcal{R}[b^N]\right) = \begin{pmatrix} \sum_{j=2}^{N}\Gamma(x_1;x_j)k_f(x_j)\alpha_j\Delta x-\frac{1}{2}k_f(x_1)\alpha_1-\mu(x_1)\alpha_1 \\ \sum_{j=3}^{N}\Gamma(x_2;x_j)k_f(x_j)\alpha_j\Delta x-\frac{1}{2}k_f(x_2)\alpha_2-\mu(x_2)\alpha_2 \\ \vdots \\ \Gamma(x_{N-1};x_N)k_f(x_N)\alpha_N\Delta x-\frac{1}{2}k_f(x_{N-1})\alpha_{N-1}-\mu(x_{N-1})\alpha_{N-1} \\ -\frac{1}{2}k_f(x_N)\alpha_N-\mu(x_N)\alpha_N \end{pmatrix}.$$

In the following lemma we show that the numerical scheme satisfies Condition 5.7.

Claim 5.15. The function $g^N : H^N \times \mathscr{F} \to H^N$ as defined by

$$g^N(b^N,F)=\mathcal{A}[b^N]+\mathcal{B}[b^N;F]+\mathcal{R}[b^N] \tag{5.21}$$

satisfies the Lipschitz-type property in Condition 5.7.

Proof. We consider the integrand

$$\left\|\pi^N\left(\mathcal{A}[b^N]+\mathcal{R}[b^N]+\mathcal{B}[b^N;F]-\mathcal{A}[\tilde{b}^N]-\mathcal{R}[\tilde{b}^N]-\mathcal{B}[\tilde{b}^N;\tilde{F}]\right)\right\|,$$

and note that

$$\begin{aligned} \leq \quad & \left\|\pi^N\right\|\left(\left\|\mathcal{A}[b^N]-\mathcal{A}[\tilde{b}^N]\right\|\right. \\ & +\left\|\mathcal{R}[b^N]-\mathcal{R}[\tilde{b}^N]\right\| \\ & \left.+\left\|\mathcal{B}[b^N;F]-\mathcal{B}[\tilde{b}^N;\tilde{F}]\right\|\right). \end{aligned}$$

The induced L^1-norm on the projection operator will not be an issue as

$$\begin{aligned} \left\|\pi^N\right\| &= \sup_{h\in H,\|h\|=1}\left\|\pi^N h\right\| \\ &= \sup_{h\in H,\|h\|=1}\left\|\sum_{j=1}^{N}\frac{\beta_j^N(\cdot)}{\Delta x}\int_{x_{j-1}^N}^{x_j^N}h(x)dx\right\| \\ &= 1\,. \end{aligned}$$

As illustrated in the proof of Claim 5.14, the bounding constants for $\mathcal{A}+\mathcal{R}$ and $\mathcal{B}$ are $3C_0\left\|k_a\right\|_\infty+$

$\|\mu\|_\infty$ and $\|k_f\|_\infty \left(\frac{1}{2} + \overline{x}\,\|\Gamma\|_\infty\right)$, respectively. Combining these results, we have that

$$\left\|\tilde{b}^N(t,x;\tilde{F}) - b^N(t,x;F)\right\| \leq C_N \left\|\tilde{b}^N(t,x;\tilde{F}) - b^N(t,x;F)\right\| + \mathcal{T}^N(\tilde{F},F)$$

where $\mathcal{T}^N(\tilde{F},F) = \int_0^{t_f} \pi^N \mathscr{T}(\tilde{F},F)ds$, independent of t, and $C_N = \|k_f\|_\infty \left(\frac{1}{2} + \overline{x}\,\|\Gamma\|_\infty\right) + 3C_0\,\|k_a\|_\infty + \|\mu\|_\infty$. □

Corollary 5.16. *The semi-discrete solutions to (5.19) converge uniformly in L^1-norm to the unique solution of (5.12) on a bounded time interval as $N \to \infty$.*

Proof. From results in (Bortz et al., 2008), we can obtain semi-discrete solutions b^N to the forward problem that converge uniformly in norm to the unique solution of (5.12)-(5.13) on a bounded time interval as $N \to \infty$.

For fixed N, we rewrite (5.19) in integral form and consider

$$\begin{aligned}\left\|b^N(t,x;F) - \pi^N b(t,x;F)\right\| \;\leq\; & \int_0^t \left\|\pi^N\left(\mathcal{R}[b^N(s,x;F)] - \mathcal{R}[b(s,x;F)]\right)\right\| ds \\ & + \int_0^t \left\|\pi^N\left(\mathcal{A}[b^N(s,x;F)] + \mathcal{B}[b(s,x;F)]\right.\right. \\ & \left.\left. -\mathcal{A}[b^N(s,x;F)] - \mathcal{B}[b(s,x;F]\right)\right\| ds.\end{aligned}$$

for $t \in T$. The general strategy is to use the fact that the discretized version of g, defined in (5.21), is locally Lipschitz and then apply Gronwall's inequality. We refer readers to (Ackleh, 1997; Bortz et al., 2008) for the detailed discussion about the convergence of the numerical scheme. □

5.3.2 Convergence of the numerical scheme

In this section, we provide numerical evidence for the linear convergence of the approximation scheme described in Section 5.3.1. Towards this end, we choose the following model rates.

To describe the aggregation within a laminar shear field (orthokinetic aggregation (Dobias, 1993)) we used the kernel,

$$k_a(x,\,y) = 10^{-6}\left(x^{1/3} + y^{1/3}\right)^3 . \tag{5.22}$$

As in (Bortz et al., 2008; Ackleh & Fitzpatrick, 1997; Mirzaev & Bortz, 2015a,b) we assume that the breakage and removal rate of a floc of volume x is proportional to its radius,

$$k_f(x) = 10^{-1}x^{1/3} \quad \mu(x) = 10^{-3}x^{1/3}\,. \tag{5.23}$$

For the post-fragmentation density function we chose a uniform distribution in x for fixed y,

$$\Gamma(x, y) = \mathbb{1}_{[0,\,y]}(x)\frac{1}{y}\,, \tag{5.24}$$

a Beta distribution with $\alpha = \beta = 2$.

The main advantage of this semi-discrete scheme, defined in (5.12)-(5.13), is that it can be initialized very fast using Toeplitz matrices Matveev et al. (2015). This in turn proves useful in the optimization process, where the approximate forward problem is initialized and solved multiple times for each iteration. For solving the approximate forward problem we used an adaptive step size integration method implemented in an open-source Python library[2]. The simulation was run with initial size-distribution $b_0(x) = \exp(x)$ on $Q = [0,\,1]$ for $t_f = 1$. L^1-error between actual solution $u(t,\,x)$ and approximate solution $u_N(t,\,x)$ was computed as

$$\|u - u_N\| = \int_0^{t_f}\int_0^{\overline{x}} |u(t,\,x) - u_N(t,\,x)|\,dx\,dt\,.$$

Since no analytical solution is available for the nonlinear flocculation equations, defined (5.12)-(5.13), we estimate the error with a fine grid solution, i.e., $u(t,\,x) \approx u_{1000}(t,\,x)$.

Figure 5.2 depicts loglog plot of the error, which implies that the numerical algorithm has a linear convergence rate. This is due to the fact that we chose zeroth order functions as basis functions for approximate subspaces. In general, if one desires a higher order convergence for Galerkin-type approximations, choosing higher order basis functions gives higher convergence rate (Kappel & Kunisch, 1981).

5.3.3 Numerical optimization and results

[2] `scipy.integrate.odeint`

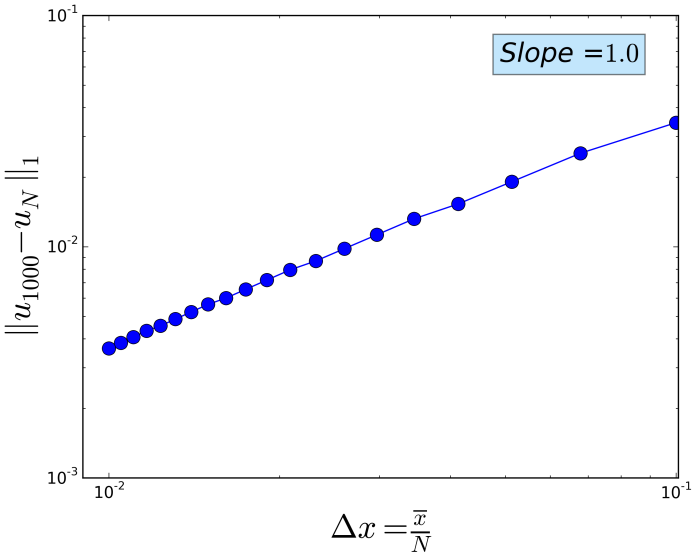

Figure 5.2: Loglog plot of the L^1-error

As an initial investigation into the utility of this approach, we apply the framework presented in this chapter to the flocculation equations. Towards this end, we generate two sets of artificial data.

In Byrne et al. (2011), we found that the resulting post-fragmentation density for *small* parent flocs resembles a Beta distribution with $\alpha = \beta = 2$ (see Figure 5.1a for an illustration). Therefore, the first artificial data set was generated from the forward problem by assuming model rates given in (5.22)-(5.23) and a post-fragmentation density function a Beta distribution with $\alpha = \beta = 2$,

$$\Gamma_{\text{true}}(x, y) = \mathbb{1}_{[0,\, y]}(x) \frac{6x(y-x)}{y^3}\,. \tag{5.25}$$

As in Section 5.3.1, we chose exponential initial size-distribution $b_0(x) = 10^3 \exp(x)$ on $Q = [0,\, 1]$ for $t_f = 10$. We also note that constants for the rate functions were chosen to emphasize the fragmentation as a driving factor. Moreover, Figure 5.3 illustrates the simulation of the forward problem for different post-fragmentation density functions. When the fragmentation is the driving mechanism, one can observe in Figures 5.3a-5.3c that model behaves significantly different for various post-fragmentation density functions.

Recall from Section 5.1.1 that data required for the inverse problem needs to be of the form $n_j(t_i)$, representing the number of flocs with volume between x_j and x_{j+1} at time t_i. In general, the number of bins for floc volume N_x comes fixed with measurement device (flow-cytometers, Coulter

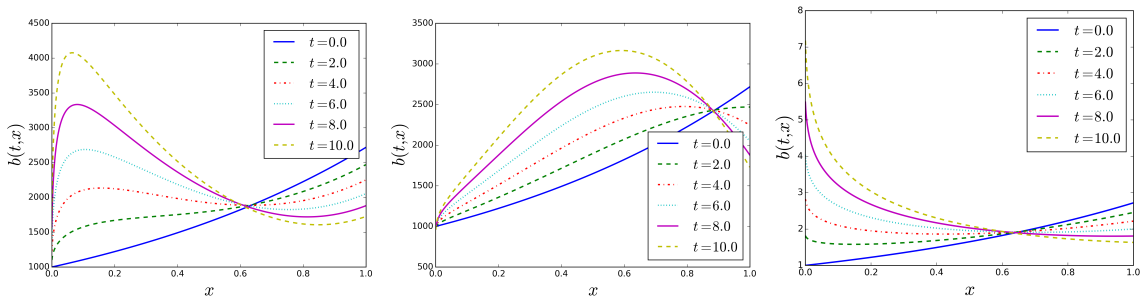

(a) (b) (c)

Figure 5.3: Direct model simulation results. a) Simulation of the forward problem for Beta distribution with $\alpha = \beta = 2$. b) Simulation of the forward problem using Beta distribution with $\alpha = 5$ and $\beta = 1$. c) Simulation of the forward problem using a uniform distribution in x for fixed y.

counters, etc). Therefore, for the synthetic data generation we choose fixed volume bins $N_x = 10$. Nevertheless, one has control of number of measurements taken in time, N_t.

The simulation results with fine grid ($N = 1000$ and $\Delta t = 0.001$) were interpolated onto the function $b(t,\, x,\, F_0)$ using linear interpolation[3]. Consequently, aggregate data of the form (5.3) were obtained from the integration of the interpolated function $b(t,\, x,\, F_0)$ on the interval $[x_j,\, x_{j+1}]$ and at time t_i. Furthermore, normal $i.i.d$ noise with zero mean and standard deviation $\sigma = 20$ were added to the aggregate data. For this choice of initial size-distribution and volume bins N_x values of the data are in the range [100, 300] and thus we note that $\sigma = 20$ is a significant noise.

To minimize the approximate cost functional in (5.8) we used nonlinear constrained optimization[4] employing Powell's iterative direct search algorithm (Powell, 1994, 1998). At each iteration the algorithm forms linear approximations to nonlinear objective and constraint functions and thus performs well even when no derivative information is available. For better results we set the maximum number of iterations to 10^4. The optimization was seeded with an initial density comprised of a uniform distribution in x for fixed y, illustrated in Figure 5.1c. Naturally, we constrained $\Gamma(\cdot, y)$ to be a probability density for each fixed y, i.e.,

$$F(x, y) = \int_0^x \Gamma(\xi;\, y)\, d\xi = 1 \text{ for all } x \in (y,\, \overline{x}].$$

[3] `scipy.interpolate.interp2d`
[4] `scipy.optimize.fmin_cobyla`

The optimization procedure is computationally very expensive. That is because at each iteration the algorithm solves the approximate forward problem with dimension N. Moreover, recall from Section 5.2 that for each approximate space $\mathcal{F}^{ML}$ the optimization entails finding L probability measures discretized with M Dirac measures. Therefore, time required for minimizing the cost functional (5.8) increases substantially for larger dimensions of the approximate space $\mathcal{F}^{ML}$, defined in Section 5.2. Towards this end, dimension of the approximate space and the approximate forward solution was set to 30, i.e., $N = M = L = 30$. For this case note that, since $F(x, y) \equiv 1$ for $x \geq y$ and fixed $y \in Q$,

$$\frac{N(N-1)}{2} = 435$$

discrete parameters need to be optimized for the simulation of the inverse framework.

For computational convenience, the error plots are in terms of the total variation metric (also called the *statistical distance*) defined as

$$\rho_{\mathrm{TV}}(F, \tilde{F}) = \sup_{\Omega \in \mathscr{A}} |F(\Omega) - \tilde{F}(\Omega)|\,,$$

where $\mathscr{A}$ is the Borel σ-algebra on Q as defined in Section 5.1.1. Note that convergence in the total variation metric implies the convergence of probability measures in the Prohorov metric (Gibbs & Su, 2002), i.e.,

$$\rho_{\mathrm{proh}}(F, \tilde{F}) \leq \rho_{\mathrm{TV}}(F, \tilde{F})\,. \tag{5.26}$$

The result of the optimization for the density function (5.25) is shown in Figure 5.4. The optimization was carried out with $N = M = L = 30$, $N_x = 10$, $N_t = 20$. In Figure 5.4d, we have illustrated error plots for different observation duration $t_f \in \{1, 2, \cdots, 20\}$. Observe the general trend that having larger observation duration improves the error in estimates. Figures 5.4a and 5.4b depict the result of the optimization for $t_f = 10$. One can see that fit between the *true* F_0 and approximate probability measures F_{30} is satisfactory (though there is room for improvement).

Moreover, Figure 5.4c also illustrates the satisfactory fit between F_0 and F_{30}, for two fixed values of y.

To investigate the behavior of the estimators for different probability distributions we applied our inverse methodology for another artificial data set. The artificial data set was generated with a post-fragmentation density function equal to a Beta distribution with $\alpha = 5$ and $\beta = 1$ (see Figure 5.1a for an illustration),

$$\Gamma_{\text{true}}(x, y) = \mathbb{1}_{[0,\, y]}(x)\frac{5x^4}{y^5}\,. \tag{5.27}$$

Other model rates were chosen same as in the first artificial data set. The application of our inverse problem framework to this second artificial data set is depicted in Figure 5.5. Figure 5.5d illustrates error plots in total variance norm for different observation duration $t_f \in \{1, 2, \cdots, 20\}$. Once again having larger observation duration is generally improving the error in estimates. Furthermore, Figures 5.5a-5.5c, depict that the fit between F_0 and F_{30} is satisfactory.

We also note that our simulations gave better convergence results for larger values of $t_f \geq 5$ as depicted in Figures 5.4d and 5.5d. For the last few values of t_f, the error does appear to exhibit an increasing trend, possibly due a lack of sufficient resolution in time. This result is consistent with the literature (Banks et al., 2007b; Keck & Bortz, pear; Thomaseth & Cobelli, 1999) in that the size and resolution of the observation interval can have a substantial effect on identifiability of parameters. For instance, Thomaseth & Cobelli (1999) developed generalized sensitivity functions that can be used for the qualitative analysis of the impact of the observation intervals on identifiability of parameters in dynamical systems. These sensitivity functions help to identify the most relevant data and time subdomains for identification of certain parameters. Later, Banks et al. (Banks et al., 2010a, 2007b) offered a quantitative means to choose the duration t_f required for an optimal experiment design. Moreover, Keck & Bortz (pear), provided an extension of this sensitivity functions to the size-structured population models. Hence, as a future research direction, we plan to incorporate these sensitivity functions for choosing the optimum observation duration t_f.

Figure 5.6 depicts the effect of increasing noise on the reconstruction of the conditional probability measures. In particular, in Figure 5.6a (and Figure 5.6b) we plotted the error between *true* cdf F_0 and approximate cdf F_{30} for increasing standard deviation σ of artificial noise added to the first

data set (and the second data set). The optimization was carried with $t_f = 10$, $N = M = L = 30$ and $N_t = N_x = 10$. One can observe that for both data sets the optimization performs well for the standard deviations in the range [0, 25].

5.4 Concluding Remarks

Our efforts here are motivated by a class of mathematical models which characterize a random process, such as fragmentation, by a probability distribution. We are concerned with the inverse problem for inferring the conditional probability distribution in measure-dependent evolution equations, and present the specific problem for the flocculation dynamics of aggregates in suspension which motivated this study. We then developed the mathematical framework in which we formulate the inverse problem as a least squares problem for inferring the conditional probability distributions. We prove existence and consistency of the least squares estimates using the Prohorov metric framework. We also include results for overall method stability for numerical approximation, confirming a computationally feasible methodology. Finally, we verify that our motivating example in flocculation dynamics conforms to the developed framework, and illustrate its utility by identifying sample distributions.

To conclude, this work is one piece of a larger effort aimed at advancing our abilities for identifying microscale phenomena from size-structured population measurements. In particular, we are interested in the propensity of suspended bacterial aggregates to fragment in a flowing system. The model proposed in (Byrne et al., 2011) uses knowledge of the hydrodynamics to predict a breakage event and thus the post fragmentation density Γ. With this work, we now have a tool to bridge the gap between the experimental and microscale modeling efforts for fragmentation. Our future effort will focus on using experimental evidence to validate (or refute) our proposed fragmentation model.

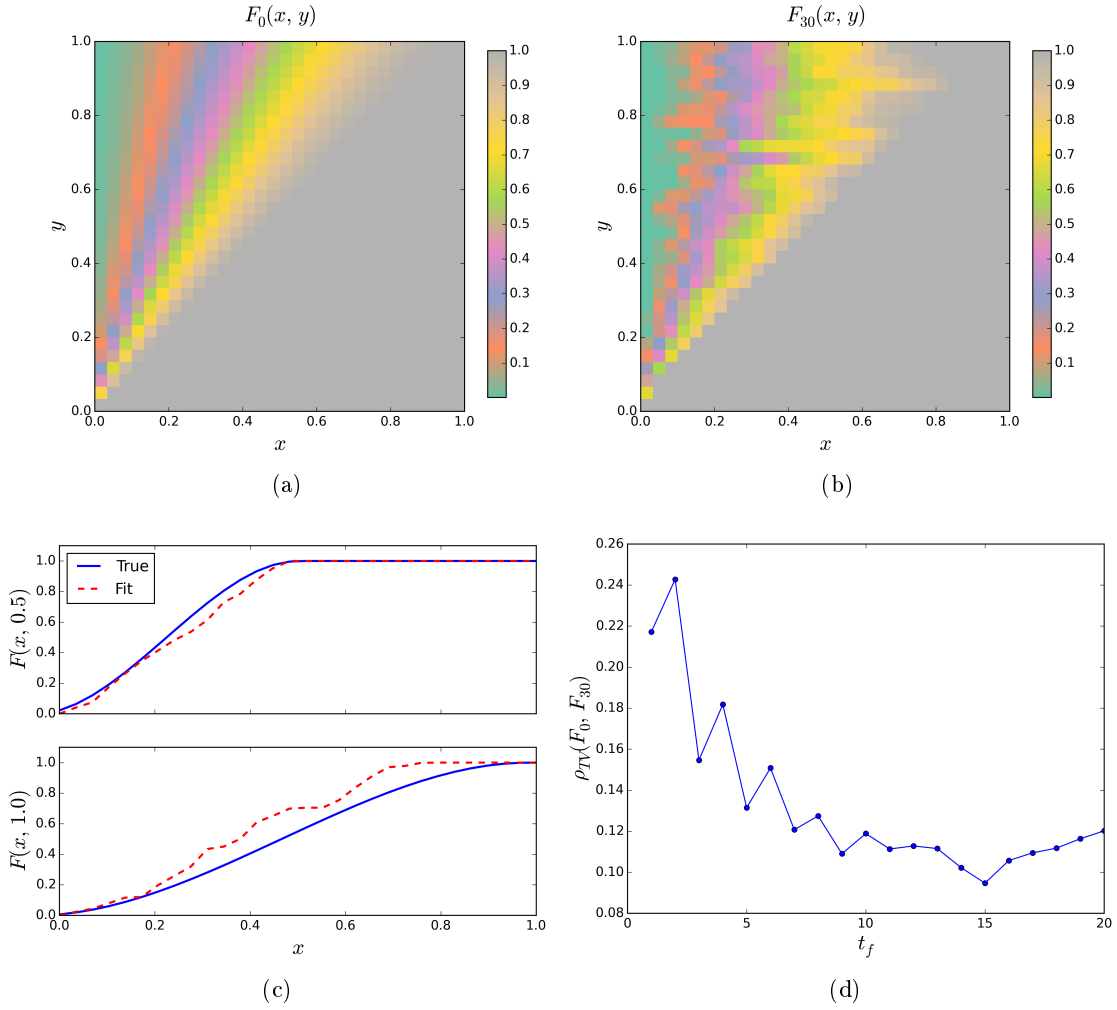

Figure 5.4: Simulation results for the artificial data generated using Beta distribution with $\alpha = \beta = 2$, and normal i.i.d error with mean zero and standard deviation $\sigma = 20$. (a) *True* cdf $F_0(x, y)$ (b) Approximate cdf $F_{30}(x, y)$ for $N = M = L = 30$, $N_x = 10$, $N_t = 20$ and $t_f = 10$. (c) Comparison of $F_0(x, y)$ and $F_{30}(x, y)$ for $y = 0.5$ and $y = 1.0$ (d) Error plots in total variance norm for $t_f \in \{1, 2, \cdots, 20\}$ and $N_t = 20$.

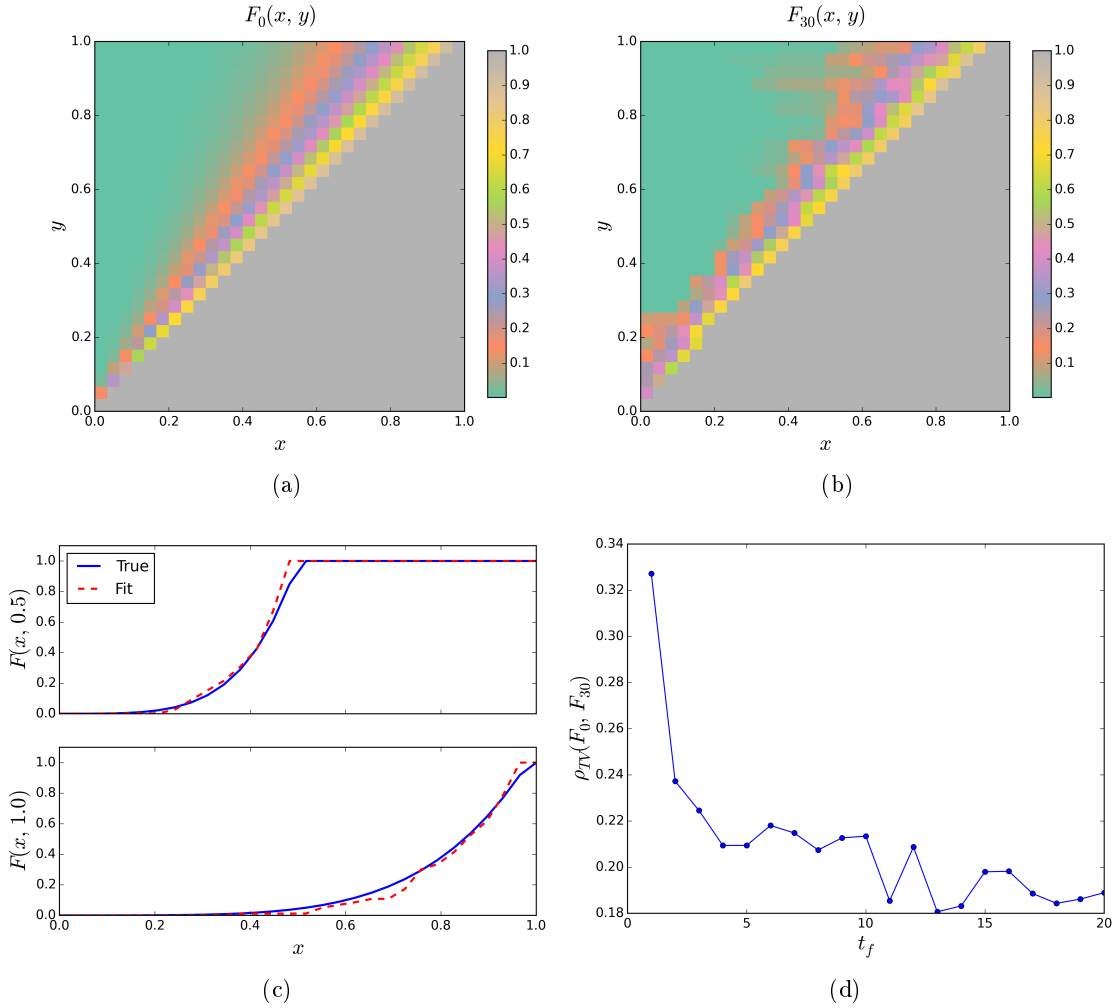

Figure 5.5: Simulation results for the artificial data generated using Beta distribution with $\alpha = 5$ and $\beta = 1$ and normal i.i.d error with mean zero and standard deviation $\sigma = 20$. (a) *True* cdf $F_0(x, y)$. (b) Approximate cdf $F_{30}(x, y)$ for $N = M = L = 30$, $N_x = 10$, $N_t = 20$ and $t_f = 10$. (c) Comparison of $F_0(x, y)$ and $F_{30}(x, y)$ for $y = 0.5$ and $y = 1.0$ (d) Error plots in total variance norm for $t_f \in \{1, 2, \cdots, 20\}$ and $N_t = 20$.

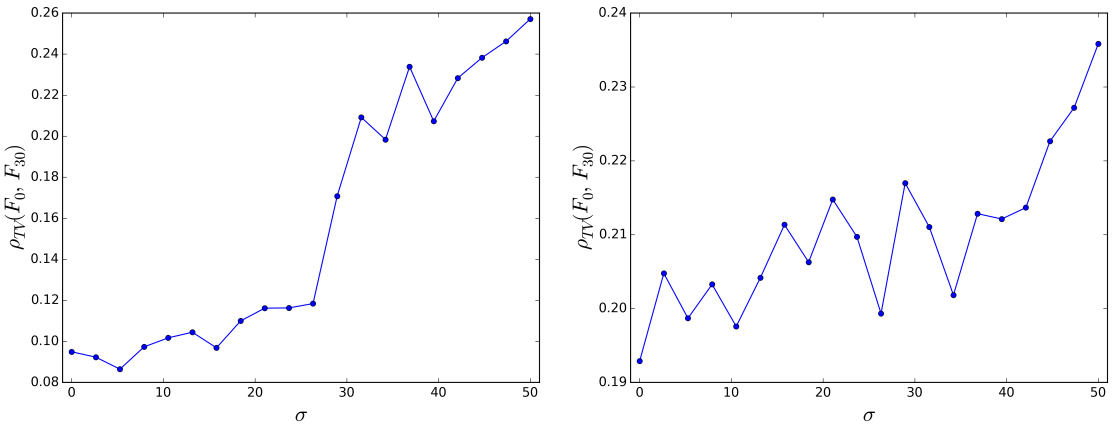

(a) (b)

Figure 5.6: Effect of noise on reconstruction of the conditional probability measure with $N = M = L = 30$ and $N_t = N_x = 10$. a) Artificial data set generated using Beta distribution with $\alpha = \beta = 2$ and increasing normal i.i.d error with mean zero and standard deviation $\sigma \in [0, 50]$. b) Artificial data set generated using Beta distribution with $\alpha = 5$ and $\beta = 1$ and increasing normal i.i.d error with mean zero and standard deviation $\sigma \in [0, 50]$.

Chapter 6

Conclusions

6.1 Industrial applications of flocculation

Flocculation of suspended particles is ubiquitous in many different fields such as meteorology, marine science, astronomy, polymer science, and biotechnology. Flocculation is an efficient liquid-solid separation technique and has a broad range of industrial applications including fermentation, biofuel production, mineral processing, wastewater treatment, just to name a few. Particularly, almost all of the modern wastewater treatment plants have bioreactors where microbial metabolism and flocculation are exploited in the removal of hazardous material from the surface waters, often referred to as activated sludge process. The activated sludge process is the most commonly used pollutant removal method for municipal and industrial wastewater treatment. The sewage water in an aeration tank is seeded with bacteria, which use soluble and insoluble contaminants as a substrate for metabolism. Floc formation of newly formed cells is controlled in a settling tank. Consequently, the flocculated biomass is removed from the clarified effluent before its discharge by gravitational solid-liquid separation technique. Flocculation of microorganisms is crucial for the proper operation and efficiency of the gravitational separation technique. The failure of flocculation process may result in an excess discharge of solids to the rivers, which in turn results in the spreading of disease and destruction of aquatic life.

The final clarification step is often modeled using simple ordinary differential equations which describe time-evolution of an averaged variable for the biomass concentration in the tank. Recent technological advance in online monitoring of activated sludge flocculation has enabled development

of so-called segregated models. In segregated models, mostly referred to as population balance models, the individual interactions of flocs are accurately described and transient time evolution of floc size distribution in the tank is tracked. The mathematical model for the microbial flocculation is a 1D nonlinear partial integro-differential equation, which has been successful in matching many flocculation experiments (Li et al., 2004; Ducoste, 2002; Spicer & Pratsinis, 1996; Nopens et al., 2005). The microbial flocculation equations (1.1) accounts for a broad range of biological phenomena (necessary for the survival of a community of microorganism in a suspension) including growth, aggregation, fragmentation, removal due to predation and gravitational sedimentation. Moreover, the number of cells that erode from a floc and enter the single cell population is modeled with McKendrick-von Foerster-type renewal boundary equation.

The microbial flocculation equations have been a focus of an extensive mathematical analysis over the past several decades. Well-posedness of the microbial flocculation equations has been established in many different space settings. Analytical solutions were found for a few special cases and thus many different numerical schemes have been proposed for the approximation of the solutions. Nevertheless, the nonlinear terms introduced by aggregation have made investigating the long-term behavior of the microbial flocculation equation a very challenging task. Towards this end, in this dissertation report, we rigorously investigated the long-term behavior of the microbial flocculation equations described in (1.1).

6.2 Summary of the mathematical results

We first showed that, under relatively simple restrictions on the model rates, the microbial flocculation equations possess a unique, non-trivial, positive stationary solution. Consequently, we employed the principle of linearized stability to provide sufficient conditions for the local stability and instability of the non-trivial stationary solutions. Microbial flocculation equations can be classified as evolution equations. There are many analytical techniques for establishing existence and stability of stationary solutions of evolution equations. However, finding closed form stationary solutions of evolution equations is rather challenging and thus making linearized stability analysis very difficult. To this end, we developed a numerical framework for computing approximations to stationary solutions of general evolution equations, which can also be used to produce approximate

existence and stability regions for steady states.

Moreover, to approximate stationary solutions of the microbial flocculation equations, we proposed several different numerical techniques based on Finite Difference and Spectral Collocation methods. In particular, our numerical scheme with spectral collocation method yielded very precise approximations with at high rate of convergence. We exploited this increased precision in the approximation scheme for the numerical spectral analysis of Freched derivative of the operator $\mathcal{F}$ (1.1) evaluated at a computed stationary solution, which allowed us to numerically evaluate the local stability of computed stationary solutions. Furthermore, we explored the stationary solutions of the model for various biologically relevant parameters and gave valuable insights for the efficient removal of suspended particles. For instance, our results indicate that for a given growth rate of a microbial floc one can adjust the shear rate within a stirring tank to yield an optimal average floc size.

We also presented and investigated an inverse problem for estimating the conditional probability measures in size-structured population models from size-distribution measurements. We illustrated that a particular form of the microbial flocculation equations (without the growth of the flocs, i.e., $g(x) \equiv 0$) is one realization of a system satisfying the hypotheses of our framework. In particular, we showed that our inverse methodology can be utilized to infer the post-fragmentation density function $\Gamma(x, y)$ from size-distribution measurements. Furthermore, we presented numerical examples to demonstrate the feasibility of our methodology for artificial data sets.

6.3 Discussion

We found that the growth and renewal rates, accounted in the boundary conditions, are crucial for the existence and the stability of the non-trivial steady states. As stated in Theorem 2.1, for the existence of the stationary solutions the growth rate needs to be sufficiently large. In Figure 4.10, we numerically validated that the stationary solutions fail to exist for the small growth rates. Moreover, for the large growth rates the growth dominates and thus stationary solution of the nonlinear microbial flocculation equation approaches the stationary solutions of the linear Sinko-Streifer equations. Furthermore, for the existence of a positive stationary solution half of the fragmentation rate should be larger than the removal rate. This in turn can be interpreted as

fragmentation rate needs to be fast enough such that not all of the large flocs are removed by the gravitational sedimentation. Conversely, when the removal rate is sufficiently large, as illustrated in Figure 1.3a, the solutions converge to a zero stationary solution.

As illustrated in Figure 1.3, the magnitude of the renewal rate can cause the solutions to diverge or converge to trivial or non-trivial stationary solutions. In fact, one of the main assumptions of the steady state existence theorem (Theorem 2.1) is to adjust the renewal rate to satisfy

$$g(0)p(0) = \int_0^{\overline{x}} q(y)u_*(y)\,dy = 1\,. \tag{6.1}$$

The numerical spectral analysis of Section (4.4) suggest that the stationary solutions satisfying the condition (6.1) are all locally stable. However, note that the numerical results of the Chapters 3 and 4 indicate existence of stationary solutions even when the condition (6.1) is not satisfied. Hence, as a future research, we plan to further investigate stability of non-trivial steady states of the microbial flocculation equations.

Appendix A

Model Rates used in Chapter 4

Having the approximation scheme in hand, we now present our preliminary numerical results. For the purpose of illustration, the aggregation kernel was chosen to describe flow within laminar shear flow (Saffman & Turner, 1956) (i.e., *orthokinetic* aggregation)

$$k_a(x,\, y) = 1.3 \left(\frac{\epsilon}{\nu}\right)^{1/2} \left(x^{1/3} + y^{1/3}\right)^3 ,$$

where ϵ represents the homogeneous turbulent energy dissipation rate of the stirred tank and ν is the kinematic viscosity of the suspending fluid. The quantity

$$\dot{\gamma} := \left(\frac{\epsilon}{\nu}\right)^{1/2}$$

is often referred to as a "volume average shear rate" (hereby, referred to as the "shear rate") of the stirring tank.

We employ the fragmentation rate given by Spicer (1995)

$$k_f(x) = C_f x^{1/3} ,$$

where C_f is the breakage rate coefficient for shear-induced fragmentation. Pandya & Spielman (1983); Spicer & Pratsinis (1996) have experimentally shown that there is a power law relation between the shear rate $\dot{\gamma}$ and the breakage rate C_f,

$$C_f = a\dot{\gamma}^b$$

Parameter	Symbol	Value	Source
Kinematic viscosity of water at 20°C	ν	$10^{-6}\, m^2/s$	Jewett & Serway (2008)
Shear rate	$\dot{\gamma}$	$1\, s^{-1}$	Piani et al. (2014)
Fitting parameter	a	7×10^{-4}	(Flesch et al., 1999)
Fitting parameter	b	1.6	(Flesch et al., 1999)
Removal rate	C_μ	$1/\dot{\gamma}$	Assumed
Growth rate	C_g	1	Assumed
Renewal rate (surface erosion)	C_q	$\left(\int_0^1 (y+1)p_*(y)\, dy\right)^{-1}$	This chapter (6.2)

Table 6.1: Model parameters and their values used in simulations

where a and b fitting parameters specific to a flow type. For our purposes we use the parameters for laminar shear flow found by Flesch et al. (1999),

$$a = 7 \times 10^{-4}, \qquad b = 1.6\,.$$

For a post-fragmentation density function we chose the well-known Beta distribution[1] with $\alpha = \beta = 2$,

$$\Gamma(x,\, y) = \mathbb{1}_{[0,\, y]}(x) \frac{6x(y-x)}{y^3}\,,$$

where $\mathbb{1}_I$ is the indicator function on the interval $I = [0,\, 1]$. Removal rate is assumed to be linearly proportional to the volume of the floc,

$$\mu(x) = C_\mu x\,.$$

Since flocs sediment slower under large shear rates, the removal rate should be inversely proportional to the shear rate of the stirring tank. Therefore, for the remaining of the chapter we set the removal rate to

$$C_\mu = \exp\left(-\dot{\gamma}\right)\,.$$

Renewal (or surface erosion rate) is assumed to be proportional to the surface area of a floc, i.e.,

$$q(x) = C_q x^{2/3}\,.$$

[1] Although normal and log-normal distributions are mostly used in the literature, Byrne et al. (Byrne et al., 2011) have provided evidence that the Beta density function describes the fragmentation of small bacterial flocs.

where C_q some positive real number. Finally, we chose growth rate arbitrarily to fulfill positivity condition (**A**1),

$$g(x) = C_g(x+1)\,.$$

Note that, once a stationary solution is found, the constant C_q needs to be set to

$$C_q := \left(\int_0^1 (y+1)p_*(y)\,dy\right)^{-1}\,. \tag{6.2}$$

The remaining parameters C_g and $\dot{\gamma}$ can be set to an arbitrary positive real number. Unless otherwise stated, all the parameters used for the simulations are given in Table 6.1.

Bibliography

Aceto, N., Bardia, A., Miyamoto, D. T., Donaldson, M. C., Wittner, B. S., Spencer, J. A., Yu, M., Pely, A., Engstrom, A., Zhu, H., Brannigan, B. W., Kapur, R., Stott, S. L., Shioda, T., Ramaswamy, S., Ting, D. T., Lin, C. P., Toner, M., Haber, D. A., & Maheswaran, S. (2014). Circulating Tumor Cell Clusters Are Oligoclonal Precursors of Breast Cancer Metastasis. *Cell*, 158(5), 1110–1122.

Ackleh, A. S. (1997). Parameter estimation in a structured algal coagulation-fragmentation model. *Nonlinear Analysis*, 28(5), 837–854.

Ackleh, A. S. & Fitzpatrick, B. G. (1997). Modeling aggregation and growth processes in an algal population model: analysis and computations. *J. Math. Biol.*, 35(4), 480–502.

Adachi, Y. (1995). Dynamic aspects of coagulation and flocculation. *Advances in Colloid and Interface Science*, 56, 1–31.

Adams, R. & Fournier, J. (2003). *Sobolev spaces*. Oxford, UK: Elsevier Ltd.

Aldous, D. J. (1999). Deterministic and Stochastic Models for Coalescence (Aggregation, Coagulation): A Review of the Mean-Field Theory for Probabilists. *Bernoulli*, 5(1), 3–48.

Appell, J., Pascale, E. D., & Vignoli, A. (2004). *Nonlinear spectral theory*. Walter de Gruyter GmbH & Co.

Arnold, V. I. (1992). *Ordinary Differential Equations*. Berlin, Heidelberg: Springer Science & Business Media.

Bäbler, M. U., Morbidelli, M., & Baldyga, J. (2008). Modelling the breakup of solid aggregates in turbulent flows. *Journal of Fluid Mechanics*, 612, 261–289.

Bache, D. H. & Gregory, R. (2007). *Flocs in Water Treatment*. London, UK: IWA Publishing.

Banasiak, J. (2011). Blow-up of solutions to some coagulation and fragmentation equations with growth. *Discrete and Continuous Dynamical Systems*, (pp. 126–134).

Banasiak, J. & Lamb, W. (2009). Coagulation, fragmentation and growth processes in a size structured population. *Discrete Contin. Dyn. Syst. - Ser. B*, 11(3), 563–585.

Banks, H. T., Banks, J. E., Dick, L. K., & Stark, J. D. (2007a). Estimation of Dynamic Rate Parameters in Insect Populations Undergoing Sublethal Exposure to Pesticides. *Bull. Math. Biol.*, 69(7), 2139–2180.

Banks, H. T. & Bihari, K. L. (2001). Modeling and Estimating Uncertainty in Parameter Estimation. *Inverse Problems*, 17(CRSC-TR99-40), 95–111.

Banks, H. T. & Bortz, D. M. (2005). Inverse problems for a class of measure dependent dynamical systems. *Journal of Inverse and Ill-posed Problems*, 13(2), 103–121.

Banks, H. T., Dediu, S., & Ernstberger, S. L. (2007b). Sensitivity functions and their uses in inverse problems. *Journal of Inverse and Ill-posed Problems jiip*, 15(7), 683–708.

Banks, H. T., Dediu, S., Ernstberger, S. L., & Kappel, F. (2010a). Generalized sensitivities and optimal experimental design. *Journal of Inverse and Ill-posed Problems*, 18(1).

Banks, H. T. & Fitzpatrick, B. G. (1990). Statistical methods for model comparison in parameter estimation problems for distributed systems. *Journal of Mathematical Biology*, 28(5), 501–527.

Banks, H. T. & Fitzpatrick, B. G. (1991). Estimation of growth rate distributions in size structured population models. *Quarterly of Applied Mathematics*, 49(2), 215–235.

Banks, H. T., Fitzpatrick, B. G., Potter, L. K., & Zhang, Y. (1999). Estimation of Probability Distributions for Individual Parameters Using Aggregate Population Data. In W. M. McEneaney, G. G. Yin, & Q. Zhang (Eds.), *Stochastic Analysis, Control, Optimization and Applications*, Systems & Control: Foundations & Applications (pp. 353–371). Birkhäuser Boston.

Banks, H. T. & Kappel, F. (1989). Transformation semigroups andL 1-approximation for size structured population models. *Semigroup Forum*, 38(1), 141–155.

Banks, H. T., Kareiva, P. M., & Murphy, K. A. (1987). Parameter estimation techniques for interaction and redistribution models: a predator-prey example. *Oecologia*, 74(3), 356–362.

Banks, H. T., Kenz, Z. R., & Thompson, W. C. (2012). A review of selected techniques in inverse problem nonparametric probability distribution estimation. *Journal of Inverse and Ill-Posed Problems*, 20(4), 429–460.

Banks, H. T. & Kunisch, K. (1989). *Estimation Techniques for Distributed Parameter Systems*, volume 1 of *Systems & Control: Foundations & Applications*. Boston, MA: Birkhäuser.

Banks, H. T., Sutton, K. L., Thompson, W. C., Bocharov, G., Roose, D., Schenkel, T., & Meyerhans, A. (2010b). Estimation of Cell Proliferation Dynamics Using CFSE Data. *Bull. Math. Biol.*, 73(1), 116–150.

Banks, H. T. & Thompson, W. C. (2012). *Least Squares Estimation of Probability Measures in the Prohorov Metric Framework*. Technical Report CRSC-TR12-21, North Carolina State University Center for Research in Scientific Computation, Raleigh, NC.

Banks, H. T. & Thompson, W. C. (2015). Existence and consistency of a nonparametric estimator of probability measures in the prohorov metric framework. *International Journal of Pure and Apllied Mathematics*, 103(4).

Banks, J. E., Dick, L. K., Banks, H. T., & Stark, J. D. (2008). Time-varying vital rates in ecotoxicology: Selective pesticides and aphid population dynamics. *Ecological Modelling*, 210(1–2), 155–160.

Bauer, F. F., Govender, P., & Bester, M. C. (2010). Yeast flocculation and its biotechnological relevance. *Applied Microbiology and Biotechnology*, 88(1), 31–39.

Becker, R. & Döring, W. (1935). Kinetische Behandlung der Keimbildung in übersättigten Dämpfen. *Ann. Phys.*, 416(8), 719–752.

Bell, G. & Anderson, E. (1967). Cell growth and division: I. a mathematical model with applications to cell volume distributions in mammalian suspension cultures. *Biophysical journal*.

Belleni-Morante, A. & McBride, A. (1998). *Applied nonlinear semigroups*. John Wiley & Sons.

Biggs, C. & Lant, P. (2002). Modelling activated sludge flocculation using population balances. *Powder Technol.*, 124(3), 201–211.

Billingsley, P. (1968). *Convergence of Probability Measures*. New York, NY: John Wiley & Sons.

Borenstein, J. T. (2008). Acting together, bacterial clusters initiate coagulation. *Nat Chem Biol*, 4(12), 718–719.

Bortz, D. M. (2015). Chapter 17: Modeling and simulation for nanomaterials in fluids: Nanoparticle self-assembly. In V. Tewary & Y. Zhang (Eds.), *Modeling, characterization, and production of nanomaterials: Electronics, Photonics and Energy Applications*, volume 73 of *Woodhead Publishing Series in Electronic and Optical Materials* (pp. 419–441). Cambridge, UK: Woodhead Publishing Ltd.

Bortz, D. M., Jackson, T. L., Taylor, K. A., Thompson, A. P., & Younger, J. G. (2008). Klebsiella pneumoniae Flocculation Dynamics. *Bull. Math. Biol.*, 70(3), 745–768.

Bottero, S., Storck, T., Heimovaara, T. J., van Loosdrecht, M. C. M., Enzien, M. V., & Picioreanu, C. (2013). Biofilm development and the dynamics of preferential flow paths in porous media. *Biofouling*, 29(9), 1069–1086.

Bourgade, J.-P. & Filbet, F. (2008). Convergence of a Finite Volume Scheme for Coagulation-Fragmentation Equations. *Mathematics of Computation*, 77(262), 851–882.

Bourgeron, T., Doumic, M., & Escobedo, M. (2014). Estimating the division rate of the growth-fragmentation equation with a self-similar kernel. *Inverse Problems*, 30(2), 025007.

Breda, D. (2006). Solution operator approximations for characteristic roots of delay differential equations. *Applied Numerical Mathematics*, 56(3–4), 305–317.

Breda, D., Diekmann, O., Maset, S., & Vermiglio, R. (2013). A numerical approach for investigating the stability of equilibria for structured population models. *J. Biol. Dyn.*, 7, 4–20.

Breda, D., Maset, S., & Vermiglio, R. (2004). Computing the characteristic roots for delay differential equations. *IMA J Numer Anal*, 24(1), 1–19.

Breda, D., Maset, S., & Vermiglio, R. (2005). Pseudospectral Differencing Methods for Characteristic Roots of Delay Differential Equations. *SIAM J. Sci. Comput.*, 27(2), 482–495.

Breda, D., Maset, S., & Vermiglio, R. (2006). Pseudospectral approximation of eigenvalues of derivative operators with non-local boundary conditions. *Applied Numerical Mathematics*, 56(3–4), 318–331.

Breda, D., Maset, S., & Vermiglio, R. (2009). Numerical approximation of characteristic values of partial retarded functional differential equations. *Numer. Math.*, 113(2), 181–242.

Buyel, J. F. & Fischer, R. (2014). Downstream processing of biopharmaceutical proteins produced in plants. *Bioengineered*, 5(2), 138–142.

Byrne, E., Dzul, S., Solomon, M., Younger, J., & Bortz, D. M. (2011). Postfragmentation density function for bacterial aggregates in laminar flow. *Phys. Rev. E*, 83(4).

Calvez, V., Doumic, M., & Gabriel, P. (2012). Self-similarity in a general aggregation–fragmentation problem. Application to fitness analysis. *Journal de Mathématiques Pures et Appliquées*, 98(1), 1–27.

Calvez, V., Lenuzza, N., Doumic, M., Deslys, J.-P., Mouthon, F., & Perthame, B. (2010). Prion dynamics with size dependency–strain phenomena. *J. Biol. Dyn.*, 4(1), 28–42.

Caridi, A. (2006). Enological functions of parietal yeast mannoproteins. *Antonie Van Leeuwenhoek*, 89(3-4), 417–422.

Carrera, J. & Neuman, S. P. (1986). Estimation of Aquifer Parameters Under Transient and Steady State Conditions: 2. Uniqueness, Stability, and Solution Algorithms. *Water Resour. Res.*, 22(2), 211–227.

Chavent, G. (1979). Identification of distributed parameter systems: about the output least square method, its implementation and identifiability. In *Proc. 5th IFAC Symposium on Identification and System Parameter Estimation*, volume 1 (pp. 85–97).

Chen, R. E. & Thorner, J. (2007). Function and regulation in MAPK signaling pathways: Lessons learned from the yeast Saccharomyces cerevisiae. *Biochimica et Biophysica Acta (BBA)-Molecular Cell Research*, 1773(8), 1311–1340.

Cooley, R. L. (1982). Incorporation of prior information on parameters into nonlinear regression groundwater flow models: 1. Theory. *Water Resour. Res.*, 18(4), 965–976.

Dacosta, F. P. (1995). Existence and Uniqueness of Density Conserving Solutions to the Coagulation-Fragmentation Equations with Strong Fragmentation. *Journal of Mathematical Analysis and Applications*, 192(3), 892–914.

Dagan, G. (1982). Stochastic modeling of groundwater flow by unconditional and conditional probabilities: 1. Conditional simulation and the direct problem. *Water Resources Research*, 18(4), 813–833.

Darzynkiewicz, Z., Robinson, J. P., & Crissman, H. A. (1994). Flow Cytometry. In *Methods in Cell Biology* (pp. 1–697). San Diego, CA: Academic Press, 2nd edition.

Davis, R. H. & Hunt, T. P. (1986). Modeling and Measurement of Yeast Flocculation. *Biotechnol Progress*, 2(2), 91–97.

De Roos, A. M. (2008). Demographic analysis of continuous-time life-history models. *Ecol. Lett.*, 11(1), 1–15.

De Roos, A. M. (2014). PSPManalysis. https://staff.fnwi.uva.nl/a.m.deroos/PSPManalysis/index.html.

De Roos, A. M., Diekmann, O., Getto, P., & Kirkilionis, M. a. (2010). Numerical equilibrium analysis for structured consumer resource models. *Bulletin of mathematical biology*, 72(2), 259–97.

DeVita, V. T., Lawrence, Theodore, S., & Rosenberg, S. A. (2008). *Cancer: Principles and Practice of Oncology*, volume 1. Lippincott Williams & Wilkins.

Diekmann, O., Gyllenberg, M., & Metz, J. A. J. (2003). Steady-state analysis of structured population models. *Theoretical Population Biology*, 63(4), 309–338.

Diekmann, O., Heijmans, H. J. A. M., & Thieme, H. R. (1984). On the stability of the cell size distribution. *J. Math. Biol.*, 19(2), 227–248.

Dobias, B. (1993). *Coagulation and Flocculation: Theory and Applications*. CRC Press.

Dorao, C. A. & Jakobsen, H. A. (2006a). Application of the least-squares method for solving population balance problems in Rd+1. *Chemical Engineering Science*, 61(15), 5070–5081.

Dorao, C. A. & Jakobsen, H. A. (2006b). A least squares method for the solution of population balance problems. *Computers & Chemical Engineering*, 30(3), 535–547.

Dorao, C. A. & Jakobsen, H. A. (2007). Least-squares spectral method for solving advective population balance problems. *Journal of Computational and Applied Mathematics*, 201(1), 247–257.

Doumic, M., Perthame, B., & Zubelli, J. P. (2009). Numerical solution of an inverse problem in size-structured population dynamics. *Inverse Problems*, 25(4), 045008.

Doumic, M. & Tine, L. M. (2012). Estimating the division rate for the growth-fragmentation equation. *J. Math. Biol.*, 67(1), 69–103.

Doumic-Jauffret, M. & Gabriel, P. (2009). Eigenelements of a General Aggregation-Fragmentation Model. *ArXiv09075467 Math*.

Dubovskii, P. B. (1994). *Mathematical Theory of Coagulation*. Number 23 in Lecture Notes Series. Seoul National University, Seoul 151-742, Korea: Seoul National University, Research Institute of Mathematics, Global Analysis Research Center.

Dubovskii, P. B. & Stewart, I. W. (1996). Existence, Uniqueness and Mass Conservation for the Coagulation-Fragmentation Equation. *Mathematical Methods in the Applied Sciences*, 19(7), 571–591.

Ducoste, J. (2002). A two-scale PBM for modeling turbulent flocculation in water treatment processes. *Chemical Engineering Science*, 57(12), 2157–2168.

Engel, K.-J. & Nagel, R. (2000). *One-Parameter Semigroups for Linear Evolution Equations*, volume 194 of *Graduate Texts in Math*. New York, NY: Springer Science & Business Media.

Engelborghs, K., Luzyanina, T., & Roose, D. (2002). Numerical Bifurcation Analysis of Delay Differential Equations Using DDE-BIFTOOL. *ACM Trans Math Softw*, 28(1), 1–21.

Engl, H. W., Rundell, W., & Scherzer, O. (1994). A Regularization Scheme for an Inverse Problem in Age-Structured Populations. *Journal of Mathematical Analysis and Applications*, 182(3), 658–679.

Enmon, R. M., O'Connor, K. C., Song, H., Lacks, D. J., & Schwartz, D. K. (2002). Aggregation kinetics of well and poorly differentiated human prostate cancer cells. *Biotechnol. Bioeng.*, 80(5), 580–588.

Escobedo, M., Mischler, S., & Perthame, B. (2002). Gelation in Coagulation and Fragmentation Models. *Communications in Mathematical Physics*, 231(1), 157–188.

Farkas, J. (2005). Stability conditions for a non-linear size-structured model. *Nonlinear Anal. Real World Appl.*, 6(5), 962–969.

Farkas, J. Z. (2005). Stability conditions for a non-linear size-structured model. *Nonlinear Analysis: Real World Applications*, 6, 962–969.

Farkas, J. Z. & Hagen, T. (2007). Linear stability and positivity results for a generalized size-structured Daphnia model with inflow. *Applicable Analysis*, 86(9), 1087–1103.

Farkas, J. Z. & Hagen, T. (2007). Stability and regularity results for a size-structured population model. *J. Math. Anal. Appl.*, 328(1), 119–136.

Farkas, J. Z. & Hagen, T. (2010). Hierarchical size-structured populations: The linearized semigroup approach. *Dynamics of Continuous, Discrete and Impulsive Systems Series A: Mathematical Analysis*, 17(5), 639–657.

Farkas, J. Z. & Hinow, P. (2012). Steady states in hierarchical structured populations with distributed states at birth. *Discrete Contin. Dyn. Syst. - Ser. B*, 17(8), 2671–2689.

Fitzpatrick, B. (1993). Modeling and Estimation Problems for Structured Heterogeneous Populations. *Journal of Mathematical Analysis and Applications*, 172(1), 73–91.

Flesch, J. C., Spicer, P. T., & Pratsinis, S. E. (1999). Laminar and turbulent shear-induced flocculation of fractal aggregates. *AIChE Journal*, 45, 1114–1124.

Fornberg, B. (1998). *A Practical Guide to Pseudospectral Methods*. Cambridge University Press.

Fournier, N. & Laurençot, P. (2005). Existence of self-similar solutions to Smoluchowski's coagulation equation. *Communications in Mathematical Physics*, 256(3), 589–609.

Gamma, C. D. & Jimeno, C. L. (1993). Rock fragmentation control for blasting cost minimization and environmental impact abatement. In P. P. Roy (Ed.), *Rock Fragmentation by Blasting* (pp. 273). Amsterdam, The Netherlands: A. A. Balkema Publishers.

Gibbs, A. L. & Su, F. E. (2002). On Choosing and Bounding Probability Metrics. *International Statistical Review*, 70(3), 419–435.

Gourley, S. A., Liu, R., & Wu, J. (2008). Spatiotemporal Patterns of Disease Spread: Interaction of Physiological Structure, Spatial Movements, Disease Progression and Human Intervention. In P. Magal & S. Ruan (Eds.), *Structured Population Models in Biology and Epidemiology*, number 1936 in Lecture Notes in Mathematics (pp. 165–208). Springer Berlin Heidelberg.

Greiner, G. & Nagel, R. (1988). Growth of cell populations via one-parameter semigroups of positive operators. *Mathematics applied to science*, 13(2), 934937.

Gurtin, M. & MacCamy, R. (1974). Non-linear age-dependent population dynamics. *Archive for Rational Mechanics and Analysis*, (pp. 66–76).

Gurtin, M. E. & MacCamy, R. C. (1979). Some Simple Models for Nonlinear Age-Dependent Population Dynamics. *Math. Biosciences*, 43, 199–211.

Gyllenberg, M., Osipov, A., & Päivärinta, L. (2002). The inverse problem of linear age-structured population dynamics. *J.evol.equ.*, 2(2), 223–239.

Haaber, J., Cohn, M. T., Frees, D., Andersen, T. J., & Ingmer, H. (2012). Planktonic Aggregates of Staphylococcus aureus Protect against Common Antibiotics. *PLOS ONE*, 7(7), e41075.

Hall, P., Racine, J., & Li, Q. (2004). Cross-Validation and the Estimation of Conditional Probability Densities. *Journal of the American Statistical Association*, 99(468), 1015–1026.

Han, B., Akeprathumchai, S., Wickramasinghe, S. R., & Qian, X. (2003). Flocculation of biological cells: Experiment vs. theory. *AIChE J.*, 49(7), 1687–1701.

Henry, D. (1981). Geometric theory of semilinear parabolic equations.

Hounslow, M. J. (1990). A discretized population balance for continuous systems at steady state. *AIChE J.*, 36(1), 106–116.

Ilana, N., Elkinb, M., & Vlodavsky, I. (2006). Regulation, function and clinical significance of heparanase in cancer metastasis and angiogenesis. *The International Journal of Biochemistry & Cell Biology*, 38, 2018.

Iori, G., Kapar, B., & Olmo, J. (2015). Bank characteristics and the interbank money market: a distributional approach. *Studies in Nonlinear Dynamics & Econometrics*, 19(3).

Ito, K. & Kappel, F. (1998). The Trotter-Kato theorem and approximation of PDEs. *Math Comp*, 67, 21–44.

Jewett, J. W. & Serway, R. A. (2008). *Physics for Scientists and Engineers with Modern Physics*. Cengage Learning EMEA.

Kappel, F. & Kunisch, K. (1981). Spline Approximations for Neutral Functional Differential Equations. *SIAM J. Numer. Anal.*, 18(6), 1058–1080.

Kato, N. (1995). A principle of linearized stability for nonlinear evolution equations. *Transactions of the American Mathematical Society*, 347(8), 2851–2868.

Kato, N. (1995). A Principle of Linearized Stability for Nonlinear Evolution Equations. *Transactions of the American Mathematical Society*, 347(8), 2851–2868.

Kato, T. (1959). Remarks on pseudo-resolvents and infinitesimal generators of semi-groups. *Proc. Japan Acad.*, 35(8), 467–468.

Kato, T. (1976). *Perturbation Theory for Linear Operators*. Classics in Mathematics. Berlin, Heidelberg: Springer Berlin Heidelberg.

Keck, D. D. & Bortz, D. M. (2016 (to appear)). Generalized sensitivity functions for size-structured population models. *Journal of Inverse and Ill-posed Problems*.

Kelley, J. L. (1955). *General Topology*. Princeton, NJ: Van Nostrand-Reinhold.

Kirkilionis, M. A., Diekmann, O., Lisser, B., Nool, M., Sommeijer, B., & De Roos, A. M. (2001). Numerical continuation of equilibria of physiologically structured population models i: theory. *Math. Models Methods Appl. Sci.*, 11(06), 1101–1127.

Krishnaswamy, S., Spitzer, M. H., Mingueneau, M., Bendall, S. C., Litvin, O., Stone, E., Pe'er, D., & Nolan, G. P. (2014). Conditional density-based analysis of T cell signaling in single-cell data. *Science*, 346(6213), 1250689–1250689.

Kuratowski, K. (1966). *Topology.* New York, NY, USA: Academic Press.

Ladisch, M. R. (2001). *Bioseparations Engineering: Principles, Practice and Economics.* New York: John Wiley & Sons.

Laskowski, J. S. & Ralston, J. (2015). *Colloid Chemistry in Mineral Processing.* Elsevier.

Laurençot, P. & Walker, C. (2005). Steady States for a Coagulation-Fragmentation Equation with Volume Scattering.

Laurencot, P. & Walker, C. (2005). Steady States for a Coagulation-Fragmentation Equation with Volume Scattering. *SIAM Journal on Mathematical Analysis. doi:10.1137/S0036141004444111.*

Li, X.-y., Zhang, J.-j., & Lee, J. H. W. (2004). Modelling particle size distribution dynamics in marine waters. *Water Research*, 38(5), 1305–1317.

Lu, C. F. & Spielman, L. A. (1985). Kinetics of floc breakage and aggregation in agitated liquid suspensions. *Journal of Colloid and Interface Science*, 103(1), 95–105.

Luzyanina, T., Mrusek, S., Edwards, J. T., Roose, D., Ehl, S., & Bocharov, G. (2006). Computational analysis of CFSE proliferation assay. *J. Math. Biol.*, 54(1), 57–89.

Luzyanina, T., Roose, D., & Bocharov, G. (2008). Distributed parameter identification for a label-structured cell population dynamics model using CFSE histogram time-series data. *J. Math. Biol.*, 59(5), 581–603.

Luzyanina, T., Roose, D., Schenkel, T., Sester, M., Ehl, S., Meyerhans, A., & Bocharov, G. (2007). Numerical modelling of label-structured cell population growth using CFSE distribution data. *Theor Biol Med Model*, 4(1), 1–15.

Makino, J., Fukushige, T., Funato, Y., & Kokubo, E. (1998). On the mass distribution of planetesimals in the early runaway stage. *New Astronomy*, 3(7), 411–417.

Matveev, S. A., Smirnov, A. P., & Tyrtyshnikov, E. E. (2015). A fast numerical method for the Cauchy problem for the Smoluchowski equation. *Journal of Computational Physics*, 282, 23–32.

Menon, G. & Pego, R. L. (2004). Approach to self-similarity in Smoluchowski's coagulation equations. *Communications on Pure and Applied Mathematics*, 57(9), 1197–1232.

Menon, G. & Pego, R. L. (2005). Dynamical Scaling in Smoluchowski's Coagulation Equations: Uniform Convergence. *SIAM Journal on Mathematical Analysis*, 36(5), 1629.

Menon, G. & Pego, R. L. (2006). Dynamical Scaling in Smoluchowski's Coagulation Equations: Uniform Convergence. *SIAM Review*, 48(4), 745.

Metz, J. A. J. & Diekmann, O. (1986). *The Dynamics of Physiologically Structured Populations.* Springer-Verlag.

Miao, H., Xia, X., Perelson, A., & Wu, H. (2011). On Identifiability of Nonlinear ODE Models and Applications in Viral Dynamics. *SIAM Rev.*, 53(1), 3–39.

Michel, P., Mischler, S., & Perthame, B. (2005). General relative entropy inequality: an illustration on growth models. *Journal de Mathématiques Pures et Appliquées*, 84(9), 1235–1260.

Mirzaev, I. (2015). Steady state approximation. *https://github.com/MathBioCU/SteadyStateApproximation*.

Mirzaev, I. (2017). Spectral Collocation Methods for numerical approximation of steady states of the microbial flocculation equations. *https://github.com/mirzaevinom/SpectralCollocationMethods*.

Mirzaev, I. & Bortz, D. M. (2015a). Criteria for linearized stability for a size-structured population model. *arXiv:1502.02754*.

Mirzaev, I. & Bortz, D. M. (2015b). Stability of steady states for a class of flocculation equations with growth and removal. *arXiv:1507.07127*.

Mirzaev, I. & Bortz, D. M. (2017). A numerical framework for computing steady states of structured population models and their stability. *Mathematical Biosciences and Engineering*, (to appear).

Mirzaev, I., Byrne, E. C., & Bortz, D. M. (2016). An Inverse Problem for a Class of Conditional Probability Measure-Dependent Evolution Equations. *Inverse Problems*, 32(9), 095005.

Nicmanis, M. & Hounslow, M. J. (1998). Finite-element methods for steady-state population balance equations. *AIChE J.*, 44(10), 2258–2272.

Nicmanis, M. & Hounslow, M. J. (2002). Error estimation and control for the steady state population balance equation: 1. An a posteriori error estimate. *Chemical Engineering Science*, 57(12), 2253–2264.

Niwa, H.-S. (1998). School Size Statistics of Fish. *J. Theor. Biol.*, 195(3), 351–361.

Nopens, I., Koegst, T., Mahieu, K., & a Vanrolleghem, P. (2005). PBM and activated sludge flocculation: From experimental data to calibrated model. *AIChE Journal*, 51, 1548–1557.

Pandya, J. D. & Spielman, L. A. (1982). Floc breakage in agitated suspensions: Theory and data processing strategy. *Journal of Colloid and Interface Science*, 90(2), 517–531.

Pandya, J. D. & Spielman, L. A. (1983). Floc breakage in agitated suspensions: Effect of agitation rate. *Chemical Engineering Science*, 38(12), 1983–1992.

Pazy, A. (1992). *Semigroups of Linear Operators and Applications to Partial Differential Equations*, volume 44 of *Applied Mathematical Sciences*. New York, NY: Springer-Verlag.

Persson, P.-A., Holmberg, R., & Lee, J. (1994). *Rock Blasting and Explosives engineering*. CRC Press.

Perthame, B. & Zubelli, J. P. (2007). On the inverse problem for a size-structured population model. *Inverse Problems*, 23(3), 1037–1052.

Piani, L., Rizzardini, C. B., Papo, A., & Goi, D. (2014). Rheology Measurements for Online Monitoring of Solids in Activated Sludge Reactors of Municipal Wastewater Treatment Plant. *ScientificWorldJournal*, 2014.

Pilant, M. & Rundell, W. (1991). Determining a Coefficient in a First-Order Hyperbolic Equation. *SIAM J. Appl. Math.*, 51(2), 494–506.

Powell, M. (1970). A hybrid method for nonlinear equations. In P. Rabinowitz (Ed.), *Numerical Methods for Nonlinear Algebraic Equations* (pp. 87–114). Gordon & Breach.

Powell, M. J. (1994). A direct search optimization method that models the objective and constraint functions by linear interpolation. In *Advances in optimization and numerical analysis* (pp. 51–67). Springer.

Powell, M. J. D. (1998). Direct search algorithms for optimization calculations. *Acta Numerica*, 7, 287–336.

Pruppacher, H. R. & Klett, J. D. (2012). *Microphysics of Clouds and Precipitation: Reprinted 1980*. Springer Science & Business Media.

Prüss, J. (1983a). On the qualitative behaviour of populations with age-specific interactions. *Computers & Mathematics with Applications*, 9(3), 327–339.

Prüss, J. (1983b). Stability analysis for equilibria in age-specific population dynamics. *Nonlinear Analysis: Theory, Methods & Applications*, 7(1), 1291–1313.

Ramkrishna, D. (2000). *Population Balances: Theory and Applications to Particulate Systems in Engineering*. Academic Press.

Saffman, P. G. & Turner, J. S. (1956). On the collision of drops in turbulent clouds. *Journal of Fluid Mechanics*, 1(01), 16–30.

Salim, S., Bosma, R., Vermuë, M. H., & Wijffels, R. H. (2011). Harvesting of microalgae by bio-flocculation. *Journal of Applied Phycology*, 23(5), 849–855.

Schreiber, S. J. & Ryan, M. E. (2011). Invasion speeds for structured populations in fluctuating environments. *Theor. Ecol.*, 4(4), 423–434.

Sinko, J. W. & Streifer, W. (1967). A new model for age-size structure of a population. *Ecology*, 48, 910–918.

Sinko, J. W. & Streifer, W. (1967). A New Model For Age-Size Structure of a Population. *Ecology*, 48(6), 910–918.

Smoller, J. (1983). *Shock waves and reaction-diffusion equations*, volume 258. New York and Heidelberg: Springer-Verlag.

Spicer, P. T. (1995). *Shear-Induced Aggregation-Fragmentation: Mixing and Aggregate Morphology Effects*. PhD thesis, University of Cincinnati.

Spicer, P. T. (1997). Shear-Induced Aggregation- Fragmentation : Mixing and Aggregate Morphology Effects by. *PHD Thesis*, (pp. 283).

Spicer, P. T. & Pratsinis, S. E. (1996). Coagulation and fragmentation: Universal steady-state particle-size distribution. *AIChE journal*, 42(6), 1612–1620.

Spicer, P. T., Pratsinis, S. E., Raper, J., Amal, R., Bushell, G., & Meesters, G. (1998). Effect of shear schedule on particle size, density, and structure during flocculation in stirred tanks. *Powder Technology*, 97(1), 26–34.

Spicer, P. T., Pratsinis, S. E., Trennepohl, M. D., & Meesters, G. H. M. (1996). Coagulation and Fragmentation: The Variation of Shear Rate and the Time Lag for Attainment of Steady State. *Industrial & Engineering Chemistry Research*, 35(9), 3074–3080.

Thomas, D. N., Judd, S. J., & Fawcett, N. (1999). Flocculation modelling: a review. *Water Research*, 33, 1579–1592.

Thomaseth, K. & Cobelli, C. (1999). Generalized sensitivity functions in physiological system identification. *Annals of biomedical engineering*, 27(5), 607–616.

Trefethen, L. (2000). *Spectral Methods in MATLAB*. Software, Environments and Tools. Society for Industrial and Applied Mathematics.

Trotter, H. F. (1958). Approximation of semi-groups of operators. *Pacific J. Math.*, 8(4), 887–919.

van Smoluchowski, M. (1916). Drei Vortrage uber Diffusion, Brownsche Bewegung und Koagulation von Kolloidteilchen. *Zeitschrift fur Physik*, 17, 557–585.

van Smoluchowski, M. (1917). Versuch einer mathematischen theorie der koagulation kinetic kolloider losungen. *Zeitschrift f{ü}r physikalische Chemie*, 92, 129–168.

Wattis, J. A. (2006). An introduction to mathematical models of coagulation–fragmentation processes: A discrete deterministic mean-field approach. *Phys. Nonlinear Phenom.*, 222(1-2), 1–20.

Wattis, J. A. D. (2006). An introduction to mathematical models of coagulation-fragmentation processes: A discrete deterministic mean-field approach.

Webb, G. F. (1985). *Theory of nonlinear age-dependent population dynamics*. Number 89 in Pure and Applied Mathematics. New York, NY: CRC Press.

White, W. H. (1980). A Global Existence Theorem for Smoluchowski's Coagulation Equations. *Proceedings of the American Mathematical Society*, 80(2), 273–276.

Wyckoff, J. B., Jones, J. G., Condeelis, J. S., & Segall, J. E. (2000). A critical step in metastasis: in vivo analysis of intravasation at the primary tumor. *Cancer research*, 60(9), 2504–2511.

Yeh, W. W.-G. (1986). Review of Parameter Identification Procedures in Groundwater Hydrology: The Inverse Problem. *Water Resour. Res.*, 22(2), 95–108.

Ziff, R. M. & Stell, G. (1980). Kinetics of polymer gelation. *J. Chem. Phys.*, 73(7), 3492–3499.